THEORY OF LONGITUDINAL EMISSION COMPUTED TOMOGRAPHY AND THE PRACTICAL APPLICATION TO CARDIAC IMAGING

BY

JOHN ALEXANDER MILLS

THESIS
SUBMITTED FOR THE
DEGREE OF DOCTOR OF PHILOSOPHY
OF THE
UNIVERSITY OF WARWICK

FROM RESEARCH
CONDUCTED IN THE PHYSICS DEPARTMENT
UNIVERSITY OF WARWICK

NOVEMBER 1986

ACKNOWLEDGEMENTS

Dr. T.A. Delchar, Physics Department, University of Warwick, for guidance and encouragement of ideas.

Mr. J.A. McIntosh, Department of Clinical Physics and Bio-Engineering, Walsgrave Hospital, Coventry for the provision and the use of the facilities.

Dr. D.N. Taylor, Department of Clinical Physics and Bio-Engineering, Walsgrave Hospital, Coventry for the assistance and encouragement.

Dr. J.N. Flint and Dr. J. Pilcher, Department of Cardiology, Walsgrave Hospital, Coventry for practical assistance in the clinical work.

Coventry Health Authority for financial assistance.

Many friends for the encouragement and interest.

Sara and Deirdre for typing.

DECLARATION

THE THEORY OF LECT SYSTEMS AND THE PRACTICAL APPLICATION TO CARDIAC IMAGING IS ORIGINAL.

THE CLINICAL WORK ON THALLIUM PERFUSION IMAGING IS SHARED WITH J. FLINT MRCP AND D.N. TAYLOR PhD.

THIS WORK IS SUBMITTED FOR THE DEGREE OF DOCTOR OF PHILOSOPHY OF THE UNIVERSITY OF WARWICK.

PUBLICATIONS

"Thallium-201 Scintigraphy for Ischaemic Heart Disease and Infarct Detection: Comparison of Rotating Slant Hole Tomography and Planar Imaging".

J.A. Mills, J. Flint, D.N. Taylor, T.A. Delchar, J.A. McIntosh and J Pilcher. 1985 Br. J. Radiology 58,625 - 634.

"Longitudinal Emission Computed Tomography: A Critical Analysis".

J.A. Mills, T.A. Delchar.
Accepted for publication in Nuclear Instruments and Methods in Physics Research. Section A.

DEDICATION

TO

MY SISTER,

ANNE.

SUMMARY

Longitudinal Emission Computed Tomography (LECT) is a radioisotope imaging technique which has found particular use in cardiac investigations. However, its clinical use has revealed imaging problems which show themselves as reconstruction artefacts or false defects. The basis for the imaging problem of LECT is established theoretically using a simple analysis which shows that the reconstruction will predict that activity lies outside the object volume. The volume of the reconstruction lying outside the object volume is considered as an error volume, by using simple, unmodified back projection. This is the first time such a concept has been developed and it is used to calculate an error volume index (EVI). This index is shown to be useful for assessing and comparing LECT systems. It is used to examine the reduction of the error volume by modifications to LECT systems.

Thallium-201 perfusion imaging for ischaemic heart disease and infarct detection using a rotating slant hole (RSH) LECT system is compared to conventional planar imaging and X-ray contrast arteriography. RSHLECT is shown not to improve the diagnostic performance of planar imaging. The tomograms suffer from artefacts which appear as defects in the myocardium. Although the presence of these artefacts have been demonstrated by other workers this study shows that they have a significant affect on the diagnostic performance of the technique. A computer simulation and experimental studies using a simulated cardiac chamber are used to study the source of the problem. The origin of the artefacts is demonstrated for the first time.

The problem of the error volume in reconstructing the cardiac blood pool is considered. Three techniques to correct the reconstruction volume are examined and one is recommended which will reduce the error volume. Computer simulation and experimental studies with a simulated blood pool are used to examine this problem. It is shown that it is not possible to correct the reconstruction volume when an iterative least squares reconstruction technique is used together with the assumption of a uniform activity distribution; this implies the need for an alternative predictive function. The inability to correct the reconstruction volume for a simple uniform activity distribution show that, for Thallium-201 perfusion imaging where the distribution is non-uniform, there is a need for an imaging system modified to reduce the error volume. This work conderning a blood pool LECT reconstruction and correction of the reconstruction volume is original.

For the clinical trial of Thallium-201 perfusion imaging and the experimental work with a simulated cardiac chamber, a rotating slant hole LECT system was used. The physical performance of this system was measured and compared with other LECT systems. In doing this a relationship between plane density in the reconstruction and inter-planar resolution is demonstrated for the first time.

C O N T E N T S

GLOSSARY OF ABBREVIATIONS

ECG	ELECTROCARDIOGRAM
ECT	EMISSION COMPUTED TOMOGRAPHY
EVI	ERROR VOLUME INDEX
IHD	ISCHAEMIC HEART DISEASE
ILSRT	ITERATIVE LEAST SQUARES RECONSTRUCTION TECHNIQUE
LAO	LEFT ANTERIOR OBLIQUE
LECT	LONGITUDINAL EMISSION COMPUTED TOMOGRAPHY
LPO	LEFT POSTERIOR OBLIQUE
LV	LEFT VENTRICLE
RAO	RIGHT ANTERIOR OBLIQUE
RHECT	ROTATING HEAD EMISSION COMPUTED TOMOGRAPHY
RSHECT	ROTATING SLANT HOLE EMISSION COMPUTED TOMOGRAPHY
RV	RIGHT VENTRICLE
SPECT	SINGLE PHOTON EMISSION COMPUTED TOMOGRAPHY
TCGBP	TOMOGRAPHIC CARDIAC GATED BLOOD POOL

CHAPTER

1

INTRODUCTION

1.1 Radioisotopes in Clinical Diagnosis

Radio isotopes or radioactive tracers are now routinely used in the diagnosis of clinical pathologies. Developments in pharmaceuticals have led to radioactive tracers which can be safely administered to patients and which will follow one or sometimes several functional processes in the body. These radiopharmaceuticals or radiotracers are used to investigate and measure the performance of the body as well as to reveal the distribution of functioning tissue in the body.

There is a wide range of radioisotopes used for diagnostic purposes with photon emission energies ranging from 28KeV for Iodine-125 up to 412KeV for Gold-198. Radiation arising from electron capture, positron anihilation, beta decay as well as γ-ray disintegration including isomeric transitions giving very short half-lifes are used clinically. It is the ability of such radiation to penetrate the body which provides such an important and useful tool for medical diagnosis.

The development of radiation measuring equipment such as Geiger and scintillation detectors has made it possible to determine quantitatively the uptake of radioactive tracer which, in turn, permits the measurement of certain functions in the body and the relative distribution of functioning tissue. By surveying the body surface above an organ where the radioactive tracer has accumulated, an indication of the distribution of functioning tissue within an organ can be obtained. To perform such a survey the detector needs to be collimated, since the radiation from the radioactive decay of the tracer is omnidirectional. Collimation of the detector ensures that the area of the body surface monitored is always defined. The radiation which is detected arises from the activity within a column lying across the organ. The column has a cross sectional area of the collimator and the length of the column is defined by the position of the detector in relation to the organ and by the direction of collimation, see Fig. 1.1. Although the majority of the detected radiation will arise from the radioactive tracer within a column through the organ defined by the collimator, some scattered radiation from the surrounding organs and tissues will also be collected. The result of such a survey is a 2-dimensional image of the radiotracer distribution in 3-dimensions.

1.2 Radioisotope Imaging System

The uptake of a radioactive tracer in an organ can be surveyed by the motion of a detector over the surface of the body above the organ. This process is carried out systematically by the rectilinear scanner, which was introduced around 1951 (Mayneord et al, Cassen et al). With this device a collimated detector is driven mechanically in parallel rows across a defined area above an organ. The detected activity is recorded at fixed intervals and a 2-dimensional distribution reflects, (in the direction of collimation), the detected activity due to the uptake of a

Fig. 1,1

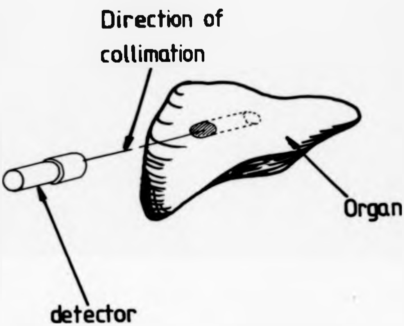

COLLIMATED DETECTOR SURVEYING THE RADIOACTIVITY IN AN ORGAN radioactive tracer in the 3-dimensional organ.

The development of scanning systems has proceeded in parallel with the development of multi-crystal and large crystal detecting systems. These are scintillation crystals which transform the energy of incident gamma or X-ray photons into visible photons. They are usually made from sodium iodide with Thallium doping (NaI(T1)). With large crystal systems there is a compromise to be made between sensitivity and resolution. To determine the position of a scintillation on a crystal as accurately as possible it is desirable to make the crystal as thin as possible. However, to collect the maximum amount of incident radiation and thus made the system as sensitive as possible, requires a thick crystal.

With multicrystals devices (Bender and Blau, 1962) an array of collimated detectors can monitor the distribution of activity throughout an organ. These crystals can be made thick as the resolution of the system is dependent on the physical position and size of the crystals. Hence, resolution may be poor but extremely high count rates can be accommodated.

The most important large crystal device is known as the anger camera after H.O. Anger (1958). These devices consist of a large NaI(T1) crystal, the diameter of which may range from around 250mm for a standard field of view (SFOV) camera to 450mm for a large field of view (LFOV) camera. The thickness of the crystal is chosen to give optimal performance of the camera depending on the range of isotope photon energies to be used and the sensitivity needed for the system application. A collimator is placed in front of the crystal; these are constructed from a thickness of lead chosen to suit the energy of the isotopes to be used. The collimator essentially consists of a large number of short parallel tubes all at right angles to the crystal. A compromise must be made between sensitivity and resolution in collimator design, thus the choice of collimator used in a study is made by the operator on the basis of the particular requirements of that study. Collimators are also designed to produce magnified images or images reduced in size. This is done by inclining the small tubes which form the collimator, and are known as diverging and converging collimators respectively.

The scintillations within the crystal are detected by an array of photomultiplier tubes. For each of two orthoganol axes in the camera face, two signals are derived from the photomultiplier pulses which arise rom each incident photon. One signal is simply an integration of all the scintillation pulses giving a signal proportional to the total incident energy. The other signal is an integration of the same pulses with the pulse level weighted by the distance of the photomultiplier from a reference axis. Using the two signals appropriate to each axes the displacements of the incident photon from the reference axes can be estimated. By placing detected photons at the calculated positions, a 2-dimensional image of the 3-dimensional radioactive tracer distribution in an organ is obtained.

The benefit of an Anger camera over a scanning device lies principally in the fact that there are no moving mechanical parts required in order to obtain the survey of activity; as the position of the scintillation is estimated electronically. Also, since the distribution of activity is surveyed at all points in the field of view of the camera virtually simultaneously, the positioning of a patient to obtain an adequate image of the organ under investigation is easily achieved. Digitisation of the scintillation data from a camera, along with the use of a computer, make it possible to follow, in real time, the flow and uptake of a radioactive tracer. This development has extended and increased the benefits from the imaging of radioactive tracers for clinical diagnosis.

Anger cameras however can only detect single photons. To specifically detect emissions due to a positron emitting isotope a diametrically opposed detecting device is needed. Most isotopes used for imaging work are single photon types and so this does not pose a serious limitation to Anger cameras.

With all of these imaging devices the resultant image is a 2-dimensional display of the radioactive tracer distribution within a 3-dimensional organ. Organs of the body tend to be of irregular shape and inhomogenous function. Estimating regions of reduced or absent function within an organ with generally known shape, but individual variations, cannot be done with only one 2-dimensional image. Indeed it can be very difficult even with several 2-dimensional images taken from different viewing directions. The problem which must be solved is how to reveal the distribution of radioactive tracer uptake across a slice of an organ by removing from the view the overlying and underlying radiotracer uptake.

1.3 Tomographic Imaging Systems with Radioactive Tracers

Before the development of tomographic imaging systems using either Anger cameras or dedicated scanners, the problem of overlying activity was tackled by the use of a focussed collimator on a rectilinear scanner. Such a collimator achieves blurring of the radiation detected from parts of the organ above and below the depth of focus. This reveals, to a limited extent, the distribution of the radiotracer through the organ at the depth of focus. However, with this device the depth of interest needs to be known approximately at the time of scanning. This can involve several views being taken which lengthens the scanning time. A more attractive proposition which is achieved by modern tomographic techniques is to provide, simultaneously, images of several slices of the organ. Viewed together these reveal more explicitly the 3-dimensional distribution of the radiotracer within the organ.

Developments of radioisotope tomographic imaging facilities have led to some dedicated multiple-crystal or single-crystal scanning devices. These devices use the information from several scans through a single plane of an organ, each in different directions to construct a tomogram. Some of these devices utilise positron emitting isotopes and the information which is obtained from the resulting pair production. However, these positron emitting isotopes have very short half-lives and so reqire production facilities in close proximity to the imaging devices. Since this is only possible at a few establishments it makes the very versatile Anger camera the principal means for producing radioisotope tomograms. Tomographic techniques using an Anger camera come within the description of single photon emission tomography (SPECT).

1.4 The Development of Longitudinal Single Photon Emission Tomography

Tomograms were being produced using X radiation in a transmission mode as early as the 1930's as described by Andrews, 1936 and Andrews and Stava in 1937. These early techniques relied on the relative motion between the radiation source and film to smear the effect of the attenuation outside a plane of interest across the image. In the 1960's this technique began to be investigated for radioisotope imaging. In 1961 Oldendorf demonstrated that an electrical signal could be produced which represented the attenuation profile across an object of known cross-section. This was basically an application of the blurring technique and was examined with a view to its medical application of detecting the variations in the soft tissue of the brain. A radisiaotope was used in transmission mode, but the demonstration was equally applicable to the emission mode. Kuhl and Edwards used this technique with a rectilinear scanner in 1963 to produce longitudinal and transverse body sections. In this work the terms longitudinal and transverse were first defined in their relationship to the use of radioisotope imaging equipment in tomography.

To obtain longitudinal tomograms using a scanner involves taking several separate views of the object. In each view the detecting head is inclined by a different arc about a centre of rotation somewhere below the patient. The 2-dimensional images so obtained are then superimposed and displaced by a known distance for a particular plane. This has the effect of enhancing data from the plane, Fig. 1.2. For transverse tomograms the scanner moves in the plane of interest across the patient, Fig. 1.3. Several such scans are taken and the backprojection of the resulting scans is displayed electronically on an oscillascope or VDU if computational facilities are used. The superposition of the backprojections produces enhancement within a profile which approximates to that of the object and this produces the tomogram.

Following this work, longitudinal tomographic systems were developed which used Anger cameras. In 1970 Muehllehner and in 1973 Freedman described the use of an Anger camera to produce oscillascope displays of tomograms. Both techniques used collimators which rather than accepting radiation perpendicular to the crystal, accepted radiation incident on the camera at some angle less than $\pi/2$. These are known as slant hole collimators and view an object in the direction of the angle of the collimator. In Muehllehner's work the patient was rotated to obtain several views from different orientations; Freedman rotated the collimator to achieve the same result. In both cases several longitudinal tomograms were displayed simultaneously on an oscilloscope.

In 1978 Kirch and Vogel first applied an iterative computer algorithm to reconstruct a set of planes. They also used a

Fig. 1.2

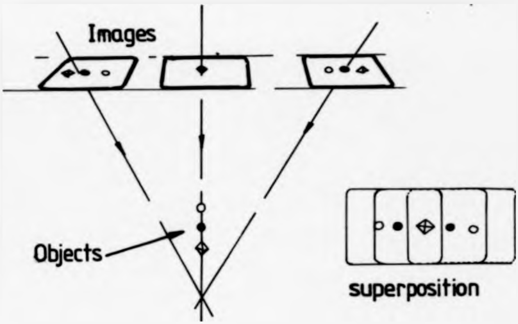

BASIS OF TECHNIQUE TO OBTAIN LONGITUDINAL TOMOGRAMS WITH A RECTILINEAR SCANNER

Fig. 1.3

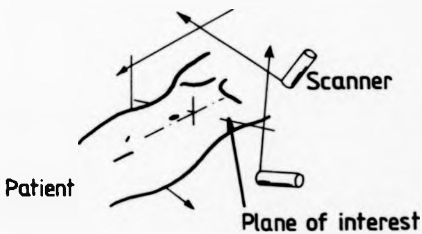

SCANNING DIRECTIONS TO OBTAIN TRANSVERSE TOMOGRAMS multiple pinhole collimator for the first time to acquire views for the reconstruction. Several suitable computer algorithms had been developed since the work of Muehllehner and Freedman, notably those of Gordon 1974 and Budinger et al 1974, for transverse X-ray and emission computed tomography. Kirch and Vogel however, successfully applied them to longitudinal emission tomography for the first time. Because all the views obtained in longitudinal tomography are as a result of the superposition of the activity within a set of planes the algorithm must reconstruct all the tomograms simultaneously. This results in a set of tomograms which forms a reconstruction volume. Longitudinal emission computer tomographic (LECT) systems are now widely available commercially. Slant hole and multiple pinhole collimators can be supplied for both large and standard field of view Anger cameras. These systems take views of an object in only a few directions, usually six to twelve and are thus known as limited angle LECT systems.

As opposed to LECT where the camera remains in one position, with rotating head computed tomography (RHECT) the camera is rotated around the patient. In this way several different views of the object are acquired. Many commercially available RHECT systems have been developed and are in widespread use. The use of computers to reconstruct transverse tomograms using images acquired by an Anger camera was well established by 1974 (Budinger and Gullberg). A great deal of research and development has subsequently been undertaken to improve the performance of RHECT systems and to determine the clinical usefulness of RHECT.

1.5 Current Developments in SPECT

Recent research and development into SPECT has mainly been in relation to RHECT systems. No new LECT system has been introduced since the multiple pinhole collimator system of Vogel and Kirch in 1978 and currently there is little work being done on LECT system development.

However, both LECT and RHECT have benefitted from the continual improvement in Anger camera performance. Improvements in linearity and uniformity of cameras has provided better quality scintigraphic data for reconstruction. This is achieved by improving balancing of the response of the photomultipliers and by techniques which set the energy windows of the photomultipliers more accurately. Camera countrate capability has been increased so decreasing the statistical uncertainty in images (Budinger 1980). Digitisation of the camera head signals allows sophisticated computations to be made on the data. Correction maps are stored for linearity, energy and sensitivity and these can be used to correct, automatically, incoming data.

Some deficiencies in tomogram production are due to factors which with careful setting-up procedures and routine checks can be eliminated. The actual centre of rotation of the camera in RHECT and the centre of images for LECT must coincide with that of the reconstruction program. If they do not then serious loss of resolution can occur. This aspect can be checked and altered by an operator. Likewise, the operator should ensure that the axis of rotation or axis of symmetry is lying correctly in relation to the couch or patient. Finally sufficient counts need to be acquired to reconstruct a good tomogram. These are operator dependent features and their significance has been brought out in work done over the past few years (Greer et al, 1983; Harkness et al, 1983). The improvements in camera performance have added greatly to RHECT tomogram improvement. Artefacts in the form of rings are produced in tomograms where there is excessive uniformity variation (Rogers et al, 1982); Harkness et al 1983 recommends that camera uniformity should be kept within ± 1%. The improvements in camera uniformity help in reducing this problem. The improved linearity is a major contribution to the improved uniformity. However, by itself it provides more accurate information for the reconstruction. Inaccuracy in the positioning of incident radiation leads to a blurring of the tomogram.

The only development in LECT has been the addition of views to the reconstruction by utilising an existing system in an extended manner. Koral et al, 1982 has demonstrated experimentally using a phantom object which simulates the radioisotope distribution in the heart that the performance of a basic slant hole LECT system can be improved. The additional views were acquired by moving the camera through $\pi/2$ and these views were then used in the reconstruction. Collimator designs still fall into the categories of multiple pinhole and slant hole types and no improvements or changes in design have been made recently.

On the other hand, with RHECT there are continuing developments and improvements to systems. One of the potential uses for ECT is the measurement of radiotracer uptake by quantifying the radioisotope within an organ. In order to do this attenuation and scatter in surrounding tissue must be taken into account. Also, the reconstruction of a uniform radioisotope distribution is detrimentally affected when scatter and attenuation are not adequately accounted for. Thus, one important aspect being investigated by several workers is the improvement in the performance of RHECT systems by making allowance for scatter and attenuation (Macey et al, 1985; Webb et al, 1985; Harris et al, 1984; Jaszczak et al, 1984). Modern cameras are capable of imaging simultaneously in two separate energy windows. Hence both an overall image, centered on the total absorption peak and a scatter image centered somewhere in the Compton scatter region can be acquired simultaneously. These can be used in combinaation to produce a more accurate image (Jaszczak et al, 1984). Another technique being examined is the use of asymmetric energy windows to reduce the amount of scatter in the image (LaFontaine et al, 1984).

A further development with RHECT has been the use of two diametrically opposed Anger cameras (Jaszczak et al, 1979). This system increases the amount of information available for a reconstruction. However, it introduces the problem of registration between the two cameras as well as the additional quality control of the extra camera. This is on top of the additional cost of the extra camera.

Most RHECT systems rotate at a set distance from an axis of rotation fixed somewhere in the cross-section of the patient. This results in a loss of resolution over the sections of rotation where there is the greatest difference between body surface and the camera face. Non-circular orbits are being studied (Gottschalk et al, 1983; Pokropek 1983; Faber et al, 1985) to evaluate the improvements in resolution and uniformity which may be obtained. This work has been done for elliptical orbits and more complex profile tracking systems have not yet been studied.

The reconstruction techniques in general use have remained unchanged and are well described by Budinger, 1974. Recently Roff, 1984 has described an improvement in myocardial reconstructions by using a pre-processing filter. Corrections for organ movement has also been studied by Freedman, 1984.

1.6 Physical Performance of SPECT System

Satisfactory physical performance of all ECT systems highly dependent on great care and attention being paid to the operation of the Anger camera and the associated tomographic equipment. This involves two aspects; firstly the routine quality control of the system and secondly, a satisfactory setting up procedure for the tomographic acquisitions. For routine quality control of the camera there are well established techniques to monitor and check intrinsic resolution, energy resolution, linearity and uniformity and these are comprehensively outlined in the standards of the National Engineering Manufacturers Association; the NEMA standards. Quality control for the overall tomographic system is achieved using a suitably chosen phantom object of well defined physical size and shape. The reconstruction of a uniform source and the resolution variations with contrast and depth are usually assessed. For RHECT two widely accepted phantoms for system assessment are those developed by Jaszczak and Carlson, (Scientific and Industrial Equipment Ltd.). These phantoms are not applicable to LECT due to the reconstruction volume. They would not give the same compre tomographic system as they do in RHECT.

For both LECT and RHECT, the setting up procedure prior to using the system for image acquisition is important. In LECT it is essential that a system is calibrated by acquiring images of a point source at a known distance from the camera face. By doing this the displacement of the centre of planes parallel to the camera face is accurately known with respect to the images subsequently acquired. For pinhole collimator systems there is a uniformity variation across the image and this must be corrected for. This can be done using the acquisition of a uniform source prior to image acquisition.

With RHECT systems it is important that the centre of rotation is in a fixed position as the camera rotates. The mechanical alignment of this should be checked regularly. The relationship between the centre of rotation and the imaging axis of the camera must be such that there is an exact agreement as the camera rotates. In the same way as LECT systems can be calibrated for the displacement of plane centres, a point source can be used to check the image of the centre of rotation as the camera rotates. This should be done prior to acquiring images and any necessary corrections made. Failure to maintain satisfactory registration between the centre of rotation and the reconstruction software results in blurring of images, (Harkness, et al, 1983; Greer, 1983). Another major problem for RHECT is uniformity correction. Small variations in uniformity lead to ring artefacts in images. Thus, for image correction for non-uniform camera performance, correction images of a uniform activity source need to contain a very large number of counts to ensure low enough statistical variation in the uniformity. Harkness (1983) recommends a flood count in excess of 30.10^6 to obtain 1% statistical variation for a 64 x 64 image matrix. Greer (1983) suggests a $40-50.10^6$ count image for a 128 x 128 matrix. Both recommendations indicate the large number of counts needed for adequate uniformity correction. The choice of filter to be used in the reconstruction in RHECT is important and needs to be chosen depending on the number of counts acquired in the image. If the filter over smooths the data there will be a loss of resolution. Also, attenuation correction must be done with care in order to avoid introducing false variations in the tomogram density.

For both LECT and RHECT the acquisition of images containing adequate counts is important. Tomographic reconstruction techniques act as a high pass filter and produce very noisy tomograms from very low noise images. Budinger (1980) states that the act of reconstruction can result in a decrease of the signal to noise ratio by an order of magnitude. Although this depends on the volume of interest and resolution of the system there is clearly a need to acquire images with high counts to obtain satisfactory tomograms.

With LECT there is an inherent ripple in the density of the reconstructed tomogram due to the limited angle nature of the systems. This makes the reconstructions rather insensitive to small variations in image uniformity and generally a lower quality image is acceptable compared with RHECT.

The physical performance of SPECT system is dependent on the energy of the radioisotope being imaged. The isotope being imaged affects in the first place the collimator used in rotating head and slant hole collimator LECT systems. This in turn alters the resolution of the images acquired for the reconstruction and so changes the physical performance of the SPECT system. With pinhole collimator LECT systems this effect is apparent in the size of the pinhole.

There is a loss of resolution with distance from the collimator of an Anger camera and this is reflected in the physical performance of ECT systems. With RHECT, the resolution, measured by the full width half maximum (FWHM) of a point or line source reconstruction increases with distance from the collimator.

Most routine applications of SPECT systems are with Technetium-99m which has an ideal imaging energy of 140KeV and most published results of physical performance use this isotope. With a Technetium-99m point or line source the intra planar resolution will vary typically between 13mm and 30mm over a radius of rotation of from 80mm to 320mm from the camera face (Myers et al, 1983). It is important in physical performance measurements that the parameters chosen for the acquisition should correspond to those to be expected in a

typical clinical application. For example, Myers figures are quoted from a radius of rotation of 80mm. Such small distances will not occur clinically and resolutions at distances of rotation between 200mm to 300mm are more typical of what will be encountered. Over this range, the intra planar resolution is of the order of between 14mm and 35mm (Myers 1983). The inter planar resolution is of the order of the imaging resolution as pointed out by Myers (1983).
Resolution measurements using the FWHM of either a reconstructed point or line source have been published by several workers and they are presented in Fig. 1.4a,b,c,d. Neither RHECT nor LECT systems correctly reconstruct a uniform source. With RHECT this is due to inadequate correction for attenuation and scatter. No simple technique can overcome this and uniform objects can have different reconstruction variations depending on the attenuation correction use. With LECT systems the uniform object is reconstructed with a hump or convex transverse profile. This is assumed to be due to the interplanar propagation referred to by Budinger (1980) and Williams (1980).

1.7 Clinical Applications of SPECT

Emission computed tomography has found many clinical applications, principally in the examination of the liver, brain, heart and lung. It has also been used for imaging of joints and bone lesions (Mortelmans et al, 1983; Sakatu et al, 1983) and in renal imaging (Kawamura et al, 1984) with a view to quantifying the uptake of radiotracer in the kidneys. Much more diagnostic information about renal function can be

Fig.1.4

INTER AND INTRA PLANAR RESOLUTION MEASUREMENTS FOR ROTATING SLANT HOLE (RSH) AND SEVEN PINHOLE (7-PINHOLE) LECT SYSTEMS

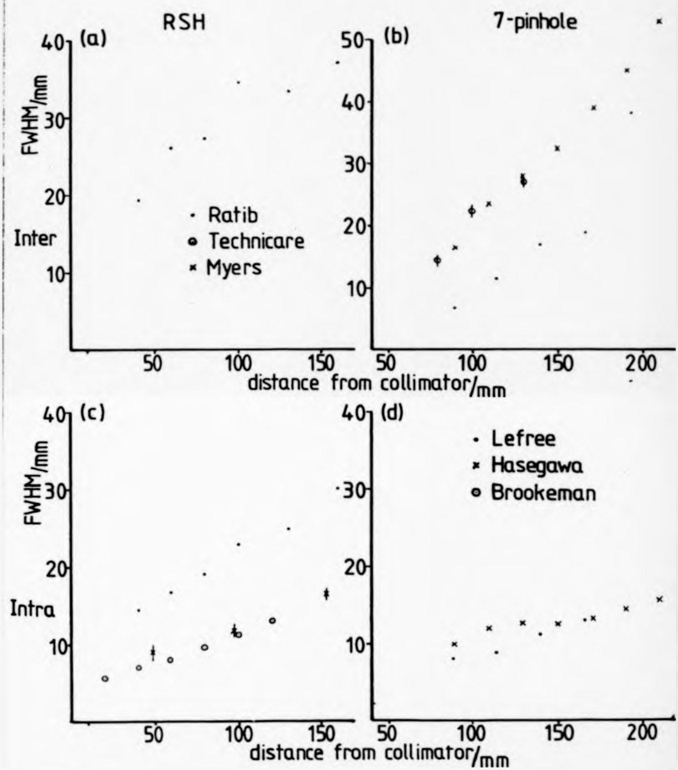

obtained from tomograms than is available from planar renal scans. The major problem is to achieve adequate quantification of the radiotracer uptake by accounting for scatter and attenuation in the organ and surrounding tissue. In all these applications the RHECT system has been used almost exclusively.

The use of LECT for brain imaging has been demonstrated by the author and Dale et al, (1985) but only Dale (1985) has published results. In cardiac imaging there is an almost equal application of RHECT and LECT. In fact LECT has found its main application in cardiac imaging. In liver radioisotope imaging RHECT has never shown an improvement over planar imaging such as to make the additional scanning and processing time worthwhile. There is a variation in the diagnostic performance of the test depending on the disease being investigated. For metastatic liver disease the detection rate is significantly higher than for other diseases. Dendy et al, 1981, demonstrated that the use of a tomogram did not improve the use of liver scintigraphy compared with planar imaging. The specificity decreased, whilst the sensitivity increased and there was no statistically significant difference in diagnostic accuracy. Research since then has examined how RHECT compares with other techniques and how it may be combined with other techniques. Berche et al, 1981 examined how the diagnostic ability of RHECT liver imaging compared with surgery, ultrasound and biochemistry tests. The contribution from ECT to the overall diagnostic process was studied by Reid et al, 1983. Oyamadu et al, 1984 suggests a segmental analysis to improve the diagnostic capability of the test, but its use has not been demonstrated clinically. Many centres use RHECT in liver scintigraphy with the view that it provides a useful adjunct to planar scans when the planar results are equivocal.

There has been several comparative studies made of planar imaging and RHECT for lung perfusion and ventilation imaging; for example LaJeune et al, 1982, Ronaldson et al, 1982 and Osborne et al, 1983. The well tried radiopharmaceutical Technetium-99m macro albumin aggregates has been used for perfusion imaging. Ventilation studies with Krypton-81m and radioactive aerosol have been made and a transmission technique has also been used to delineate the ventilated regions of the lung (Maeda et al, 1981). All these studies have given indications that identification of segmental defects are improved by the use of RHECT. None of the studies were compared with an absolute criterion such as post mortem. To find an accepted standard with which to gauge the use of RHECT lung scanning remains a problem. The studies which have been made involving human patients have compared the response of operators to planar and tomographic images. Without an absolute standard diagnosis with which the comparison can be made it is impossible to gauge how useful RHECT is in lung imaging. RHECT is also applied to brain imaging. Its application in this field has been greatly overshadowed by positron emission tomography which has been applied to brain imaging extensively as a consequence of the radioisotopes which are available in this field. However, several studies examining the role of RHECT in the diagnosis of cerebal pathologies have been done, for example; Ell et al, 1980; Watson et al, 1980; Fazio et al, 1980. Its use in brain imaging continues and particularly with a view to quantitation of radioisotopes uptake. More useful single photon radiopharmaceuticals are becoming available for example Iodine-123 labelled HIPDM for regional cerebal perfusion assessment (Fazio et al, 1984) and Iodine-123 labelled N-isopropyl Iodo amphetamine for studies involving epilespsy (Magistretti, 1983) and cerebal infarction (Uren et al, 1982).

Brain imaging had been demonstrated using a rotating slant hole system as mentioned previously. These have been of an anecdotal nature and although useful tomograms were obtained, no serious clinical trials were pursued.

Both RHECT and LECT have been used extensively in cardiac investigations. The ease of use of a LECT system when imaging what may be a seriously ill patient makes it an attractive facility for cardiac imaging. Also, even with a LFOV system, the volume which can be imaged by all the views is generally very limited and this suits a small organ like the heart.

The current developments and improvements in RHECT and in the Anger camera itself may improve the diagnostic performance of RHECT in all areas where it finds a clinical application. Compensation for scatter and attenuation may establish RHECT as having a significant role in radioisotope imaging through being able to quantify adequately the uptake of radiopharmaceutical. The establishment of the requirements of quality control and setting up procedures should lead to a better and more consistent performance of systems. LECT, due to the size of the volume which can be imaged by all views, will continue to lend itself to cardiac imaging almost exclusively. Brain imaging, which has been demonstrated could be undertaken in children where this organ would be sufficiently small. The longitudinal systems known as the Ectomogram (Dale et al, 1985) lends itself well to brain imaging in children and adults. However, as a system, it requires all the facilities of the RHECT system.

1.8 Current Use ofRHECT and LECT in Cardiac Imaging

Single photon radioisotope tracers have been very successfully applied in two aspects of cardiac investigation. In the investigation of blood flow to and within the heart wall, known as myocardial perfusion, Thallium-201 and Technetium-99m labelled pyrohosphates are used. Thallium is taken up in the same way as potassium in all muscle tissue. Hence it gives an indication of diminished blood flow, ischaemia of the myocardium, by accumulating in regions of adequately perfused myocardium and not in regions of ischaemia. Pyrohosphates, on the other hand, accumulate in muscle which has recently suffered irreversible damage due to a lack of blood supply: muscle which has infarcted. Hence it indicates regions of myocardial infarction. While a radiopharmaceutical which will have better energy characteristics than Thallium-201 is still sought after, Thallium-201 is used extensively and routinely in investigations for ischaemic heart disease (IHD). The

Technetium-99m labelled pyrophosphates although having energy, half-life and reduced toxicity advantages compared with Thallium-201 are only useful for the detection of acute infarcts. Ischaemia and old infarction cannot be assessed with it and the uptake of the pharmaceutical in the ribs complicates the interpretation of images. Further, for the detection of acute infarction, Thallium-201 imaging can commence with 5-10 minutes from injection while the phosphates require imaging at several hours post injection. Thallium-201 is currently the radiotracer of choice for the assessment of myocardial perfusion. The other aspect of radioisotope cardiac investigation is the assessment of the function of the heart. The widely accepted method is to label red blood cells with Technetium-99m and to gate the Anger camera to the electrocardiograph (ECG) signal. A series of images are acquired through each heart cycle and over several heart cycles, each series is superimposed. The resulting series of images is then displayed cinematographically to show the contraction of the cardiac chambers. This is known as cardiac gated blood pool imaging and although it is used almost entirely to assess the function of the left ventricle (LV), the right ventricle (RV) and valvular problems known as regurgitation and incompetence, can also be assessed using this technique.

In both Thallium-201 perfusion and cardiac blood pool imaging the attraction of tomography has been the improved visualisation of the isotope distribution. Developments in Thallium-201 imaging and image processing techniques seek to provide images with greater contrast between ischaemic and non-ischaemic regions of the myocardium without increasing the rate of false positive response. Another objective is to specify the coronary arteries which are responsible for the ischaemia. Tomography is an attractive proposition to attain both of these objectives. Thallium-201 however, is a poor radioisotope for use in tomography due to the low energy of the emitted photons and the small amount of activity which can be administered. Both of these aspects result in a relatively small number of counts being acquired within a reasonable scanning time. Other imaging and processing developments have been, backjground subtraction, statistical algorithms and the ECG gating of image to remove blurring due to contraction of the LV. Background subtraction has not been reported as giving an overall improvement. Both Massie et al, (1981) and McKillop et al (1980) have reported that the rate of true positives detected, the sensitivity increased but the rate of true negatives detected, the specificity decreased with background subtraction. McKillop et al (1981) compared the interpretation of ECG gated and non ECG gated Thallium-201 images for IHD detection. No significant advantages were demonstrated and sensitivity and specificity were about the same. Faris et al (1982) demonstrated an improvement in the true detection rate of positives and negatives by application of a statistical algorithm. The predictive accuracy increased from 79% to 95%.

An analysis technique involving space and time quantitation of planar images has been developed in an attempt to improve the diagnostic capability of the test (Garcia et al, 1981; Berger et al, 1981). Berger showed an improvement in sensitivity from 83% to 90%.

Results comparing the use of emission computed tomography (ECT) with planar imaging in Thallium scanning have been reported by several authors (Kirch et al, 1978; Ritchie et al, 1981; Rizi et al, 1981; Tamaki et al, 1981; Maublant et al, 1982; Prigent et al, 1983). These studies involved the 7-pinhole collimator LECT and rotating head ECT systems. An improvement in sensitivity was demonstrated in IHD detection by Rizi et al, (1981) using a 7-pinhole system. The sensitivity was improved from 75% to 94% with the specificity remaining at 91%. Using a rotating head system, Tamaki et al (1981) reported an improvement in the diagnostic accuracy of infarct detection to 94% from 81% for planar imaging.

Maublant et al (1982) improved the sensitivity from 89% to 98% using a RHECT system, with specificity remaining the same at 93%.

The main goal of tomographic cardiac blood pool imaging is the assessment of the inferior/posterior wall of the LV. It has been demonstrated that gated planar images can be used to assess adequately the anterior, lateral and septal walls as well as the apex of the LV. The problem with planar imaging of the LV is that to view the motion of the infero-posterior wall the RV lies across and partially obscures this part of the LV wall, see Fig. 1.5. There are two planar viewing directions from which the infero-posterior wall is viewed tangentially. These are known as the right anterior oblique

Fig.1.5

RIGHT ANTERIOR OBLIQUE VIEW OF THE CARDIAC CHAMBERS SHOWING THE OVERLAP OF RIGHT VENTRICLE (RV) ON LEFT VENTRICLE (LV)

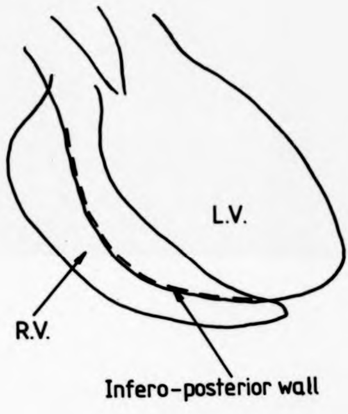

(RAO) and left posterior oblique (LPO) views. Both these viewing directions result in the overlap although the LPO view has the advantage that the LV is nearer to the camera and the radiation from it will suffer from less attenuation and scatter relative to that from the RV.

One technique which has been used to try and overcome the overlap problem is a first pass method. This involves imaging the passage of a pulse of radiotracer as it passes through the LV, a cinematographic image of the LV can be obtained. This technique suffers from two disadvantages. One is the count rate limit of Anger cameras with an accompanying loss of resolution. The other is the limited amount of activity which can be administered when an isotope like Technetium-99m is used resulting in a low number of counts being acquired in a scan. This limitation can be overcome by using the radioisotope ^{195m}Au (Elliot et al, 1983) which has a half-life of 18s and permits very high activities to be administered.

Tomographic cardiac gated blood pool (TCGBP) imaging is thus an attractive means of separating the right and left ventricles to permit the infero-posterior wall to be assessed. The clinical usefulness of TCGBP imaging is in its early stages of investigation and some early results have been published (Underwood et al, 1985; Barrat et al, 1984; Doherty et al, 1984). Underwood et al (1985) have shown good agreement between contrast ventriculography and TCGBP imaging. Doherty et al (1984) examined the parameters for data collection and reconstruction. The quantity of information required with RHECT poses a significant data handling problem for the reconstruction. Wall motion assessment and the measurement of ejection fraction with TCGBP scans is also being studied (Underwood et al, 1985 and Barat et al, 1984). The display of any tomographic images to present the three-dimensional distribution of activity in the most understandable form is a considerable problem. This is also the case for a contracting ventricle where the orientation of the LV in its presentation is also important. These studies have involved the use of RHECT systems. LECT systems also lend themselves to gated cardiac blood pool tomography, particularly multiple pinhole collimator types.

With Thallium-201 imaging, a problem for both RHECT and LECT systems is the poor count rate due to the low activity administered and low energy of the isotope. Both types of system require imaging times of the order of 15-20 minutes with a general purpose, medium sensitivity, medium resolution collimator. Multiple pinhole and quad slant hole collimator LECT systems offer an advantage over RHECT and rotating slant hole collimator LECT systems by acquiring images simultaneously. No movement is required between the camera and/or collimator with respect to the patient movement during the acquisition period. Also, the number of counts in each image will be consistent and in the event of an acquisition being terminated due to patient discomfort, gating or other clinical or technical problems, the images will have been consistently acquired. The limited angle LECT systems also acquire a small number of views, usually 6 to 12. Hence with LECT, the amount of data to be acquired and manipulated in the reconstruction is reduced compared to RHECT. A LECT system can be provided using a mobile Anger camera and so taken into an acute clinical environment: e.g. a coronary care unit. By contrast a RHECT system requires considerable rigidity in order to prevent image artefacts and so does not offer this flexibility. Patients are required to come to a RHECT system which for IHD assessment may be detrimental to the stress Thallium-201 test by introducing a delay between the injection of radiotracer and peak exercise and the start of imaging. These considerations point to LECT systems having potential advantages in the assessment of both myocardial perfusion and LV function.

1.9 Problems Associated with LECT

In the foregoing sections, the development of LECT and its current physical and clinical performance have been described. LECT is now an established radioisotope imaging technique particularly suited to cardiac imaging. As Lefree (1981) points out, the equipment is inexpensive to fabricate and most of it is common hardware found in a radioisotope imaging department. The small imaging and processing requirements also simplifies the technique compared to other radioisotope tomographic techniques such as RHECT.

A considerable amount of work has been undertaken to assess the clinical and physical performance of LECT systems. These studies have identified and in some studies attempted to explain, problems with LECT. A number of workers have documented what Williams (1980) described as an 'error propagation, of a residual forward and backward interaction from adjacent activity planes'. This same effect is described by Freedman, 1973, thus, 'information from above and below is distributed on an image and behaves as noise'. Koral (1984) refers to there being a 'well known' elongating distortion of an object in a direction perpendicular to the camera face'. None of these workers offer an explanation for this propogation or assess how significantly it affects tomograms. Lefree (1981) makes a vague reference to 'cones of revolution are missing in our sampling in the frequency domain'. This, he says, is due to a 'limited sampling angle' and the result is that 'a sheet source reconstructs ambiguously as a volume source'.

Lefrees (1981) comments about limited angular sampling are echoed by other workers. Koral (1984) states that 'sampling a 3-D volume over a solid angle less than 2π results in the elongation or propogation referred to above. Budinger (1980) also discusses 'limited angular range of sampling' and describes techniques to overcome it. Hasegawa (1982) suggests that 'some limitations of 7-pinhole tomography might be reduced by more complete angular sampling of the radionuclide distribution'. Hasegawa does not give a rationale for this and is not specific about which limitations might be reduced. He refers to another aspect discussed by Budinger (1980) regarding the criticality of patient positioning and suggests that it is made less critical by increased sampling.

Budinger (1980) discusses the dependence of object shape and the imaging orientation on the tomograms obtained. He demonstrates this on Thallium-201 tomograms obtained using a

7-pinhole collimator system. As what Budinger calls 'mispositioning' is increased, the tomograms exhibit an increasing amount of artefact until they are quite unrecognisable. Freedman (1973) discusses artefacts in tomograms more generally and suggests that the motion used to obtain the tomograms determine the type of 'information artefact' with a circular method offering 'complete blurring'. Hasegawa (1982) following on from Budingers mispositioning concept examines what he calls 'collimator misalignment artefacts' in Thallium-201 myocardial tomograms with 7 and 12 pinhole systems. He quantifies the false defects which are apparent in the tomograms and looks at the variation with misalignment. Ratib (1982) looks at the same artefacts with a rotating slant hole collimator LECT system and identifies inferior false defects in the reconstructed left ventricle. He explains these defects as being due to a 'partial volume effect' which he does not elucidate.

Of the many LECT system descriptions, none have presented a fundamental analysis of the LECT technique. Oldendorf in 1960 described the blurring effect which is obtained for out of interest activity by the selective motion between source and detector. Most other descriptions of tomogram generation by LECT has been basically this blurring of out of plane activity. Freedman (1973) discusses the selective addition of images displaced appropriately, leading to the intensification of data in the plane of interest. Kuhl and Edwards (1963) Lefree (1981) and Budinger (1980) use the extremely simplistic case of point sources to demonstrate the reconstruction technique and do not pursue larger volumes and identify the problems associated with them. Others, (Lefree, 1981; Kirch and Vogel, 1980) present LECT systems, describing the basic components, its physical performance and the reconstruction software. Lefree (1981) describes the collimator, the camera performance and acquisition parameters. Kirch and Vogel (1980) introduce the 7-pinhole collimator, describing it as fulfilling the 'notion' of viewing an object from several directions. These presentations lack a common aspect; a fundamental theory of how LECT reconstructs an object and from that how an optimum system can be designed.

However, Chiu et al, 1979 have shown theoretically that all 3-dimensional radiographic imaging systems can be treated by establishing a relationship between the measured projections and the 3-D Fourier transform of the object. They show that for imaging systems with a restricted angle of view (LECT), insufficient data will be collected to permit a complete generation of the fourier transform of the object. It is claimed by Chiu that this absent information or missing cones in fourier transform space merely degrades the resolution perpendicular to the camera face and that this is not disastrous for extended objects.

In Chapter 2 a theory of intersection of rays is considered and developed and a technique is established in Chapter 3 to allow systems to be assessed. In Chapter 3 the technique is used to optimise the design of a LECT system. The basis of this technique provides an explanation of how the backward and forward propagation arises. The effect of this on the overall reconstruction volume is demonstrated and the ideas of Lefree (1981) about 'sheet source reconstruction' and 'cones of revolution' are clarified. The technique is used to explain the improvement described by Hasegawa (1982) obtained by using a 12 pinhole collimator system rather than a 7 pinhole system for Thallium-201 myocardial imaging. Also in Chapter 3 it is demonstrated how increased sampling can be easily assessed to evaluate whether or not an improvement will be obtained.

In Chapter 4 and 5, assessment of the physical and clinical performance respectively of an actual rotating slant hole LECT system are described. A rotating slant hole LECT system is described in Chapter 4 and measurements to assess its physical performance are presented and compared with contemporary LECT systems. Chapter 5 examines how extensive false defects are in Thallium-201 myocardial tomograms. In a clinical trial, the presence of false defects are shown to have a significant effect on the diagnostic performance of the test. The origin and explanation of the defects is considered in Chapter 6. Experimental measurements are made using a left ventricle phantom and Hasegawa's (1982) finds are corroborated.

The problems to be encountered in gated blood pool tomography with LECT are considered in Chapter 7 and steps which can be takan to overcome them are examined.

CHAPTER

2

THE INTERSECTION OF BACK PROJECTED RAYS FOR LONGITUDINAL EMISSION COMPUTED TOMOGRAPHY

2.1 INTERSECTION OF RAYS FOR TOMOGRAPHY

The basic information available in all tomographic systems is a raysum, either of activity or attenuation, along a line of sight. Let this be $\sigma(l)$ where l represents a line of sight anywhere in space. For any 3-dimensional object with a distribution of activity or attenuation A (r,θ,ϕ), there will be an infinite number of raysums and associated lines of sight through that object. The entire set of raysums can be described by a function in r, θ and ϕ; each set of values of which represent a plane $\hat{p}$ which contains a raysum function continuous in r' and θ'; r' and θ' being parameters within that plane.

If a continuous function of raysums exists in a plane $\hat{p}$ then there is a unique solution to the activity or attenuation distribution A (r,θ,ϕ) within that plane, Bracewell, 1956. The continuous function in r, θ and ϕ represents all possible planes which may exist within the 3-dimensional distribution being studied.

The minimum number of planes and hence the minimum number of raysums required to reconstruct fully the distribution A (r,θ,ϕ), will be achieved when there is no redundancy of reconstructed information, i.e. when there is no overlap between planes. This can be expressed by saying that, for any chosen plane $\hat{p}_n$, any other plane $\hat{p}_m$ within the solution must not intersect $\hat{p}_n$ This means $\hat{p}_n$ and $\hat{p}_m$ must be parallel. Hence, the most efficient arrangement for acquiring the raysums to obtain a unique solution, is for all raysums to lie at right angles to a single direction. This arrangement is only found in a RHECT system where the planes are independent and may be reconstructed in isolation. Thus the ectomographic system of Dale et al, (1985) represents an inefficient use of a system which is inherently capable of rotating head tomographic performance.

In LECT, each viewing direction $\hat{d}_n$ of the camera acquires a set of raysums parallel, to $\hat{d}_n$. These raysums, when back projected, form a column of raysums with a cross-section equal to the view of the object in the direction $\hat{d}_n$. This column can be described by a set of parallel planes with direction at right angles of $\hat{d}_n$. Each plane which contains raysums has a projection of activity with a finite width, see Fig. 2.1. Let this be called a single projection plane set. This set will be just one of an infinite number of single projection plane sets S_n, each set having a direction perpendicular to $\hat{d}_n$.

Generally there are two routes to a unique reconstruction of the 3-dimensional activity distribution being imaged, See Fig. 2.2 The most efficient route, using a RHECT system is to acquire raysums which lie in a set of parallel planes. This is achieved by rotation of the camera about the object. The other route is to acquire all the possible raysums through the object. From these, an infinite number of parallel planed solutions can be obtained. All these

Fig. 2.1

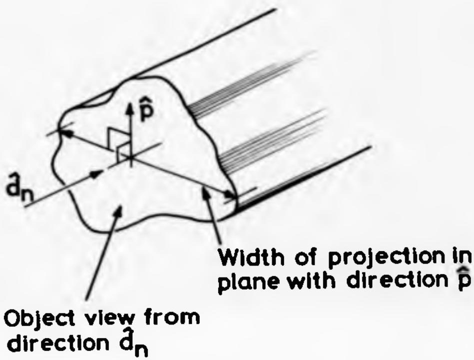

BACKPROJECTION OF AN OBJECT VIEW IN A DIRECTION $\hat{d}_n$ SHOWING TYPICAL ACTIVITY WIDTH

Fig. 2.2

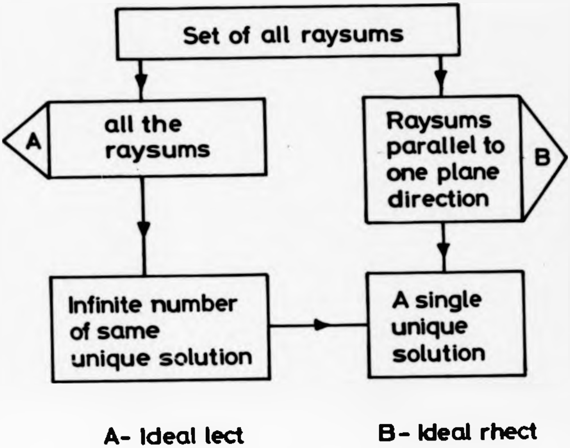

THE POSSIBLE ROUTES TO A UNIQUE RECONSTRUCTION OF A 3-DIMENSIONAL ACTIVITY DISTRIBUTION solutions would be unique reconstructions of the object and any one of them could be chosen.

Since no LECT system acquires an infinite number of raysums we cannot expect it to reconstruct the infinite number of planes which will provide a unique solution. If a LECT system has N different viewing directions $\hat{d}_1..\hat{d}_N$, then both the geometry and the distribution of activity within the object has to be approximated from the sets of single-projection planes, $S_1...S_N$, appropriate to the viewing directions. Consider a viewing direction $\hat{d}_n$ with the back projected column being represented by an infinite number of sets of single projection S_n, all at right angles to $\hat{d}_n$. If we now consider another viewing direction $\hat{d}_m$ it too will be represented by an infinite number of single-projection plane sets S_m at right angles to $\hat{d}_m$. Any reconstruction technique must use the combination of single projection plane sets.

The volume which will be described by the intersection of these two projections can be assessed by considering the set of planes from S_m and S_n which are parallel to $\hat{d}_n \wedge \hat{d}_m$. Let this be described as the common plane set for these two projections. For any complex object the common plane set from any two single-projection plane sets will contain a limited amount of information about the boundary of the object. In general, the predicted boundary will not represent exactly the shape of the object being viewed. The simplest aspect to be assessed is the difference between object and reconstruction shape which can exist wihin common plane sets. Further, the extent of the difference between the object volume and the overall reconstruction volume must be considered.

It should be emphasised that this analysis considers the geometry of the logical intersection between rays. The process of tomographic reconstruction actually involves arithmetic summation of data and the use of reconstruction algorithms. Nevertheless, we will show that the viewing geometry of a LECT system will generally indicate a difference between its outline of an object volume and the true object volume.

2.2 Interaction of Two Single-Projections

In an ideal imaging situation, with no activity outside the object and an ideal imaging system, a single projection in a direction $\hat{d}_n$ determines tangents to the object's surface in the direction $\hat{d}_n$. The combination, by back projection, of any two single projections $\hat{d}_n$ and $\hat{d}_m$ which satisfy $\hat{d}_n \wedge \hat{d}_m \neq 0$, will sweep out a volume which will contain the object, but only in the case where the object volume and the volume swept out are exactly coincident will this combination of the two projections be a unique reconstruction of the object volume boundary. The actual activity distribution which will be represented within that volume will depend on the algorithm used and this is discussed later. However, the fact that it may be possible for an object to give rise to a reconstruction volume which only represents the object boundary in directions at right angle to $\hat{d}_n$ and $\hat{d}_m$ indicates that the reconstructed activity distribution for most objects will extend into space outside the actual object volume.

Consider a direction $\hat{r}$; if $\hat{r}$ is at right angles to $\hat{d}_n$ then the object boundary in the direction $\hat{r}$ will be fixed. By comparison, for r parallel to $\hat{d}_n$ the projection $\hat{d}_n$ will provide no information about the object boundary in the direction $\hat{r}$. For $\hat{r}$ assuming any direction between these two extremes the information about the object boundary will be indeterminate, within limits which will depend on the angle between $\hat{r}$ and $\hat{d}_n$. This can be appreciated quantitatively by noting that the contribution from $\hat{d}_n$ to the boundary of the reconstruction, in a direction $\hat{r}$, decreases with the angle between $\hat{d}_n$ and $\hat{r}$. This is more usefully expressed as the contribution decreasing as $\hat{d}_n.\hat{r}$ increases.

For the combination of two viewing directions $\hat{d}_n$ and $\hat{d}_m$ the direction of $\hat{r}$ which will have the least contribution from both $\hat{d}_n$ and $\hat{d}_m$ will be the direction of greatest possible error between object and reconstruction volume boundary. We can express $\hat{r}$ in terms of $\hat{d}_n$ and $\hat{d}_m$ by

$$\hat{r} = a.\hat{d}_n + b.\hat{d}_m + c.\hat{d}_{nm} \qquad - 2.1$$

where $\hat{d}_{nm} = \hat{d}_n \wedge \hat{d}_m$ and a,b and c are constants, see Fig. 2.3

consider $\Gamma = \hat{d}_n.\hat{r} + \hat{d}_m.\hat{r} \qquad - 2.2$

$$\Gamma = \hat{d}_m. (a.\hat{d}_n + b.\hat{d}_m + c.\hat{d}_{nm})$$

$$\Gamma = (a + b)\ (1+\cos\theta) \qquad - 2.3$$

Where θ is the angle between $\hat{d}_n$ and $\hat{d}_m$

Since the comdonent c, of $\hat{r}$ in the direction $\hat{d}_{nm}$ makes no contribution to the value of Γ, it can be concluded by inspection that c must equal zero in order to maximise the value of Γ.

Fig. 2.3

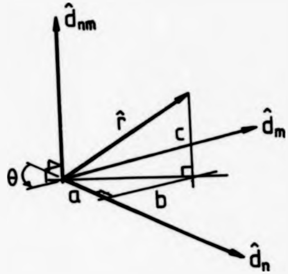

DIRECTION r IN RELATION TO d_n, d_m AND d_{nm} SHOWING ANGLE Θ AND COEFFICIENTS a, b and c.

With r a unit vector, we can then write

$$a^2 + b^2 = 1 \qquad - 2.4$$

This gives $b = (1 - a^2)^{1/2}$ $\qquad$ - 2.5

and $\Gamma = \left[a + (1 - a^2)^{1/2} \right] . (1 + \cos\theta)$

so $$\frac{d\Gamma}{da} = \left[1 - \frac{a}{(1 - a^2)^{1/2}} \right] . (1 + \cos\theta)$$

For a maximum value of Γ, $\frac{d\Gamma}{da} = 0$

$$\Rightarrow a = (1 - a^2)^{1/2}$$

$$\Rightarrow |a| = |b| \qquad - 2.6$$

Hence the direction of $\hat{r}$ which maximises the sum of the scalar products between $\hat{r}$ and $\hat{d}_n$ and $\hat{d}_m$ is such that $|a| = |b|$ and $c = 0$.

This shows that, for the combination of two single projections the maximum difference between object and reconstruction volume boundary will lie in the planes parallel to the direction $\hat{d}_{nm}$. Hence to assess the greatest error which will arise in the combination of two projections $\hat{d}_n$ and $\hat{d}_m$, the planes parallel to $\hat{d}_{nm}$ should be examined. Projections from a LECT system only have common plane sets for pairs of projections and so consideration of pairs of projections forms the basis on which to consider the error volume which will result in a LECT system reconstruction.

Within the reconstruction volume formed from the two projections $\hat{d}_n$ and $\hat{d}_m$, consider a single plane parallel to $\hat{d}_{nm}$. Let the widths of the projections be D_n and D_m and let the distance from their intersection to the viewing plane be R, Fig. 2.4a. When θ, the angle between the viewing directions tends to zero, $\hat{d}_n$ will tend towards $\hat{d}_m$ and no useful information about the object boundary is gained from the combination of these two views. The position of the camera relative to the object defines a limit to the boundary of the object in this case. When the angle betyeen the viewing directions is such that the views are separated, the limit to the object boundary is defined solely by the widths of the views D_n and D_m, and not the distance R to the intersection. When the views are not separated, as in Fig. 2.4b, there is an area of overlap as indicated. No overlap occurs if θ is greater than the value θ_c shown in Fig. 2.4a. This value of θ can be expressed in terms of R, D_n, and D_m.

Consider two intersection projections in a plane parallel to $\hat{d}_{nm}$, as shown in Fig. 2.5. The activity distribution in this plane which will give rise to these projections can be confined within a multitude of boundaries from the parallelogram formed from the intersecting widths, drawn in bold lines, to a single line of activity along either of the diagonals of the parallelogram.

The greatest difference between the area occupied by a reconstruction and the object, occurs if the object actually is a single line of activity. Realistically, the case for

Fig. 2.4

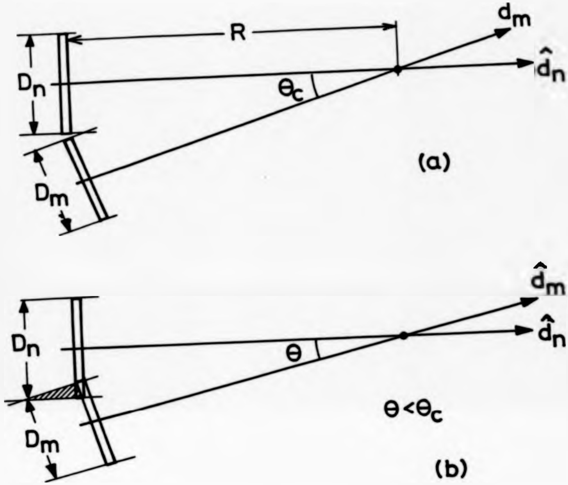

INTERSECTION OF TWO PROJECTIONS IN A COMMON PLANE FROM THE PLANE SET PARALLEL TO d_{mn}

Fig. 2.5

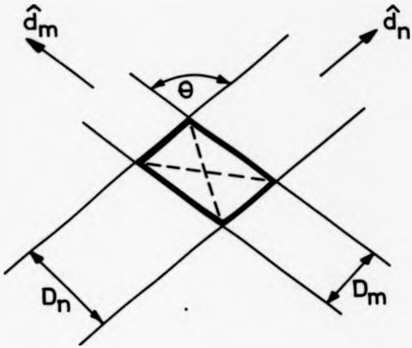

INTERSECTION OF TWO PROJECTION WIDTHS IN A PLANE PARALLEL TO $\hat{d}_{mn}$

which the true solution is a parallelogram will not arise clinically and need not be considered. The area of the parallelogram defined by the intersection of the projections gives a measure of the greatest difference between the object and reconstructed area. This area A is just

$$A = D_n D_m / \sin \theta \qquad - 2.7$$

For there to be no difference, this area needs to be zero, which will only be the case if D_n or D_m or both are zero and corresponds to an infinitesimally thin object. For a given D_n and D_m, θ may vary from θc to $\pi - \theta c$. However, we note that Dn and Dm can remain constant while varying θ, only for an object of circular cross-section in the plane of interest; in this case $D_n = D_m$. Since the widths which will arise for a variation in θ depend on the actual object shape, the value of θ which would give the minimum difference between object and reconstruction area cannot be found without prior knowledge of the object shape and hence area occupied in the plane of interest. Thus, we cannot generally specify an optimum viewing angle.

It is clear that only for an infinitesimally thin source such as a point source, a line source or a plane source in an orientation to the viewing system which results in either D_n or D_m being zero, will A be zero. Hence, only for these cases, which will not occur clinically, will a common plane set reconstruct the object volume precisely.

In practice tomographic reconstruction systems employ deconvolution techniques to modify projection data prior to back projection employing arithmetic summation in order to obtain an estimate of activity distribution. The boundary of an object must then be inferred from the reconstructed distribution of activity. The process of filtered back projection (or the equivalent Fourier deconvolution techniques) involves negative back projection values. Actual reconstructions may therefore have different boundaries from those indicated by the current analysis of intersections of back projected rays.

The limit of resolution of the imaging system will define the minimum thickness of an object which can be resolved. For any LECT viewing system an object with thickness equal to or less than the resolution of the system will have its volume shape reconstructed correctly by a common plane set, provided the object is one of the three types described above and is correctly orientated to the viewing system. Apart from these three objects and a parrallelogram shaped object, none of which occur clinically, a common plane set will not represent the object plane precisely. The volume which is generated will encompass the object and may be described as having an error volume for that common plane set.

In any situation where there are several viewing direction there will be more than one common plane set, each with its associated error volume. Combining these plane sets will result in an overall error volume for a given object and LECT system. The actual activity distribution predicted within the overall reconstruction volume will depend on the activity distribution in the object and reflected in the views acquired for the reconstruction.

CHAPTER 3

SYSTEM ASSESSMENT BY ERROR VOLUME INDEX

3.1 Assessing the Total Reconstruction Volume

The analysis in Chapter 2 has indicated that longitudinal emission computed tomography may not reconstruct a volume correctly and that in general the reconstruction volume may occupy regions which do not correspond to the object. To assess the way in which LECT systems will reconstruct an object incorrectly, it is useful to have some measure of the extent of the error volume.

In Chapter 2, Part 2, the direction $\hat{r}$ in which there was a maximum difference between each object and reconstruction area in a plane within the common plane set, resulting from views $\hat{d}_n$ and $\hat{d}_m$ was introduced. This used the scalar product of $\hat{r}$ with $\hat{d}_n$ and $\hat{d}_m$, it identified $\hat{r} = \hat{d}_n + \hat{d}_m$ and $\hat{r} = \hat{d}_n - \hat{d}_m$ as the maximum error directions. This concept for assessing the contributions made by tangents to the object in defining the object boundary in a chosen direction can be extended to the situation of N viewing directions. Each pair of viewing directions $\hat{d}_n$ and $\hat{d}_m$ will have a common plane set and two directions $\hat{d}_n + \hat{d}_m$ and $\hat{d}_n - \hat{d}_m$ in which there will be a maximum difference between object and reconstruction when only these two directions are used. In the combination of the two viewing directions considered previously the greatest difference between object and reconstructions area is for a line source, between the two points of intersection of the projections. Hence, the greatest difference between object and reconstruction volume will be for a plane source with a direction parallel to either of the two directions.

The actual extent of this difference between plane object and reconstruction volume depends on the angle between the direction of the plane and the viewing directions. Two extremes occur, if these directions are perpendicular there is no difference, while if they are parallel the difference becomes infinite and there is no information about the boundary of the plane in the direction of the plane. Hence, as the angle between the plane direction and the viewing direction increases, so the extent of the difference between plane object and reconstruction volume decreases. Thus, the extent of the error volume can be assessed from the scalar product of the maximum error volume direction and the viewing direction. Let this scalar product be called the error volume index (EVI). It will vary between zero and unity and the closer it is to zero, the smaller will be the error volume.

Although two maximum error volume directions result for each common plane set, the error volume in these directions will itself be reduced by the influence of the other common plane sets. If the EVI for all of the viewing directions can be calculated, with respect to each maximum error direction for all the common plane sets, then the smallest and largest EVI can be found and the appropriate directions identified. For a viewing system of N views the steps required are as follows:-

1) Calculate the $N!/(N-2)!$ maximum error volume directions
2) Calculate the $N(N!/(N-2)!)$ EVI for the system
3) Select the maximum EVI and the corresponding maximum error volume direction.

Thus, for any LECT system, a simple analysis can identify the direction in which the maximum difference exists between an actual plane object and its reconstruction volume. Furthermore, the EVI gives an indication of the magnitude of the reconstruction error volume which will occur. It should be noted that although the EVI gives a parameter for a particular system, in a practical application, the actual extent of the error volume will also depend on the dimensions of the plane.

3.2 Relation Between Maximum Error Volume and Reconstruction Volume

Any object can be considered as a summation of planes of activity with their directions all parallel to the direction of maximum EVI. The reconstruction volume can then be considered as the summation of the maximum error volumes for these planes. The resulting reconstruction volume will be the locus of the superimposed maximum error volumes and activity will be predicted to exist throughout this reconstructed volume even where it does not agree with the object volume. The maximum error volume for a single plane will be a double cone with an included angle $2.\cos^{-1}$ (EVI), with their bases coincident in the plane. Fig. 3.1 illustrates this for a circular plane object.

Of course, if the object shape was a double cone with an appropriate included angle, then there would be no error in the boundary of the reconstruction volume.

The superposition of maximum error volumes is demonstrated in Fig. 3.2 where a sphere is shown divided into a set of parallel planes. A reconstruction was made using the Iterative Least Squares Reconstruction Technique (ILSRT), Budinger and Gullberg, 1974. The reconstruction program was written in Fortran and its text is presented in Appendix 1. The routine reconstructs tomograms using data from a four position rotating slant hole 26.6° LECT system (QUAD 26.6°). Views on a 28 x 28 matrix are required for the program and simulated data for a solid sphere was generated.

Fig. 3.1

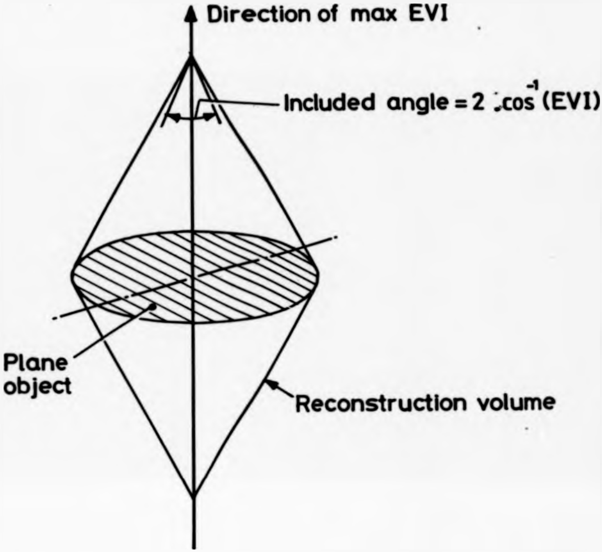

THE MAXIMUM ERROR VOLUME FOR A SINGLE CIRCULAR PLANE OBJECT

Fig. 3.2

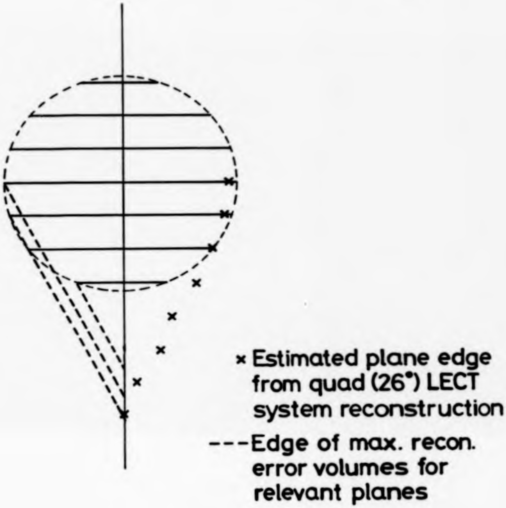

THE VOLUME BOUNDARIES FROM SUPERPOSITION OF MAXIMUM ERROR VOLUMES COMPARED TO AN ITERATIVE LEAST SQUARES RECONSTRUCTION FOR A SPHERICAL OBJECT AND A (26.6°) QUAD LECT SYSTEM

These noise free views were used to reconstruct a series of tomograms throughout the reconstruction volume.

Calculation of the EVI's for a particular set of viewing directions is straightforward and a program to do this for up to 15 different viewing directions is given in Appendix 2. For a QUAD (26.6°) LECT system the maximum EVI occurs along the axis of collimator rotation and indicates that the maximum error volume will occur for a plane orientated parallel to this axis and will be a double cone with included angle of 53°. Fig. 3.2 shows the resulting superposition of maximum error volumes for the planes of the sphere together with the reconstruction volume boundary predicted by the computer simulated reconstruction. The edges of the sphere tomograms were estimated by arbitrarily assuming a cut off of 1000 and interpolating to obtain the position of this cut off across a main axis of the tomograms.

Clinically, an organ can be considered as a summation of slices. Knowing the direction with the maximum EVI and its value, the extent of the error in the reconstruction volume can be gauged in relation to the organ's shape and size. Reductions in the extent of the overall error volume from reorientation of the imaging system can be appreciated simply using this technique. Thus, the most suitable orientation of the imaging system for a particular clinical application can be determined. On the other hand, the results from the clinical application of a system can be examined with respect to a known overall error volume generated by the system in that application.

3.3 Comparison of the Two Common LECT Systems

The most common LECT systems are of the multiple pinhole and slant hole collimator type. Fig. 3.3a and b define a coordinate system and unit vectors for the viewing directions in a 25° six-position rotating slant hole collimator and 25° 7-pinhole collimator respectively. Table 3.1 lists a selection of directions relative to the axes shown in Fig. 3.3 along with the EVI found by applying the above analysis. These are not, of course, the entire number of error directions derived from all the common plane sets, although they cover the range of EVI's for the systems. This shows that the maximum error volume is the same for the 7-pinhole and slant hole systems and occurs for the reconstruction of a planar object which has a direction parallel to the z-axis of Fig. 3.3. This is the axis of rotation of the collimator for the rotating slant hole system and perpendicular to the camera cystal in both cases. Reconstruction algorithms for such systems use this direction for the reconstructed planes. The shape of the maximum error volume for both system will be a double cone with bases coincident in the object plane and an included angle of 50°. The advantag of the 7-pinhole system compared with the slant hole system is illustrated by examining the other error direction EVI's. Table 3.1 shows that the additional view removes the error in the direction marked with an asterisk.

3.4 Optimisation of a Slant Hole Collimator System

Table 3.1 shows that, for a 25° slant hole collimator system, the majority of directions in the x-y plane have an associated error volume. Although it is not always as great as the maximum error volume for that system, object and reconstruction volume still differ significantly. By

Fig. 3.3

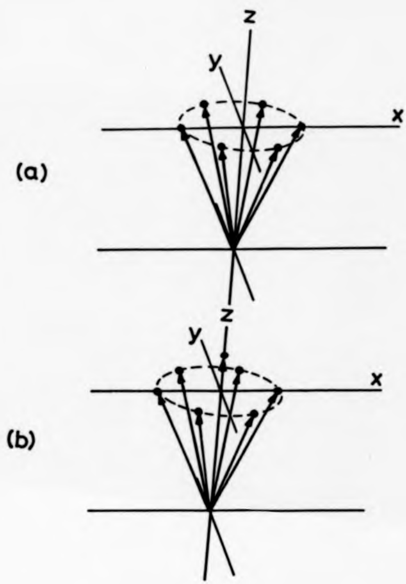

THE VIEWING DIRECTIONS FOR (a) A 25° SIX POSITION ROTATING SLANT HOLE COLLIMATOR SYSTEM AND (b) a 25° 7-PINHOLE COLLIMATOR SYSTEM, DEFINED WITH RESPECT TO A COORDINATE SYSTEM

TABLE 3.1

SYSTEM	DIRECTION			EVI
	x	y	z	
25° Hex rsh	324	.187	.927	.70
	.5	.866	0	.21*
	.113	.196	.973	.79
	.886	.5	0	0
	0	0	1	<u>.91</u>
25° 7-pinhole	324	.187	.927	.70
	.5	.866	0	0*
	.113	.196	.973	.79
	.866	.5	0	0
	0	0	1	<u>.91</u>

Comparison of EVI's for hex. rotating slant-hole and 7-pinhole systems. Maximum values underlined. Comparison of the entries marked * shows the effect of an additional view.

altering the slant-hole angle though, the EVI in these directions can be made equal to that in the z direction. When this is the case the reconstruction volume will differ from the object volume by the same amount in all of these directions.

The angle of the slant hole collimator was found at which the EVI in the z-direction equalled that in the x-y plane. This was taken to be the optimum collimator angle and this angle was found for an increasing number of views equally spaced through 360°. The variation of optimum collimator angle with number of views is shown in Fig. 3.4 and indicates that all the optimum collimator angles are greater than 45°. In practice, this would result in a very shallow viewing angle and consequently the depth at which activity could be detected would be small, even in the case of a large field of view camera where the typical field width is around 400 mm. For an optimum six position slant hole collimator on a standard field of view camera with field width of around 250 mm, the maximum depth is 57 mm which would not constitute a usable system.

3.5 Modification of LECT System by the Addition of Views

The addition of further viewing directions can be assessed easily by indentifying the maximum error direction and EVI. Koral et al. (1982, 1984) have demonstrated an improvement in the tomograms obtained from using a six position 25° slant hole collimator system, by rotating the actual camera though 90° and adding a further six views. Let this be called a double HEX LECT system. Table 3.2 lists the range of EVI's and their appropriate error directions for this system to allow comparison with the six position 25° slant hole values in Table 3.1. This shows that the direction of the maximum error volume alters, but more importantly the maximum EVI is greatly reduced compared with the single HEX system.

Fig. 3.4

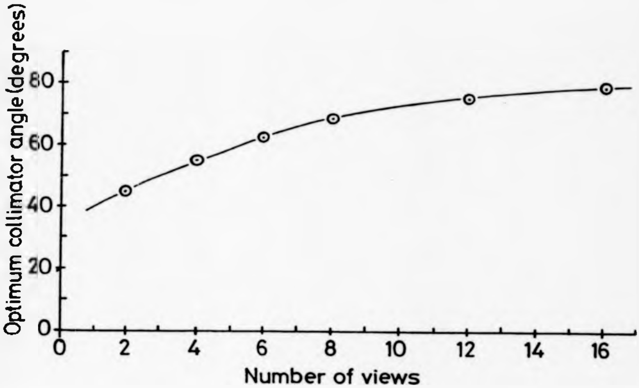

VARIATION OF OPTIMUM COLLIMATOR ANGLE WITH NUMBER OF VIEWS

TABLE 3.2

SYSTEM	DIRECTION			EVI
	x	y	z	
2 x 25° Hex	.324	.187	.927	.03
	.5	.866	0	.21
	.113	.196	.973	.13
	.551	.59	.59	.20
	0	.707	.707	.38
	.197	.843	.501	.10
	.134	.572	.807	.20
	.515	-.737	.438	.02
	.226	0	.973	.1
	.228	.688	.688	.32
	.483	-.619	.618	.23
	.292	.88	.373	.05
	0	0	1	0
25° Hex + 1	.324	.187	.927	.19
	.5	.866	0	.21
	.113	.196	.973	.20
	0	0	1	0
	.299	.707	.64	.26
	0	.374	.927	.37
	.127	.826	.548	.17
	.187	-.564	.804	.48

Range of EVI's and the corresponding error directions for double hex and hex + 1 LECT systems. Maximum values underlined.

A simpler view addition, involving less computing and data acquisition, is to add a single planar view with the camera rotated through 90°; let this be known as HEX + 1 LECT system and Table 3.2 also lists the error directions and EVI's for it. Although the directions of maximum error volume is again altered, the EVI is greatly reduced, though not quite to the level of the double HEX system. The benefit of using the HEX + 1 system as opposed to the double HEX system is that only one additional view is required.

To demonstrate this comparison, a reconstruction of a sphere was simulated using noise free projection data which was used in the program given in Appendix 1. The iterative least squares reconstruction technique (ILSRT) of Budinger and Gullberg was again used and along with the reconstruction program given in Appendix 1 for a QUAD (26.6°) LECT system two other reconstruction programs were used. These are given in Appendix 3 and 4 for a QUAD + 1 LECT and a double QUAD LECT system respectively. For the QUAD + 1 system, an additional simulated planar view is required. Fig. 3.5 shows the predicted activity profiles across the centre of the tomograms. These are shown for the basic QUAD system, a QUAD + 1 system and a double QUAD system and for comparison, the ideal distribution is also shown. For the three systems the error directions and EVI's are listed in Table 3.3. The choice of a sphere provides a simple, symmetrical object for reconstruction. The profiles for the QUAD system demonstrate the error volume projection in the z-axis direction of Fig. 3.6a. This corresponds to the max error volume direction with EVI of 0.893 listed in Table 3.3 for this system. The other two system profiles show how the error volume is greatly reduced for these systems.

THE PREDICTED ACTIVITY PROFILES ACROSS THE CENTRE OF THE TOMOGRAMS FROM QUAD, QUAD + 1 AND DOUBLE QUAD LECT SYSTEMS RECONSTRUCTING A SPHERICAL OBJECT. Fig. 3.5

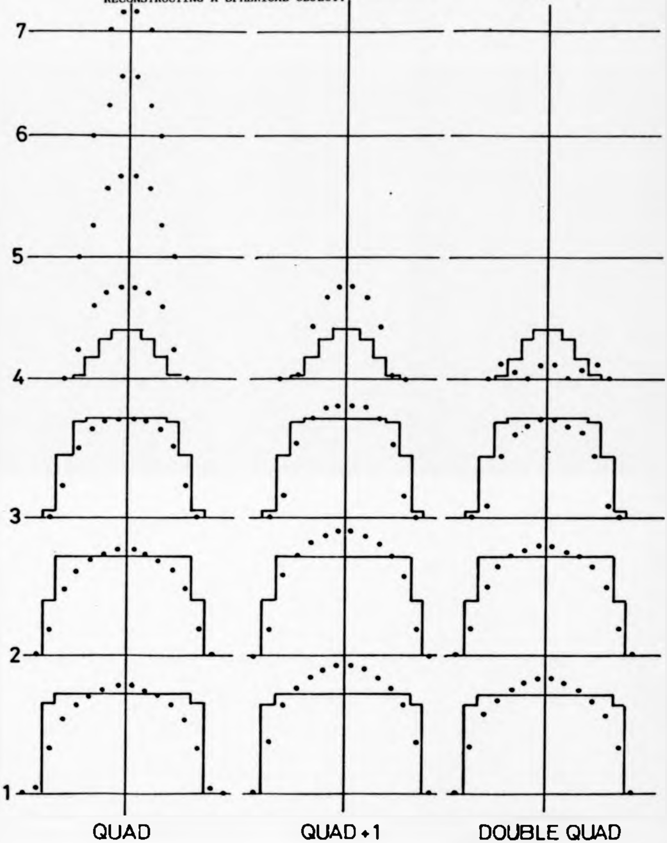

TABLE 3.3

SYSTEM	DIRECTION			EVI
	x	y	z	
26.6° quad rsh	.236 .707 0 1	.236 -.707 0 0	.924 0 1 0	.74 .12 .89 0
26.6 quad + 1	.236 .707 0 .85 .707	.236 -.707 0 0 .316	.924 0 1 .525 .632	.24 12 0 .53 .25
double quad	.236 .707 0 .236 .578 0 .267 .409 0	.236 -.707 0 -.236 .576 .711 .534 -.817 .948	.942 0 1 .942 .576 .703 .801 .407 .314	.11 .32 0 .11 .26 .31 .12 0 .14
26.6° quad + 2	.236 .707 0 .316	.236 -.707 0 .707	.942 0 1 .632	.24 .32 0 .25
1.5 x quad	.236 .707 0 .578 .267 -.41	.236 -.707 0 .576 .801 -.41	.942 0 1 .576 .534 .816	.11 .32 0 .26 .12 .18

Range of EVI's and the corresponding error directions for five different LECT systems, showing the effect of additional views. Maximum values underlined.

Fig. 3.6

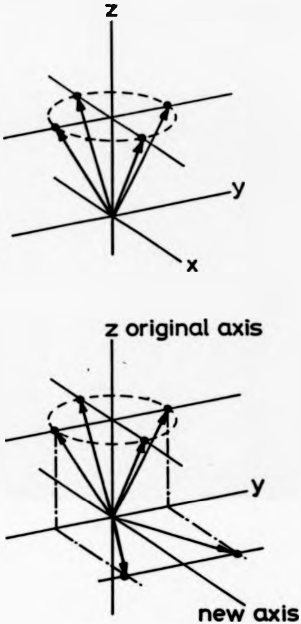

(a)

(b)

THE VIEWING DIRECTIONS FOR (a) A QUAD AND A (b) 1.5 QUAD LECT SYSTEM WITH RESPECT OF A COORDINATE SYSTEM

There are clinical situations in which there is a benefit in having to acquire only a small number of views. Fewer views mean less computing time and computer space. Additional views should be chosen such that the greatest improvement is obtained for the least number of views. This would suggest that a QUAD + 1 modification be chosen as opposed to a double QUAD. If a further planar view could be added with the camera displaced by 90° from both the original and first planar view direction, a QUAD + 2 system would result. Table 3.3 lists the direction and EVI's for this system also and shows that a maximum EVI equal to that for the double QUAD is obtained.

The major problem with the addition of such views would be the change of collimator and any consequent upset in patient positioning. This can be overcome by rotating the camera and using the slant-hole collimator, but with only two additional views, a 1.5 QUAD system. The choice of the additional views is important and this is shown in Fig. 3.6b. Table 3.3 lists the error directions and EVI's for this system and shows that the maximum EVI is the same as for the double QUAD system.

3.6 Increased Angular Sampling

It has also been suggested by Hasegawa et al, (1982) that a major problem in LECT lies with the limited angular sampling of LECT systems. For an increasing number of views with the same viewing angle, Table 3.4 shows that the maximum error volume direction and EVI remains the same and so the maximum error volume shape does not change. Thus the maximum error in the reconstruction volume will not be reduced by increasing the angular sampling in this way.

The conclusion of Hasegawa et al, (1982) that the increased sampling of a 12-pinhole collimator was responsible for

TABLE 3.4

SYSTEM	DIRECTION			EVI
	x	y	z	
4	.221	.221	.949	.77
	.707	-.707	0	.30
	0	0	1	.91
	1	0	0	0
8	.365	.151	.918	.68
	.383	-.924	0	.16
	.221	.221	.949	.73
	.067	.162	.984	.82
	0	0	1	.91
12	.396	.106	.911	.66
	.26	-.966	0	.11
	.324	.187	.927	.68
	.5	-.866	0	0
	.113	.196	.973	.79
	.031	.115	.992	.85
	0	0	1	0.91

Effect of increasing angular sampling, for a slant-hole collimator LECT system at constant viewing angle. Maximum values underlined.

a decrease in the degree to which a myocardial artefact was apparent in a phantom is true in that a decreased EVI results from the alteration in the angle of the views to accommodate the 12-pinhole collimator. From Hasegawa's figures the EVI would have been 0.796 for the 12-pinhole system compared with 0.884 for the 7-pinhole system. This would reduce the size of the maximum error volume and hence reduce the penetration between planes by an appropriate amount. Hence the improvement arises not from the increased number of views, but from the altered viewing angle of the additional views.

CHAPTER 4

DESCRIPTION AND PHYSICAL ASSESSMENT OF A ROTATING SLANT HOLE ECT SYSTEM

4.1 Description of System

The LECT system used for experimental work on phantoms and clinical trials in this research was based on a mobile standard field of view (SFOV), gamma camera. This is a type Sigma 420 gamma camera manufactured by the Technicare Corporation, Cleveland, U.S.A. The camera was designed for cardiac investigations, with a thin crystal suited to low energy isotopes and giving good resolution. It is designed primarily for standard planar imaging and adapted by the manufacturer to provide a complete LECT system.

The camera detector has 37 photomultiplier tubes coupled to a 337mm diameter NaI(Tl) scintillation crystal, 6.4mm thick. Manufacturers data about the camera performance is given in Table 4.1. The intrinsic resolution is 3.3mm FWHM and the resolution data for the range of collimators available is given in Fig. 4.1. The general, all purpose, parallel hole collimator was used for all planar imaging in this research. Energy window selection is assisted by a 128 channel multi-channel analyser. The pulse height analyser has a range from 44 to 220 KeV with a window variable between 0 and 100%. An autopeak facility tracks the required photopeak by sampling in two windows just above and just below the required energy. This maintains consistent centring on the photopeak througout the scanning period.

TABLE 4.1

Energy Resolution	13% at 140keV
Spacial Linearity	3.8mm across 248mm
Integral Uniformity	± 5% for Strip 8% of field width
Differential Uniformity	± 3% for any 17.8mm
	All above within useful FOV
Count Rate Capability	$200 . 10^3 S^{-1}$ at 100% window $150 . 10^3 S^{-1}$ at 50% window $100 . 10^3 S^{-1}$ at 20% window
Field Size	Hexagonal, 248mm across flats 286mm circumscribed circle
Intrinsic Resolution	3.3mm FWHM
Efficiency	
Tl-201	80keV, 98%
Tc-99m	140keV 70%

Technicare Sigma 420 SFOV Gamma Camera Performance Data.

Fig 4.1

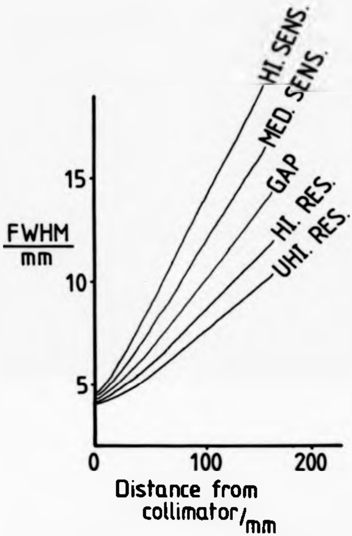

VARIATIONS IN RESOLUTION AS MEASURED USING FULL WIDTH HALF MAXIMUM (FWHM) FOR THE RANGE OF COLLIMATORS WHICH CAN BE USED WITH THE TECHNICARE (SFOV) GAMMA CAMERA

A micro-computer based on the 6800 microprocessor, forms an integral part of the system. This has two on board floppy disk drives for the system software for acquiring and processing data and also for the storage of image data. A LECT reconstruction program for use with a six position 25° rotating slant hole collimator is supplied by Technicare. The manufacturer also supplied the collimator which is a low energy, medium sensitivity type, similar to the GAP collimator for the planar imaging. It is of light construction and is manually oriented through the six viewing positions for the LECT acquisitions. Because of commercial interest Technicare would not permit the candidate access to the reconstruction software. However, the algorithm used is based on a least squares technique known as the Iterative Least Squares Reconstruction Technique (ILSRT) as described by Budinger et al, 1974.

4.2 Physical Assessment of a Rotating Slant Hole Collimator LECT System

In the next sections a comprehensive physical assessment of the system described in the previous section is presented. Measurements were made of the intra planar resolution, i.e. the resolution within a plane and of the inter planar resolution, ie. the resolution between planes. The position of reconstructed planes was correlated with the true plane position and a quantitative assessment of the reconstructed geometry was made. The sensitivity of the system and of the reconstruction was measured and lastly, the reconstruction of a uniform source was examined.

In X-ray transmission computed tomography, a single phantom which permits several parameters to be measured is used to assess the physical performance of a system (White et al, 1981). The concepts in this X-ray phantom were combined into a box phantom shown in Fig. 4.2. This consists of 1.0mm diameter tubing fixed diagonally across the faces and along the edges shown. Caps on the tube ends allow the tubing to be filled with a radioactive solution. In this design it was anticipated that several physical parameters could be assessed simultaneously.

The line sources along diagonally opposite edges provide a source to measure intra planar resolution. They also provide reference points in a tomogram for the assessment of reconstructed geometry. The sources diagonally placed across the box faces, when cut at different depths identify the depth of the tomogram and permit geometry to be assessed from the displacement from the reference point in the plane. These diagonals are arranged to be perpendicular to each other on opposite faces which allow the reconstructed plane thickness to be calculated from

$$s = (m_1 . m_2)^{\frac{1}{2}} \qquad - 4.1$$

where s is the plane thickness and m_1 and m_2 the FWHM of the diagonals in the tomograms. This relationship avoids error being introduced because of misalignment of the phantom to the camera. The reconstruction of the uniform object can also be examined by filling the box phantom with a uniform solution of activity. Hence, within the one phantom there exists the facility to measure and assess several physical parameters of a LECT system. The majority of measurements by other workers of inter and intra planar resolutions are made using point sources.

4.3 Calculation of the Full Width Half Maximum For Resolution Measurements

Quantitative assessment of resolution requires the measurement of the full width half maximum (FWHM) of a point

Fig. 4.2

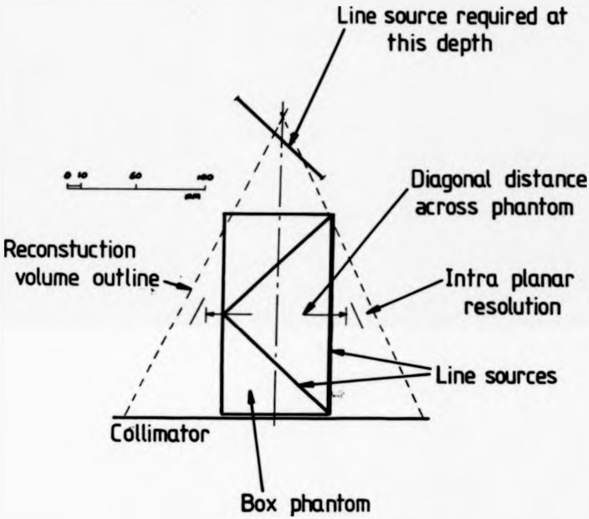

BOX PHANTOM SHOWN IN RELATION TO THE RECONSTRUCTION VOLUME OF A 25° LECT RSH SYSTEM or line source distribution in an image or tomogram. Radioisotope images are often noisy because of the low number of counts which can be acquired, or stored when a digital memory is available. Also, the limited space available in the computer memory can result in a coarse sampling of an object. With the Technicare Sigma 420 both these problems resulted in noisy acquisitions and reconstructions with a low sampling rate across a point source. The measurement of FWHM required considerable care in order to avoid wide variations in the results.

In this assessment of the Technicare system, the following technique was developed to calculate the FWHM of a point or line source distribution. Several profiles were obtained and each was given a single 3-point smooth. A spline interpolative fit was then made to each profile and from this curve the FWHM is calculated. A cubic spline interpolative curve fitting program was modified to find additionally, the maximum value of the curve and then the half maximum points were found using interpolation. Hence, the FWHM is computed.

4.4 Measurement of Inter and Intra Planar Resolution Using Line and Point Sources

The box phantom was imaged with the tubing filled with Technetium-99m in solution. The activity used was chosen to give an imaging countrate well within the Technicare systems capabilities. An energy window of $\pm$ 25% centred on the 140KeV total absorption peak was used. Tomograms were reconstructed over a depth between 15 and 65mm at 5mm intervals. Beyond 65mm it was impossible to seperate the line sources on the edges from those across the face of the phantom when interpreting the reconstructions.

Also, with increasing depth the edge of the phantom came so close to the edge of the reconstruction volume that the distance between the edges was less than the resolution of the system. This demonstrated a major fault in the phantom; its physical size severely limited the amount of the reconstruction volume which could be assessed.

Measurements of the FWHM were calculated over the usable range of depth for both intra planar resolution and plane thickness. The line sources in each tomogram provided four profiles for each measurement. These results are shown in Fig. 4.3 & 4.4. Also shown in these figures are measurements made using a point source. Besides the data provided by Technicare, point source measurements are shown which were made by the candidate for comparison with other LECT systems (Condon et al, 1983). These point sources were made by placing small spots of Technetium-99mm on chromatograph paper. The results in Fig. 4.4 show that the measurement of inter planar resolution using a point source gives a sufficient indication of plane thickness.

The problem of the relationship between box phantom and reconstruction volume is illustrated in Fig. 4.2. It shows that in order to measure the plane thickness at a depth close to the apex of the reconstruction volume, a line source which could not be imaged within the boundary of the reconstruction volume would be required. This contraindicates the use of the box phantom for resolution measurements, in favour of point sources which can be placed more extensively within the reconstruction volume.

Reusable point sources were fabricated as shown in Fig. 4.5 The small cavity in the screw can be filled with a plaster mix made with a radioisotope in solution. The reproducibility of sources is reasonable and plaster can be trimmed from

Fig. 4.3

VARIATION OF FWHM FOR INTRA-PLANAR RESOLUTION WITH DEPTH USING BOX PHANTOM ⊙ AND ALSO SHOWING MEASUREMENTS BY CONDON et al 1984 AND TECHNICARE

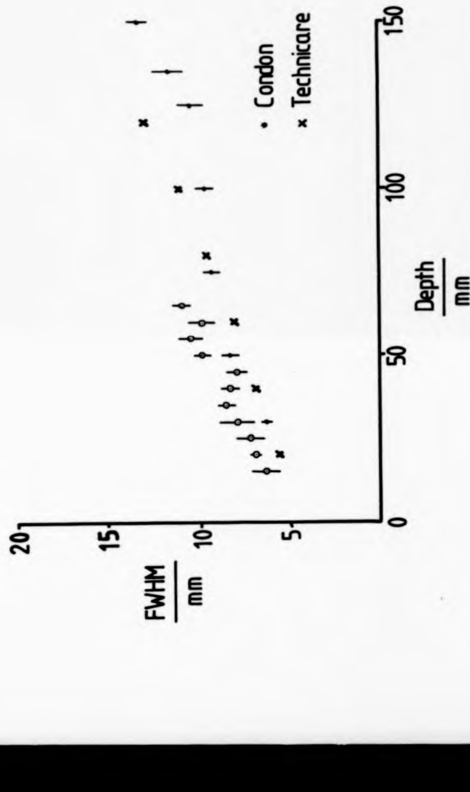

Fig. 4.4

VARIATION OF FWHM FOR INTER-PLANAR RESOLUTION WITH DEPTH USING BOX PHANTOM ⊙ AND ALSO SHOWING MEASUREMENTS BY CONDON et al 1984 AND TECHNICARE

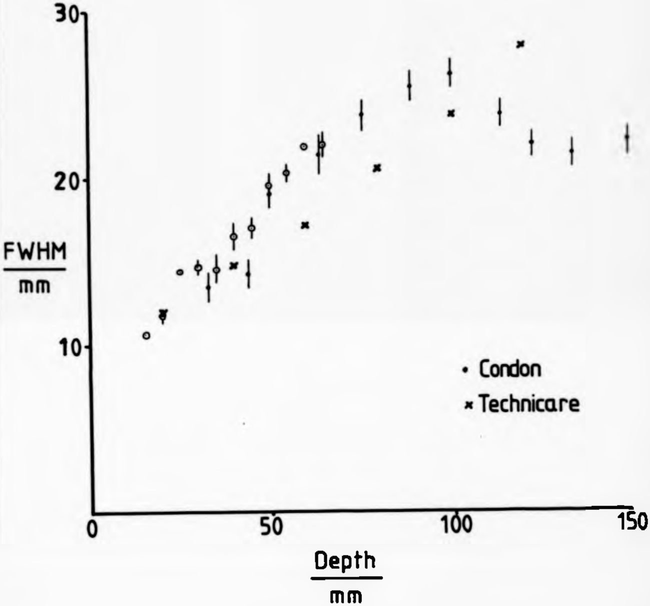

Fig. 4.5

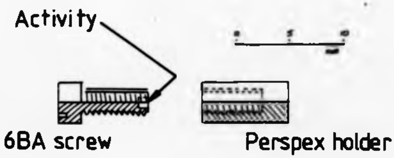

POINT SOURCES

Fig. 4.6

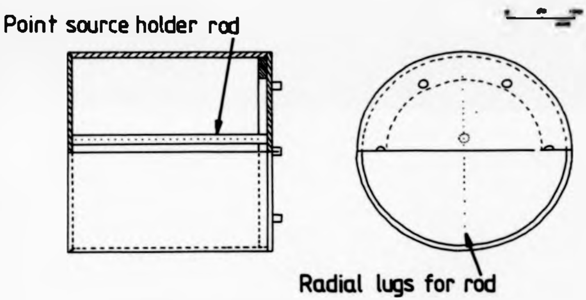

POINT SOURCE PHANTOM

the cavity to equate the activities. Table 4.2 shows the total counts obtained from the sources made on four separate occasions using Technetium-99m and counted in a simple scintillation well counter.

A drum was fabricated which can hold these point sources in any radial or axial configuration, (Fig. 4.6). The point sources can be placed at 10mm intervals along the rod which in turn can be placed radially within the drum over a range of positions. The base of the drum is as thin as possible in order to bring the drum as close as possible to the collimator. This phantom was designed to be applicable to rotating head ECT systems as well as LECT systems so allowing comparisons to be made between all ECT systems.

The air filled drum was supported on the Technicare LECT system so that the collimator was just clear of the base and could rotate. Point sources were imaged firstly at 15 and 20mm from the collimator. They were then placed at 10mm intervals up to a range of 190mm from the collimator. Up to 110mm, two sources were imaged simultaneously. These two sources were placed 60mm apart, each displaced 30mm from the centre of the drum. The drum was rotated by $\pi/2$ and another acquisition taken. This gave two acquisitions and 4 point source reconstructions for each axial position up to 110mm. Beyond this distance, it was impossible to obtain reasonable seperation between the source images and each point was imaged on the vertical axis. This again gave 4 point source reconstructions and as 2 orthogonal profiles can be obtained from each reconstruction, there were 8 profiles for each depth. The data from around 110mm was processed first to ensure there was no discontinuity due to the radial displacement of the sources. In all the reconstructions, two iterations were used. These initial results showed no significant discontinuity.

TABLE 4.2.

	TRIAL			
SOURCE	1	2	3	4
1	29387	35280	27258	25340
2	25445	34099	24902	30745
3	31102	35371	23075	27660
4	27789	34282	23498	30815

Record of counts obtained from point sources made using Tc-99m mixed with plaster.

From the 8 measurements of intra planar resolution and 4 of the inter planar resolution which were calculated, mean values of FWHM were obtained. These values are shown in Fig. 4.7. plotted against the distance from the collimator. These values are plotted up to a distance of 60mm. This was because the reconstruction program permitted a maximum of 12 reconstruction planes to be used. The reconstruction was performed using a plane separation of 5mm (plane density of $200m^{-1}$) and by a distance of 60mm the maximum span for measurement of the inter planar resolution had been reached. The significance of choosing a high plane density is discussed in Section 4.9.

4.5 Correspondence Between Actual and Reconstructed Plane Position

To assess the correspondence between actual and reconstructed plane position, the point source reconstructions described in Section 4.4 were used. It was assumed that the plane containing the maximum number of counts in the reconstruction corresponded to the centre of the point source. By identifying this plane, the reconstructed position of the point source was calculated. These results are shown in Fig. 4.8. Also given in Fig. 4.8 are point source measurements made by the candidate for a comparison with two 7-pinhole systems (Condon et al, 1983).

These results indicate that although there is a linear correlation over most of the distance studied there is an offset of approximately 20mm over most, if not all, of this distance. It is not clear what the reason for this is as the system was calibrated regularly with a point source set at a known, fixed distance from the camera. This calibration data was used to determine the position of planes within images during reconstruction.

Fig. 4.7

VARIATION OF INTER AND INTRA PLANAR RESOLUTION WITH DEPTH FROM COLLIMATOR, MEASURED BY FWHM OF RECONSTRUCTED POINT SOURCE FOR A 25° ROTATING SLANT HOLE LECT SYSTEM

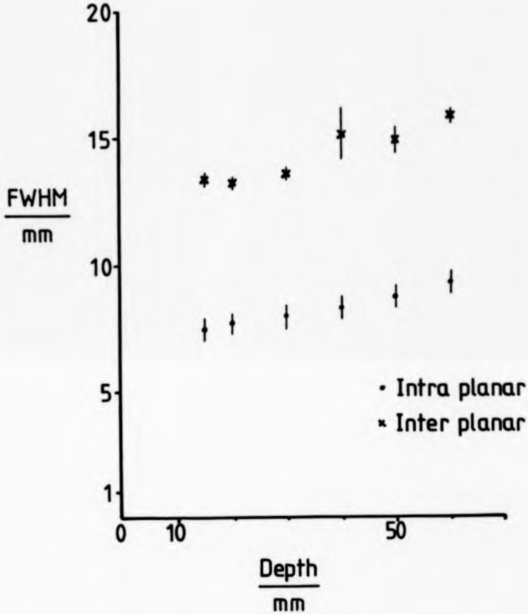

Fig. 4.8

VARIATION OF RECONSTRUCTED DEPTH WITH ACTUAL DEPTH OF POINT SOURCES

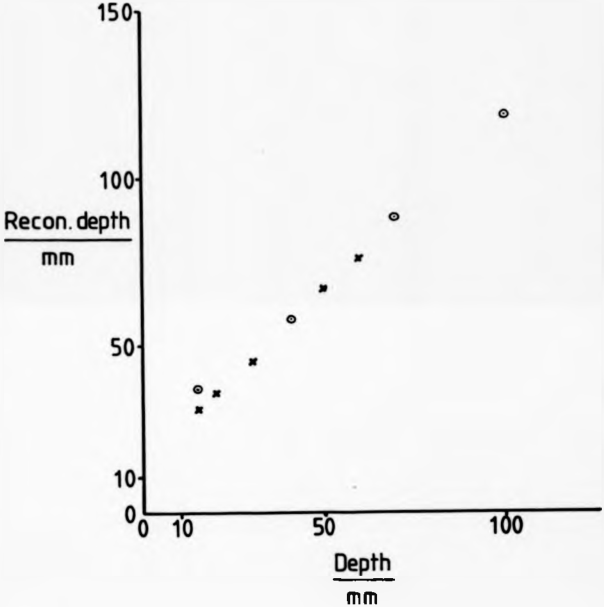

4.6 Assessment of the Geometry of the Reconstruction

The geometry of the reconstruction was assessed by examining the relationship between several point sources with known regular spacing. For this, the four radially displaced point source reconstructions described in Section 4.4 were used. These formed the regular array shown in Fig. 4.9. The position of the maximum value of the point spread functions at all the depths at which a reconstructed source had been made was recorded. From the layout of the sources in 4.9 it can be seen that the product of the intersecting gradients is -1. Table 4.3 presents for a source at 15mm, the value of the gradients and the product of the gradients. This shows that the relationship between the reconstructed sources has been maintained. In order to compare the other depths of the reconstructed sources with this, the positional data are plotted over the range 15 to 60mm, Fig. 4.10. The consistency of positions in the reconstructions with depth along with the maintenance of the relationship between the points at 15mm, as shown in Table 4.3 indicates that the geometry of reconstruction is satisfactory.

4.7 Measurement of Sensitivity of the System and of the Reconstruction

The sensitivity of the system, and of the reconstruction was measured by imaging a source of Technetium-99m at several depths from the collimator surface. The source was a 10ml Amersham vial filled so that the dimensions of the source were around 15 x 15mm. The measurements of sensitivity for the system as the source is moved away from the collimator is presented in Fig. 4.11. Since the solid angle subtended between source and collimator is altering, the sensitivity is expressed per unit of a solid angle. The variation in reconstructed sensitivity

Fig. 4.9

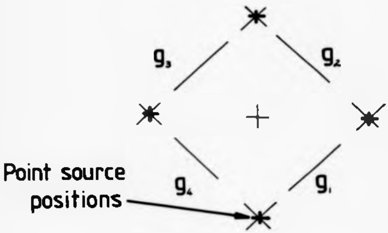

REGULAR ARRAY OF RADIALLY DISPLACED POINT SOURCES WITH INTERSECTING GRADIENTS FOR ASSESSMENT OF RECONSTRUCTION GEOMETRY

TABLE 4.3

g_1	g_2	g_3	g_4
1.0943	-0.9218	1.0157	-0.8858
$g_1 \cdot g_2$	$g_2 \cdot g_3$	$g_3 \cdot g_4$	$g_4 \cdot g_1$
-1.0087	-0.9362	-0.8994	-0.9690

Gradients and products of gradients to assess geometry. See Fig. 4.9.

Fig. 4.10

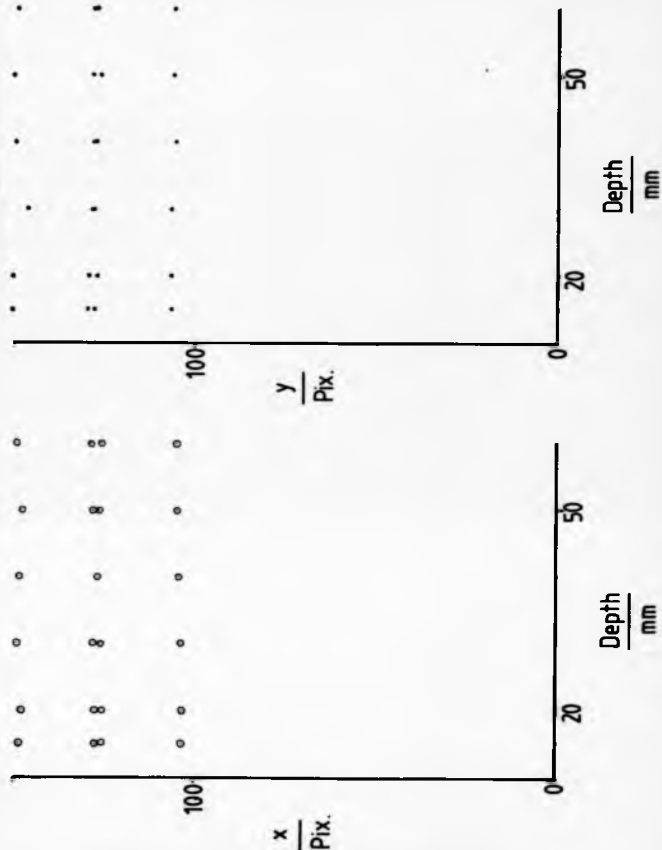

VARIATION OF POSITION OF POINT SOURCES IN RECONSTRUCTION WITH DEPTH

Fig. 4.11

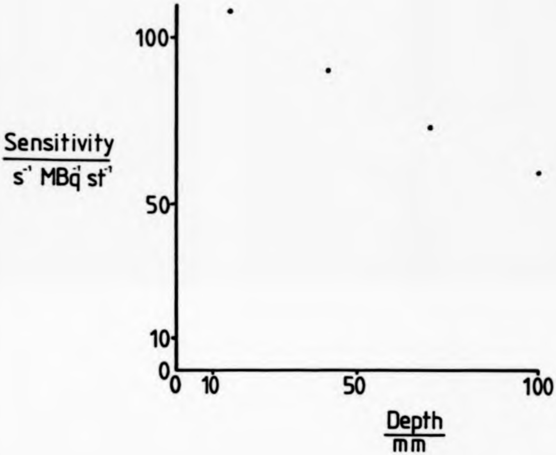

VARIATION OF SENSITIVITY OF SYSTEM WITH DEPTH is presented in Fig. 4.12 in terms of total counts per unit activity in imaged source. The reconstructions were made for the source using a combination of planes and number of iterations. The results show that there is no difference with the number of iterations, and the program iterates to the same limit of total number of counts at each depth. Furthermore, the reconstructed sensitivity appears to be almost constant with depth even though the sensitivity of the camera falls with depth. Since the sensitivity of the camera falls off, the total number of counts acquired for the images decreases with depth, Table 4.4. Since the only data which the reconstruction algorithm can iterate on is the total acquired counts, a correction for fall off must be introduced by an attenuation correction feature. This must correct the tomograms for depth in tissue after the tomograms have been computed. However, these measurements were made in air.

4.8 Uniformity

The uniformity of the reconstruction of the uniform source was assessed using the box phantom described in Section 4.2. The phantom was filled with a well mixed solution of Technetium-99m. Six images, each containing 400.10^3 counts were obtained using the 25° slant hole collimator. A 25% energy window centred on the 140KeV peak was used. Reconstruction was made using 2 iterations, 12 planes and with a plane separation of 15mm. The variation in reconstructed activity along the vertical axis of the reconstruction is shown in Fig. 4.13. Using this, the central plane was identified. Two smoothed transverse orthogonal profiles were taken and are shown in Fig. 4.14. It is clear from these that the reconstructed activity distribution is not uniform within the boundaries of the object, also marked on Fig. 4.14. The distribution demonstrates the penetration of activity from under and over-

Fig. 4.12

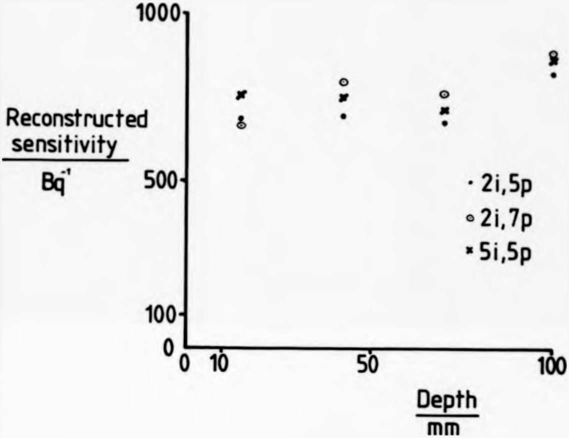

VARIATION OF RECONSTRUCTED SENSITIVITY WITH DEPTH FOR VARIOUS NUMBERS OF ITERATIONS (i) AND NUMBERS OF PLANES (p) USED IN THE RECONSTRUCTION

TABLE 4.4

Distance from Collimator mm	Total counts acquired in 4.s
15	15282
42	10825
70	7403
100	2959

Total number of counts acquired in 4 seconds for a source at increasing distance from the collimator.

VARIATION IN THE ACTIVITY ALONG THE CENTRAL AXIS OF THE RECONSTRUCTION OF A UNIFORM OBJECT

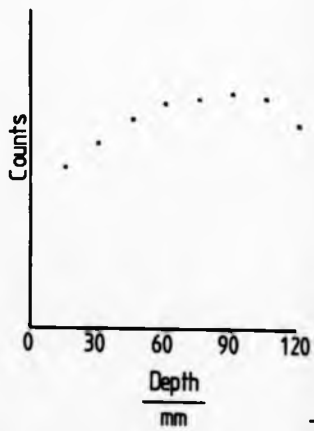

Fig. 4.13

TWO ORTHOGONAL TRANSVERSE SMOOTHED PROFILES THROUGH A TOMOGRAM OF THE RECONSTRUCTION OF A UNIFORM OBJECT

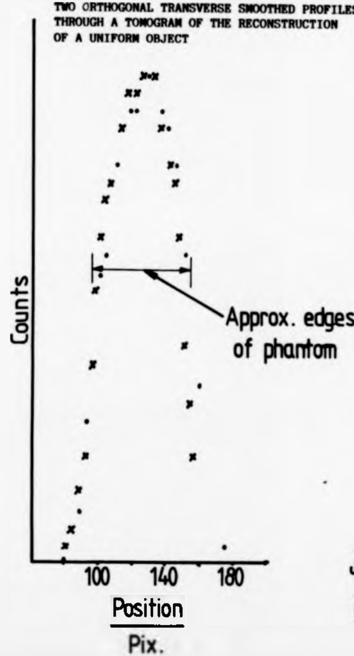

Fig. 4.14

lying planes giving rise to the peaking of activity in the centre of the profile.

4.9 Variation of Inter Planar Resolution with the Reconstruction Plane Frequency

The distribution of activity predicted within the planes in LECT can be shown to be dependent on the number of planes within the reconstruction. In any iterative reconstruction technique, the summations or raysums of the predicted activity are compared to the activity detected in the actual views. Corrections are made to the predicted plane activity to obtain reasonable agreement between the predicted raysums and the actual views. In this way, the entire viewed activity is distributed throughout the planes in the reconstruction. In the extreme case, that only one plane was chosen to exist within the reconstruction, all the activity in the views would be pushed into this plane by the algorithm. The number of planes is better referred to as the plane frequency (m^{-1}) and the inter planar resolution was shown to vary considerably with changes in plane frequency. Five point sources were placed in a regular array, Fig. 4.15, and imaged at distances from the collimator of 30 and 50mm using a 128 x 128 image matrix. The same array was also imaged at distances of 15, 30 and 60mm using a 64 x 64 image matrix. Reconstructions were made using 2 iterations for several different plane frequencies. The inter planar resolution was measured and the results are shown in Fig. 4.16 and 4.17. It can be seen that as the plane frequency increases, the inter planar resolution decreases towards a limit.

The reason for this variation lies in the fact that the iterative algorithm distributes the viewed activity throughout the planes available within the reconstruction. If

Fig. 4.15

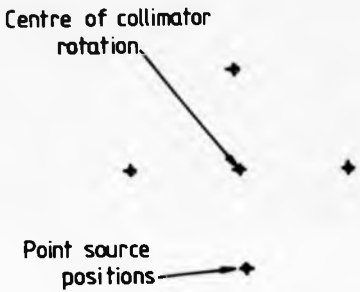

REGULAR ARRAY OF POINT SOURCES FOR RESOLUTION VERSUS PLANE FREQUENCY MEASUREMENTS

Fig. 4.16

VARIATION IN INTER-PLANAR RESOLUTION WITH RECONSTRUCTION PLANE FREQUENCY FOR A 64 x 64 IMAGE AND TOMOGRAM MATRIX

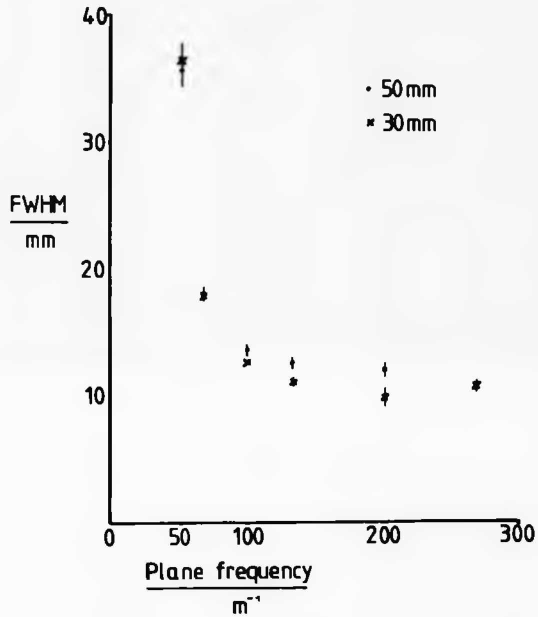

Fig. 4.17

VARIATION IN INTER-PLANAR RESOLUTION WITH RECONSTRUCTION PLANE FREQUENCY FOR A 128 x 128 IMAGE AND TOMOGRAM MATRIX

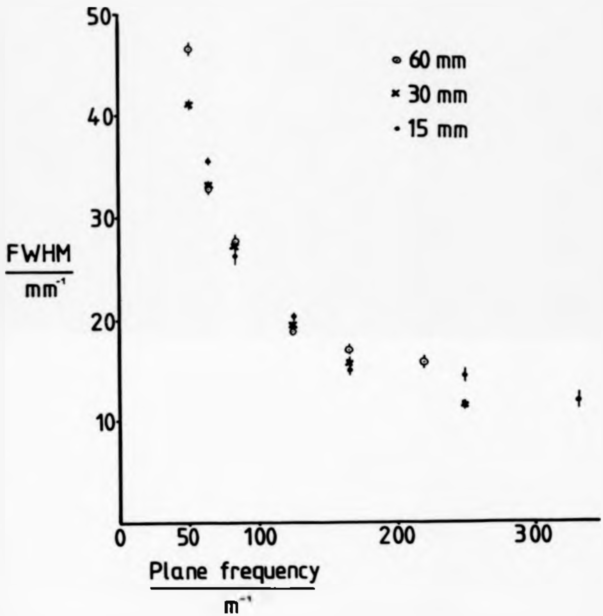

we assume an ideal viewing system with infinitesimally small image elements, then the image profile would be a continuous function. The initial prediction will use data from this profile and sample it at a frequency related to the chosen plane frequency. If the profile is assumed to be a normal distribution, then by dividing the distribution by equal intervals of increasing size, thus redistributing the area under the curve into fewer columns of activity, the effect on the full width half maximum of increasing the plane frequency can be demonstrated, Fig. 4.18.

To verify this effect on the Technicare system an acquisition of a single point source was made at a distance of 50mm from the collimator using a 128 x 128 image matrix. First approximations were made for three plane frequencies which gave coincident planes. Table 4.5 lists the resulting total counts in the appropriate planes and illustrates how the first activity prediction increases as the plane frequency decreases.

Another aspect affected by plane frequency is the predicted depth of a plane as determined by the maximum of activity. Fig. 4.19 shows for a 128 x 128 image and reconstruction matrix that as plane frequency increases, the predicted position of the plane decreases and improves. Although it does not attain the true position, the difference is minimised by a higher plane frequency. In the previous section, 4.5, the increased difference between predicted and actual position at increasing distance from the collimator may have resulted from the lower plane frequency necessary for the reconstruction at these distances.

This illustrates that the choice of plane frequency for reconstruction is important and should be chosen as high

Fig. 4.18

VARIATION IN MEASURED FWHM OF NORMAL DISTRIBUTION
WITH SAMPLING FREQUENCY

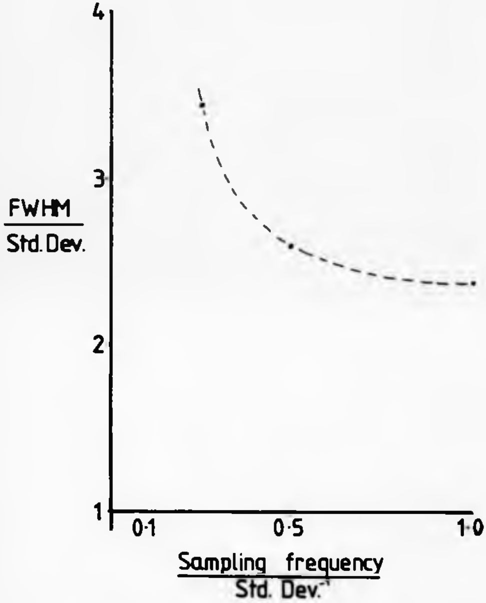

TABLE 4.5

PLANE FREQUENCY	RECON POSITION / mm								
	30	35	40	45	50	55	60	65	70
$200m^{-1}$	1	12	124	337	325	107	15	0	0
$100m^{-1}$	3		261		669		36		1
$50m^{-1}$	5				1013				1

Total counts in the planes of the reconstruction of a point source with varying reconstruction plane frequency.

Fig. 4.19

VARIATION IN RECONSTRUCTED DEPTH WITH PLANE FREQUENCY

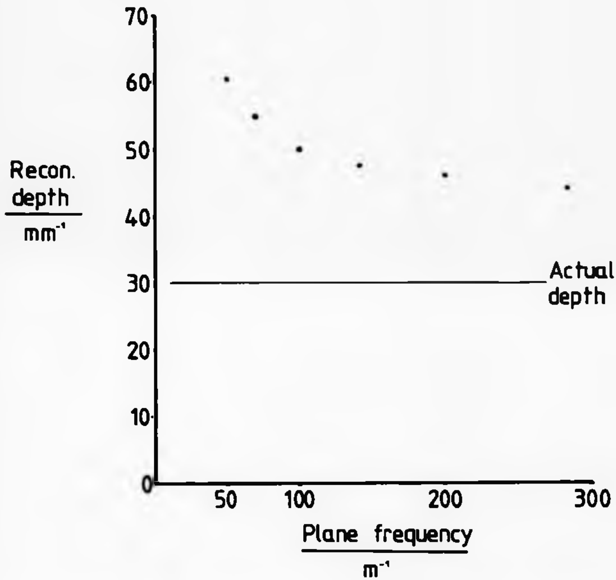

as possible within the scope of the reconstruction system being used. There is a limiting frequency which is related to the matrix size and the collimator angle and there is no point in going higher than this. Most LECT systems have a limited maximum number of planes and these can be distributed as required throughout the reconstruction volume. This distribution should be chosen so that the object is encompassed yet the plane frequency is maintained as high as possible.

4.10 Comparison of RSH Performance with Other LECT Systems

Inter and Intra planar resolution measurements have been published by several authors.

Measurements of this Technicare system were made by the candidate as part of a comparison with standard and large field of view 7-pinhole systems which was published in 1983 (Condon et al). Data from that comparison along with that from the manufacturers and other workers are presented in Figs. 4.20 to 4.21 Ratibs (1982) results for intra planar resolution are the only ones amongst the RSH measurements which show a difference. The RSHLECT system used by Ratib was a Technicare 420 Sigma, but a 0.9mm diameter Technetium-99m line source was used as opposed to a point source. The majority of measurements for the 7-pinhole systems agree Fig. 4.22 and Fig. 4.23 In the intra planar measurements, the differing results of Condon (1983) include scatter whereas all the results in agreement do not. The results by Condon without scatter suggest that scatter accounts for a slight difference in the intra planar resolution. However, the same effect is not apparent for the inter planar resolution where the inclusion of scatter makes no difference. Both of Condon's inter planar resolution measurements for the 7-pinhole system differ greatly from the measurements by other workers. A possible explanation, or contributing

Fig. 4.20

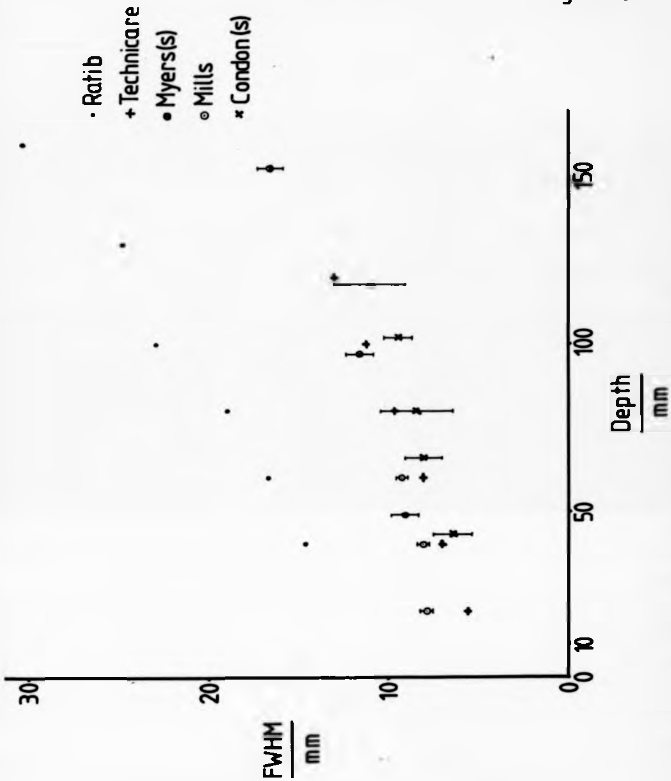

VARIATION OF INTRA PLANAR RESOLUTION AS MEASURED BY THE FULL WIDTH HALF MAXIMUM (FWHM) ON ROTATING SLANT HOLE LECT SYSTEMS ((s) INDICATES WITH SCATTER)

Fig. 4.21

VARIATION OF INTER PLANAR RESOLUTION AS MEASURED BY THE FULL WIDTH HALF MAXIMUM (FWHM) ON ROTATING SLANT HOLE LECT SYSTEMS ((s) INDICATES WITH SCATTER)

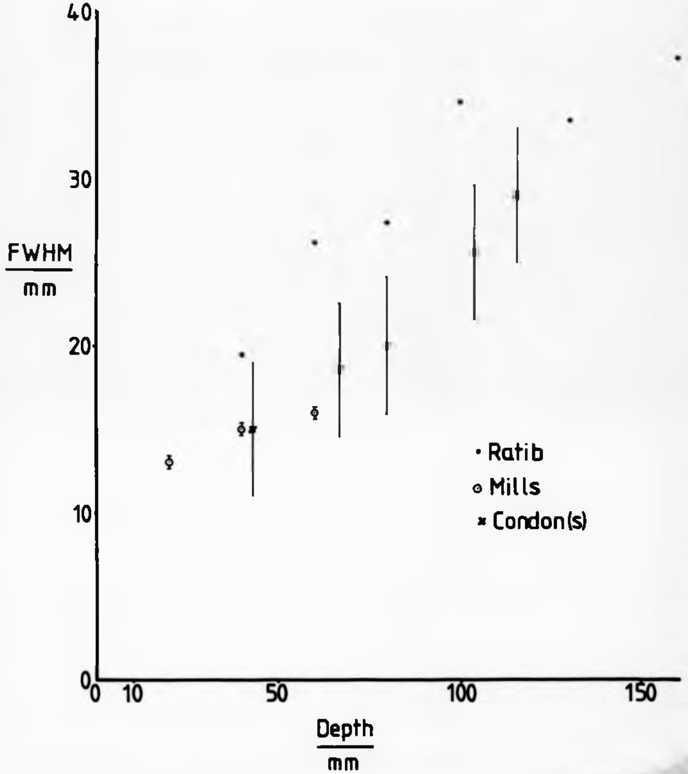

Fig. 4.22

VARIATION OF INTRA PLANAR RESOLUTION AS MEASURED BY THE FULL WIDTH HALF MAXIMUM (FWHM) ON 7-PINHOLE LECT SYSTEMS ((s) INDICATES WITH SCATTER)

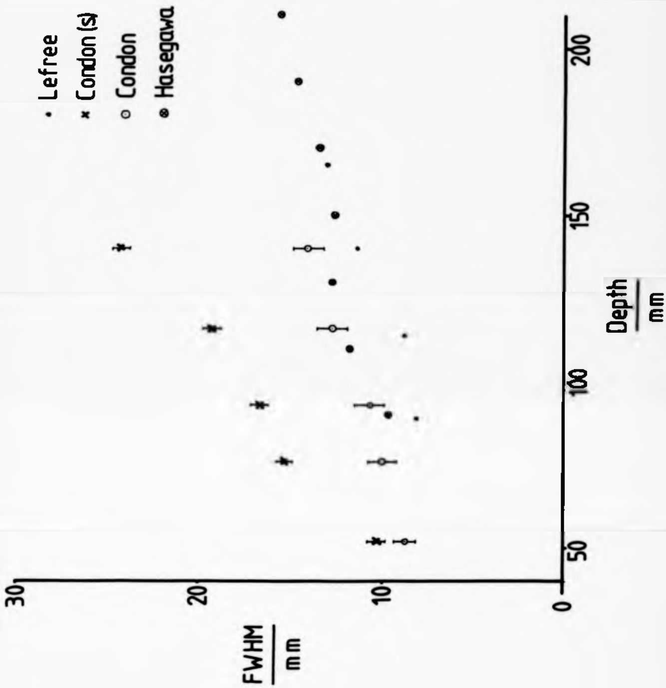

Fig. 4.23

VARIATION OF INTER PLANAR RESOLUTION AS MEASURED BY THE FULL WIDTH HALF MAXIMUM (FWHM) ON 7-PINHOLE LECT SYSTEMS ((s) INDICATES WITH SCATTER)

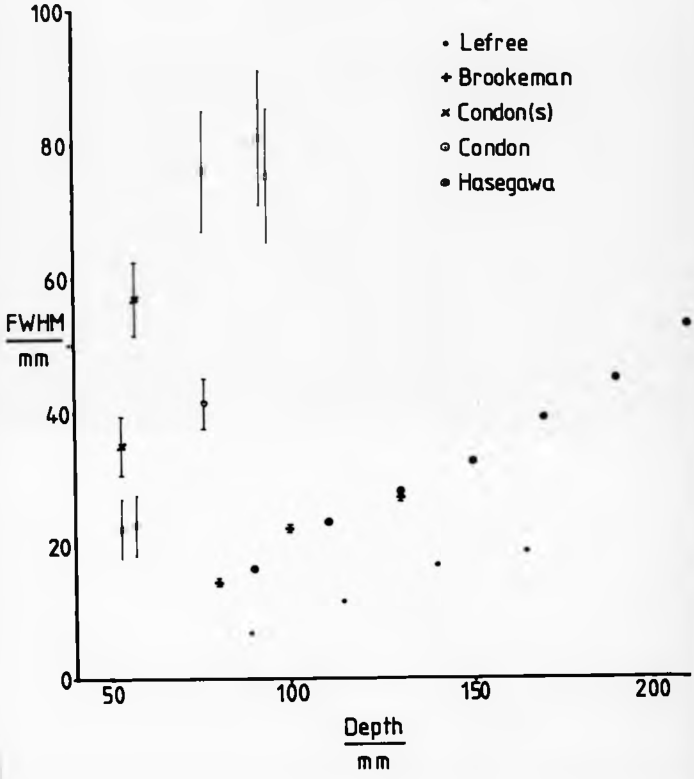

factor to the poor inter planar resolution suggested by Condon's measurements, may lie in the choice of plane frequency.

Both RSH and 7-pinhole systems have comparable intra planar resolution except when scatter is present. Then the RSH system performs better than the 7-pinhole. If the results of Condon for 7-pinhole inter planar resolution are set aside the results for both systems are comparable.

Uniformity measurements have been made by Brookeman (1981) on a 10cm cube of uniform activity distribution. These measurements demonstrated a uniformity variation both parallel and perpendicular to the camera face. Condon also assessed uniformity with a uniformily distributed active cube and found no significant variation in the uniformity of the reconstruction. The assessment described in Section 4.8 found a variation along both the central axis of the reconstruction, similar to that found by Brookeman and also across the central plane. There was no dip in the transverse activity profile, as was found by Brookeman for the 7-pinhole system. The variations in the transverse direction was very different from a uniform distribution, in contrast to the findings of Condon.

4.11 Conclusion

This Technicare RSHLECT system performs as well as other RSH and 7-pinhole LECT systems as assessed by inter and intra planar resolution. Reconstruction of a uniform source is unsatisfactory. There is a discrepancy between the positioning of an object and the actual position of the object reconstruction as demonstrated by point source measurements. This positioning is also affected by the plane frequency chosen for the reconstruction. Inter planar resolution is affected by the choice of plane frequency for reconstruction. The geometry of a reconstruction is a true reflection of the object geometry and no distortions were found to be generated. Plane frequency for reconstruction should be chosen to be as high as possible within the constraint of encompassing the object. With the Technicare system there is a possible maximum of 12 planes. The plane spacing should be chosen so that the object is just encompassed within these 12 planes. In this way, the highest plane frequency is used giving the best possible resolution and reconstructed plane positioning.

CHAPTER

5

CLINICAL TRIAL OF A ROTATING SLANT HOLE COLLIMATOR LECT SYSTEM FOR INFARCT DETECTION AND ISCHAEMIC HEART DISEASE DETECTION

5.1 The Basis for a Clinical Trial

The description of LECT developed previously has shown that in a reconstruction, activity may be predicted in a volume lying outside the imaged object. To what extent, if any, this error will affect the diagnostic performance of the technique can only be appreciated through a comparative clinical trial, using a standard technique as control. It is anticipated that in Thallium-201 perfusion imaging, tomography will show an improved diagnostic performance compared to standard planar imaging, due to the removal of overlying and underlying activity. In Chapter 3, Section 3, two common LECT systems were compared. One of these, a 6-position RSH LECT system, was assessed using the EVI technique to identify the maximum error volume. However, this analysis did not in itself give an indication of how this reconstruction error would affect the diagnostic performance of the system in its clinical application to cardiac perfusion imaging. The clinical trial to be described compares the diagnostic performance of planar imaging and RSHLECT imaging using Thallium-201 against angiography findings for ischaemic heart disease detection and ECG and enzyme criteria for infarct detection. The trial identifies the deficiencies of LECT in Thallium-201 imaging of the heart and their impact on diagnosis.

5.2 Materials and Methods

The Technicare RSHLECT system assessed in Chapter 4 is used in this study. The acquisition, processing and reconstruction were done using the standard Technicare facilities provided through the system computer. The useful field of view is 248mm and both the planar and rotating slant hole collimators were general all-purpose types. The slant hole angle was 25^{o} so that the reconstruction volume forms a cone as shown in Fig. 5.1. Thus, the size of the reconstruction volume is small in relation to most adult organs. However, with the camera head in the 45^{o} left anterior oblique (LAO 45^{o}) position, the left ventricle (LV) can be encompassed reasonably well, Fig. 5.1. Both the planar and tomographic views were taken on a 35% window centred on the 80KeV mercury X-Ray peak.

The tomographic reconstruction method used is the Iterative Least Squares Reconstruction Technique (ILSRT). This is appropriate for radioisotope imaging when there are a small number of views and the acquired data is noisy. (Budinger and Gullberg, 1974). Six views, each separated by 60^{o} are required for the reconstruction.

Three groups, comprising 29 patients with acute myocardial infarction, 20 patients being investigated for coronary artery disease and 10 normal volunteers, were studied with ethical approval. Those with acute infarction (23 men and 6

Fig. 5.1

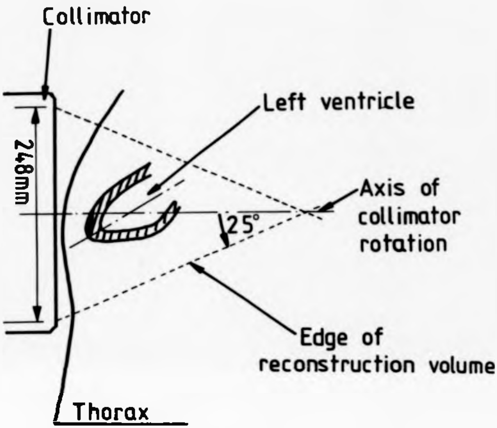

RELATIONSHIP BETWEEN RSHLECT SYSTEM RECONSTRUCTION VOLUME AND LEFT VENTRICLE WITH CAMERA IN THE LAO VIEWING POSITION women; age range 32-73 years, mean age 56 years) had rest Thallium-201 scans performed within 5 hours of the onset of symptoms of definite infarction, as shown by ECG and later enzyme criteria. Patients with other cardiac disease, apart from hypertension were excluded from the study. Stress and redistribution Thallium-201 scintigraphy was carried out on 20 patients (18 men and 2 women; age range 38 - 60 years; mean age 53 years) within six months of coronary arteriography. Five of the infarct patients were taking a diurectic at the time of the examination, but no cardiac drugs were administered. Among those investigated for ischaemic heart disease, five were on beta-blockade and two were taking a diureotic. Ten healthy male volunteers (age range 18 - 40; mean age 25 years) with no cardiac history, symptoms, signs or ECG abnormalities formally consented to have stress and redistribution Thallium-201 scintigraphy performed. 60MBq of Thallium-201 was administered intravenously to the patients and informed volunteers. This activity gave a whole body dose of 3.9mSv and a dose of 23.8mSv to the kidneys which was the critical organ. Infarct patients were injected supine and imaged in a coronary care unit. The other groups were injected erect in the stress laboratory. Planar images in the anterior (AP), LAO-45^{o} and left lateral (LLAT) positions were taken. Six tomographic views were also obtained in the LAO-45^{o} position.

Imaging started within 5 to 10 minutes after injection for stress testing and within 20 minutes for the rest scintigram in infarct patients. Acquisitions of 700,000 counts for each planar view took from between 6 and 10 minutes. Each tomographic view was acquired over 200 s, giving around 250,000 counts per view. The order of planar and tomographic imaging was reversed randomly to ensure that the effect of Thallium redistribution was spread throughout both planar and tomographic scans. The entire imaging session following stressing of the patient was completed within 45 minutes. Delayed images of myocardial redistribution were performed on exercise tested patients 4 hours after the stress testing. Both planar and tomographic views were recorded in a 128 x 128 format.

Patients being investigated for coronary artery disease and the normal group were exercised using a bicycle ergonometer. During exercise the workload was increased by 40W every 3 minutes. The V5 electrocardiogram lead and the blood pressure were monitored before each step up towards symptom-limited maximal exercise. Maximal exercise was maintained for at least 1 minute after the Thallium injection.

Coronary arteriography was performed on patients being investigated for coronary artery disease within 6 months of stress Thallium scintigraphy. A significant stenosis was defined as a reduction in coronary artery diameter equal to, or greater than 70% of the diameter. All arteriograms were reviewed independantly by two observers in ignorance of the scintigraphic findings. Particular attention was given to the site, severity and number of significant coronary stenoses and coronary occlusions and to the presence of collateral vessels.

The planar images were photographed from the computer video screen without any processing. For the tomographic reconstruction the maximum number of 12 planes allowed by the software was used. To encompass the left ventricle sufficiently, a plane separation of 8mm was chosen, giving a reconstruction depth of 88mm. The position of the first plane was chosen so that it appeared to coincide with the apex of the left ventricle. This technique gave the best encompassment of the left ventricle while maintaining reasonable inter-planar resolution. With stress and redistribution images, the position of the first plane in the redistribution scan was chosen to give the closest comparison between the two scans on a plane to plane basis. After reconstruction the images were normalised to the same maximum count and smoothed once.

Separate black and white photographs were made of each planar image while four tomographic planes were recorded on a single black and white photograph. Fig. 5.2 shows the corresponding planar and tomographic images for a normal scan. Four groups of images were presented to the observers in a random order: tomographic and planar infarcts and tomographic and planar ischaemic heart disease.

Two experienced observers viewed each group separately, the presentation order was then altered and the same two observers viewed each group a second time. This provided data for inter and intra observer variability

Fig. 5.2

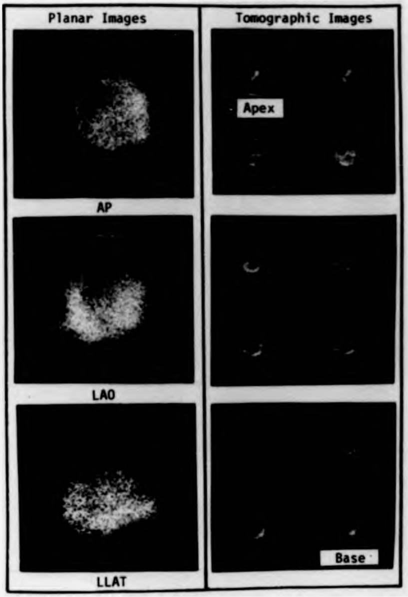

PLANAR AND TOMOGRAPHIC IMAGES FOR A NORMAL SCAN

For infarct detection observers were asked to indicate whether a scan was positive (i.e. defect present) or negative (defect not present). The observers responded either "definitely" or "probably"; and an equivocal response was also allowed. For ischaemic heart disease, as well as indicating the presence of ischaemia in the same manner, they were asked to give information about the number of vessels and the extent of the disease.

5.3 The Presence of False Myocardial Defects in the Tomographic Images of Normal Subjects

It has been demonstrated by Hasegawa et al, 1982 and Ratib et al, 1982, that, in pinhole and slant hole LECT of the myocardium, false defects can be introduced in a normal left ventricle, and in a left ventricular phantom. This occurs when the left ventricle axis is at an angle to the central axis of the reconstruction volume, as shown in Fig. 5.1. In the clinical situation it has been found to be impossible to eliminate entirely the angular separation between the axes of the left ventricle and the reconstruction volume. Fig. 5.3 shows two sets of tomograms of two normal left ventricles from this study. One set shows complete rings while the other shows a continuous break along the anterior surface of the reconstructed left ventricle. The extent of the false defect varies with the anatomical variation in the left ventricles orientation from patient to patient.

Since it was known that there would be false defects present in the tomographic images of normal subjects, Fig. 5.3, a pilot study to examine their influence on tomographic images for infarct detection, was conducted prior to the trial. The intention of this study was to see if observers could interpret the false defect phenomenon as such in a normal scan.

Fig.5.3

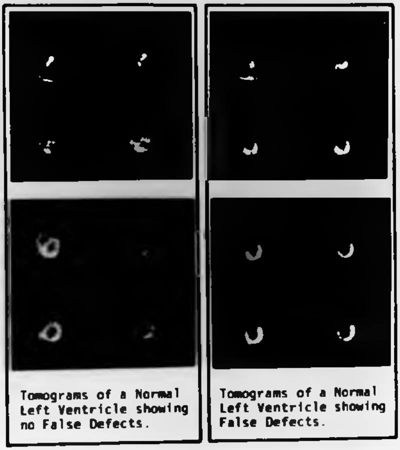

TOMOGRAMS OF TWO NORMAL VENTRICLES SHOWING THE FALSE DEFECT PHENOMENON

Two observors were presented with 30 planar and 30 tomographic scans from 23 of the patients with known infarcts and 7 normal volunteers (from the groups described above). The observers were asked to interpret the scans without making allowance for what they thought were false defects. Fig. 5.4 presents the resulting ROC analysis of these results, which are given in Table 5.1. This shows that the specificity improved greatly when the observers observed the false defects. Although this acknowledgement of a false defect may have led to an increase in false negatives, no decrease in sensitivity was demonstrated. It was concluded that observers could interpret the false defect phenomenon in a normal scan; it was identifiable as a smooth-edged discrete defect, continuous along the anterior wall of the reconstructed left ventricle. In the full trial for infarct detection and ischaemic heart disease, the observers were asked to interpret false defects as normal scans.

5.4 Results for Infarct Detection

The responses from both observers on each presentation were combined to obtain the tomographic and planar infarct detection results. Table 5.2 indicated the total responses in the various categories and Fig. 5.5 shows the resultant ROC analysis for these responses. To obtain an overall figure for sensitivity (fraction of true positive patients detected) and specificity (fraction of true negative patients detected), the equivocal scans were presented to the appropriate observers and they were asked to make a definite response. This gave an overall sensitivity, specificity and predictive accuracy (fraction of patients with correct diagnosis) of 96%, 95% and 96% respectively, for planars and of 93%, 80% and 89% respectively for tomograms.

The inter and intra observer variability was assessed by scoring the response range between +2 for definitely positive and -2 for definitely negative, with 0 as equivocal, i.e.

RECEIVER OPERATOR CHARACTERISTIC (ROC) CURVES FOR INFARCT DETECTION COMPARING PLANAR, RSHLECT AND (f) RSHLECT WITH ACKNOWLEDGEMENT OF THE FALSE DEFECTS

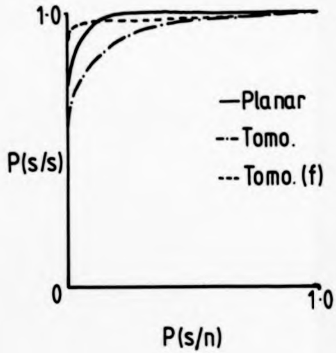

Fig. 5.4

ROC CURVES FOR INFARCT DETECTION

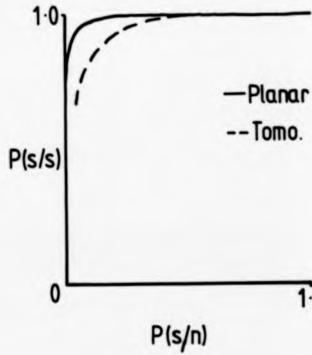

Fig. 5.5

TABLE 5.1

PRE-TRIAL RESPONSES FOR INFARCT DETECTION

	ACTUAL	+VE DEF	+VE PROB	EQU	-VE PROB	-VE DEF
PLANARS	+VE	33	10	2	1	0
	-VE	0	1	1	3	9
TOMOS	+VE	30	14	0	0	2
	-VE	0	4	0	6	4
	-VE AKFD	0	0	0	10	4

AKFD - Acknowledging False Defects

TABLE 5.2

	ACTUAL	+VE DEF	+VE PROB	EQUIV	-VE PROB	-VE DEF
PLANARS	+VE	73	38	0	5	0
	-VE	0	2	0	8	30
TOMOS	+VE	78	28	2	8	0
	-VE	2	5	1	18	14

Total Responses for Infarct Detection

a maximum absolute variation of 4. The variation in responses to the same image between observers on each presentation and between presentation for each observer, was assessed by examining the frequency of changes between 0 and 4. These are presented in Table 5.3. A change of greater than 2 was considered to be significant, and at this level both inter and intra observer variability was good, with agreement in over 95% of the responses.

5.5 Results for Ischaemic Heart Disease Detection

As with the infarct detection results, both observer's responses from each presentation were combined to obtain the ischaemic heart disease results for planar and tomographic imaging.

The group of 20 patients imaged had disease in one, two or three vessels; 13 in three vessels and 7 in one or two vessels, as diagnosed by arteriography. Table 5.4 presents the results from one observers interpretation of the number of vessles shown. This shows that neither tomographic nor planar imaging is a reliable way of obtaining adequate information on the number of vessels involved. This agrees with the results of other workers (McKillop et al, 1970, Rigo et al, 1980, Bodenheimer et al, 1980). No particular coronary artery gave more unreliable results than any other, and there was no improvement in the agreement when only arteries with a stenosis of 70% were considered.

The images were assessed by two observers for the presence of ischaemic heart disease as described above. Table 5.5 sets out the responses in the various categories. The resulting ROC analysis is presented in Fig. 5.6 to obtain an overall sensitivity and specificity figure for the technique each observer was asked to make a specific decision in place of their equivocal responses. This gave a sensitivity,

TABLE 5.3

Inter and Intra Variability for Infarct Detection Trial

		Δ	N	f		Δ	N	f
PLANARS	P1 01/02	0	22		01 P1/P2	0	28	
		1	14	95%		1	9	95%
		2	3	100%		2	2	100%
		3	0			3	0	
		4	0			4	0	
	P2 01/02	0	28		02 P1/P2	0	28	
		1	11	100%		1	10	95%
		2	0	100%		2	1	100%
		3	0			3	0	
		4	0			4	0	

		Δ	N	f		Δ	N	f
TOMOS	P1 01/02	0	19		01 P1/P2	0	31	
		1	16	85%		1	6	95%
		2	3	95%		2	1	85%
		3	1			3	1	
		4	0			4	0	
	P2 01/02	0	25		02 P1/P2	0	21	
		1	8	85%		1	11	80%
		2	4	95%		2	6	95%
		3	2			3	1	
		4	0			4	0	

KEY:
01 - Observer 1
02 - Observer 2
P1 - Presentation 1
P2 - Presentation 2

Δ - Absolute Change in Response
N - Number of Changes
f - The Fraction of Responses less than or equal to Δ

TABLE 5.4

		Agree	Disagree
Planars	To within 1 vessel	10	4
	Accurately	7	7
Tomos	To within 1 vessel	13	6
	Accurately	8	11

Relation Between One Observer's Interpretation of Number of Vessels Diseased and Arteriography Results.

TABLE 5.5

	Actual	+VE		Equiv	-VE	
		Def	Prob		Prob	Def
Planars	+ve	43	30	0	6	1
	-ve	0	4	0	16	20
Tomos	+ve	53	16	2	7	2
	-ve	2	4	5	20	9

Total Responses for Ischaemic Heart Disease

ROC CURVES FOR ISCHAEMIC HEART
DISEASE DETECTION

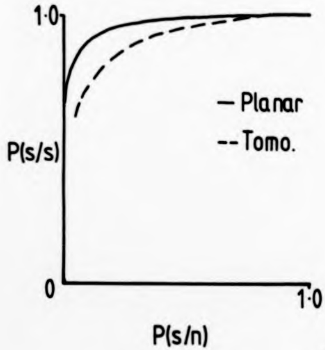

Fig. 5.6

POST SCAN PROBABILITY (P+p)
OF HAVING ISCHAEMIC HEART DISEASE
VERSUS PRIOR SCAN PROBABILITY P+
BASED ON TRIAL SENSITIVITY AND SPECIFICITY
FIGURES

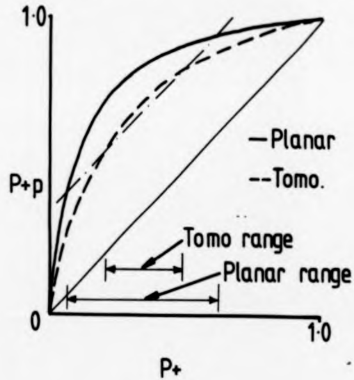

Fig. 5.7

specificity and predictive accuracy of 83%, 83% and 83% respectively for tomograms and of 91%, 90% and 91% respectively for planar images.

The inter and intra observer variability was assessed using the same scoring system as for infarct detection. The difference in responses for the same image between observers and between presentations for the same observer were assessed again using the criterion that an absolute change of 2 or less was acceptable. The frequency of changes are given in Table 5.6 and shows that inter and intra observer variability was acceptable in over 90% of the cases.

5.6 Discussion of the Results

The ROC curves for infarct detection show a clear difference between planar and tomographic images, (Fig. 5.5). The tomographic results being less sensitive or specific than the planar as shown by the displacement of the tomographic curve away from the axes. The results for the planar images were very good with an overall sensitivity of 96% and specificity of 95%. The overall figures for tomography of 93% and 80% respectively reflect a significant ($p < 0.02$) reduction in the sensitivity and specificity which was seen in the ROC curves.

It is concluded that for the detection of full transmural infarction no improvement is obtained from the use of rotating slant-hole tomography. The use of rotating slant hole tomography for the detection and assessment of non-transmural infarcts and for the estimation of infarct size remains to be examined. In these aspects it may prove to be a superior technique to planar imaging.

For ischaemic heart disease detection, a loss of sensitivity and specificity was demonstrated in the responses to tomographic images compared to the responses to the planar images. The

TABLE 5.6

Inter and Intra Variability for Ischaemic Heart Disease Dectection Trial

		Δ	N	f		Δ	N	f
PLANARS	P1 01/02	0	15		01 P1/P2	0	21	
		1	10	76%		1	12	100%
		2	6	94%		2	0	100%
		3	2			3	0	
		4	0			4	0	
	P2 01/02	0	14		02 P1/P2	0	17	
		1	14	82%		1	10	79%
		2	2	91%		2	5	97%
		3	3			3	1	
		4	0			4	0	

		Δ	N	f		Δ	N	f
TOMOS	P1 01/02	0	16		01 P1/P2	0	20	
		1	10	79%		1	12	97%
		2	4	91%		2	1	100%
		3	3			3	0	
		4	0			4	0	
	P2 01/02	0	17		02 P1/P2	0	19	
		1	13	91%		1	9	85%
		2	2	97%		2	3	94%
		3	1			3	2	
		4	0			4	0	

KEY: 01 - Observer 1
02 - Observer 2
P1 - Presentation 1
P2 - Presentation 2

Δ - Absolute Change in Response
N - Number of Changes
f - The Fraction of Responses less than or equal to Δ

ROC curves, Fig. 5.6 show this difference very clearly. The overall sensitivity and specificity for the tomograms, 83% and 83% respectively, and for the planars 91% and 90% reflect this significant reduction ($p<0.1$). Rotating slant hole tomography did not improve the diagnostic capability of the Thallium scan for the detection of ischaemic heart disease.

The effect of this reduction can be gauged using Bayesian analysis (Hamilton 1979, Murray et al, 1981). Fig. 5.7 shows a plot of post-scan probability of having ischaemic heart disease (P+p) plotted against the prior scan probability (P+). If an improvement in P+p of 35% is taken as a reference, then it can be seen that the range of patient groups to which the test is useful is reduced. With planar scanning, patients within a range of 0.55 of prior probability; between 0.07 and 0.62 would benefit from the scan. This is reduced to a range of 0.28 (from 0.2 to 0.48) with tomography: a sizeable reduction and it is concluded that rotating slant-hole tomography does not provide any improvement in Thallium scanning for the detection of ischaemic heart disease. Moreover, it involves much more time and effort than obtaining a simple planar image.

Several authors (Kirch et al, 1978; Ritchie et al, 1981; Rizi et al, 1981, Tamaki et al, 1981, Maublant et al, 1982; Prigent et al, 1983) have reported results of comparative studies between planar and tomographic Thallium imaging. These studies involved the 7 pinhole collimator and rotating head ECT systems. Some of these results along with the results from this study are given in Table 5.7. Rizi et al, (1981) using a 7 pinhole LECT system, demonstrated an improvement in sensitivity from 75% to 94% in ischaemic heart disease detection. Specificity remained the same at 91%. Using a rotating head system, Tamaki et al (1981) reported an improvement in diagnostic accuracy for infarct detection to 94% compared to 81% for planar imaging.

TABLE 5.7

MI Studies	Tomo sens	Tomo spec	System	Planar sens	Planar spec
Ritchie et al	83	71	7ph	80	93
Tamaki et al	93	68	7ph	75	89
	96	89	Rot. Head	75	89
Maublant et al	98	93	Rot. Head	89	93
Mills et al	93	80	RSH	96	95
IHD Studies					
Rizi et al	94	91	7ph	75	91
Mills et al	83	83	RSH	91	90

List of Other Published Results of Comparative Trials for Thallium-201 Scintigraphy.

Maublant et al, (1982) improved the sensitivity from 89% to 98% by using a rotating head system, with specificity remaining the same at 93%. The sensitivity and specificity results obtained from this comparative trial showed that rotating slant hole tomography was significantly worse than non-processed planar Thallium scintigraphy for the detection of both infarcts and ischaemic heart disease. This was not the general trend of the results shown in Table 5.7 from other comparative trials with tomography. This trial, however, obtained high values of sensitivity and specificity for planar scintigraphy, although the values lay well within the range of values obtained in other studies.

The general trend of high sensitivity and low specificity in the tomographic results (Table 5.7) suggests that contrast enhancement was having the same effect as has been shown for planar images (Massie et al, 1981; McKillop et al, 1980). Also, it appears that rotating head results are better in general than those for collimator tomography.

The improvement demonstrated by Rizi et al (1981) for detection of ischaemic heart disease with a 7 pinhole collimator LECT system has not been confirmed. Although studies with phantoms (Myers et al, 1983) suggested that both RHECT and LECT images would give an improved visulisation of contrast variations and hence improve ischaemic heart disease detection, no improvement has been demonstrated in this trial for a rotating slant hole LECT system.

5.7 The Influence on the Trial Results of False Myocardial Defects in the Tomograms of Normal Subjects

In order to examine the influence which the false defects had on the response of the observers, the normal group was divided into two sub-groups. One sub-group had tomograms which obviously contained false defects and the other had tomograms which did not.

The responses of both observers to the two presentations for these two groups were combined and are presented in Table 5.8 for infarct detection and in Table 5.9 for ischaemic heart disease detection. Visual examinations suggest that there is a difference in the response distribution for infarct detection, but not for ischaemic heart disease detection.

In an attempt to quantify the difference, a distribution was fitted to the responses for the sub-group with no false defects. To achieve this a Poisson distribution was used by attaching a value of 0-4 to the response (with 0 for definitely -ve) and calculating the mean response. Then the Poisson distribution for this mean value was used to generate an ideal response distribution. The X^2 test was then used to examine the goodness of fit of the response distribution to this ideal distribution.

For infarct detection there was a significant difference at the 5% level between the distribution of responses for false defects present and false defects not present. Table 5.8 presents the ideal response distribution and the X^2 values obtained for the goodness of fit X^2 test.

For ischaemic heart disease detection the difference between the sub-group was not so significant as for infarct detection, but p lay between 0.1 and 0.05. With infarct detection the false defects affected the response distribution by shifting responses away from definitely -ve, making the test less specific. With ischaemic heart disease detection, the presence of the false defects in both the stress and redistribution tomograms appeared to aid the observers in identifying these scans as normal and thus led to a significantly ($p<0.05$) better specificity with false defects present.

From this analysis it can be seen that the presence of false defects in the tomograms of normal subjects significantly affects

TABLE 5.8

	+ve			-ve	
	DEF	PROB	EQUIV	PROB	DEF
FALSE DEFECT NOT PRESENT	1			5	6
POISSON DIST. FIT, $X^2 = 0.514$	1.74			4.1	6.1
FALSE DEFECT PRESENT	7			13	8
POISSON DIST. PROJECTED TO 28 RESPONSES, $X^2 = 6.02$ N = 2	4			9.6	14

Distribution of Responses to Normal Scans With and Without False Defects in the Infarct Detection Trial.

TABLE 5.9

	+ve		Equiv	-ve	
	Def	Prob		Prob	Def
FALSE DEFECT NOT PRESENT	4		1	5	2
POISSON DIST. FIT, X^2 = 2.99 = 3	2.66		2.99	3.54	2.3
FALSE DEFECT PRESENT	3		4	14	7
POISSON DIST. PROJECTED TO 28 RESPONSES, X^2 = 7.38 n = 3	6.217		6.97	8.26	5.42

Distribution of Responses to Normal Scans With and Without False Defects in the Ischaemic Heart Detection Trial.

the responses of observers in interpreting the results. There is a decrease in the specificity of the test for infarct detection and an increase in specificity for ischaemic heart disease detection.

The effect on the diagnostic performance of the test if the phenomenon of false defects could be overcome in LECT can be estimated by using the ideal response distributions generated above. For infarct detection the resulting ROC curves are shown in Fig. 5.8. This shows that there would be no improvement in the diagnostic capability of Thallium-201 imaging compared to standard planar imaging.

Likewise, Fig. 5.9 shows the ROC curves anticipated for no false defects with ischaemic heart disease detection. This shows an even poorer performance for the technique than actually obtained.

ROC CURVES FOR INFARCT DETECTION SHOWING THE PROJECTED BENEFIT FROM THE ELIMINATION OF FALSE DEFECTS (p)

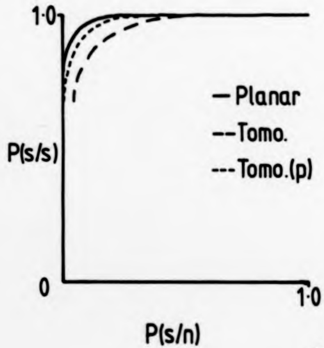

Fig. 5.8

ROC CURVES FOR ISCHAEMIC HEART DISEASE SHOWING PROJECTED DETERIORATION DUE TO ELIMINATION OF THE FALSE DEFECTS (p)

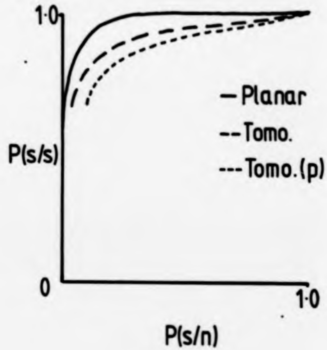

Fig. 5.9

CHAPTER

6

EXPERIMENTAL AND THEORETICAL ANALYSIS OF THE FALSE DEFECT PROBLEM IN THALLIUM-201 LEFT MYOCARDIAL IMAGING

6.1 Overview of the Problem

In imaging the heart with a RSHLECT system, the ideal tomograms would represent slices through the left ventricle (LV) at right angles to the axis of the LV. This would require the collimator to rotate about the axis of the LV. Fig. 6.1 shows that this would require a degree of tilt between the camera and the chest wall. This tilt pushes the LV up towards the apex and out of the reconstruction volume. To encompass the LV satisfactorily, the axis of the collimator rotation must be at some angle to the LV axis, Fig. 6.2. This angulation between the LV axis and axis of rotation results in false defects in the tomograms of normal subjects, Fig. 5.3. The trial described in Chapter 5 demonstrated that these false defects significantly affect the response of observers to the tomograms of normal subjects.

6.2 Left Ventricle Phantom

In order to examine the use of RSHLECT in cardiac imaging, a left ventricle (LV) phantom was designed and constructed. The phantom is basically two chambers with one sitting inside the other to form a wall, Fig. 6.3 and Fig. 6.4. Perspex defects can be inserted in the wall, along with a radioactive solution to simulate the uptake of activity in the myocardium. The phantom design is based on that by Williams et al, 1980, which although slightly oversized compared to an average left ventricle, has been used in other tomographic studies (Mueller et al, 1970; Gottschalk et al, undated). This design is more flexible, and easier to construct and use than the basic Williams et al, (1980) design.

Fig. 6.1

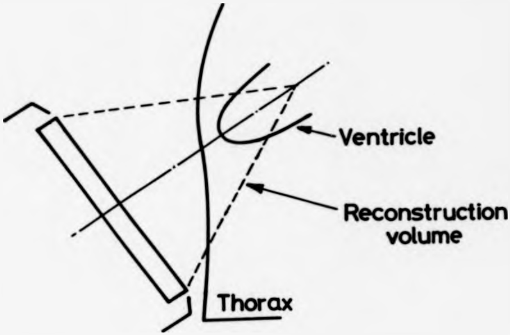

UNSATISFACTORY ENCOMPASSMENT OF THE LEFT VENTRICLE BY THE RECONSTRUCTION VOLUME

Fig. 6.2

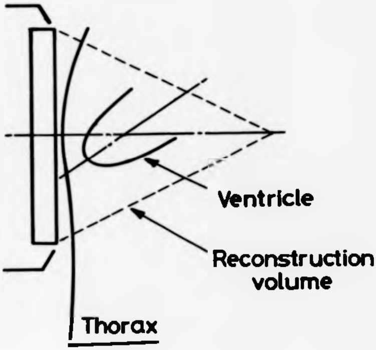

SATISFACTORY ENCOMPASSMENT OF THE LEFT VENTRICLE BY THE RECONSTRUCTION VOLUME

Fig. 6.3

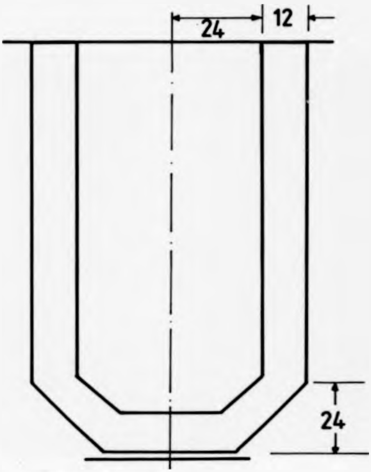

Dimensions in mm

LEFT VENTRICLE PHANTOM

Fig. 6.4

EXPLODED LEFT VENTRICLE PHANTOM WITH DEFECT IN PLACE

6.3 Quantitation of Defects in Tomograms

A consistent method is used to quantify defects throughout the study. Fig. 6.5 shows a set of tomograms from the LV phantom with a perspex defect in position. A radial plot of the count density around the annulus may be obtained for such tomograms and a typical plot is shown in Fig. 6.6(a) This is crudely smoothed to obtain a histogram plot shown in Fig. 6.6(b). From this plot a normal band is chosen and the mean and standard error calculated. A signal, or defect is taken as being present, if, using a t-test criteria there is a value different from that which reflected the 99% confidence limit. Each tomogram from a reconstruction is assessed to see if a variation in uniformity of the anulus is present. The variation in uniformity is quantified as the ratio of the lowest histogram value to the mean value. In choosing normal values some account is taken of the position of variations in adjacent tomograms.

6.4 Variation in Uniformity due to True Defects in LV Phantom

To gauge the significance of the false defects, the uniformity variation due to true defects was examined. Two defects were both imaged seperately at depths of 70mm and 100mm from the camera face. One defect was 12mm deep and the other 45mm deep and both occupied a section of ½ and Technetium-99m was the radioisotope used. The Technicare Sigma 420 RSHLECT system previously described, was used for acquiring and processing the images. The phantom was imaged with its axis at right angles to the camera face to ensure no false defects were introduced. Fig. 6.7 and 6.8 show the variation in uniformity for the 12mm and 45mm defect respectively.

Fig. 6.5

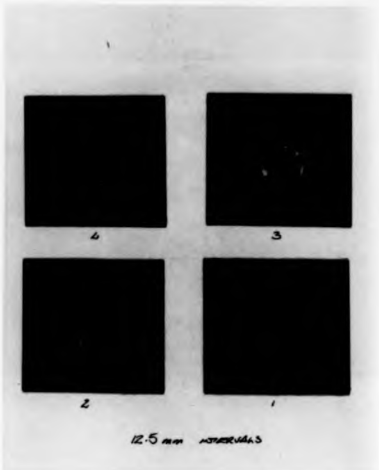

TOMOGRAMS OF LEFT VENTRICLE PHANTOM WITH DEFECT IN PLACE

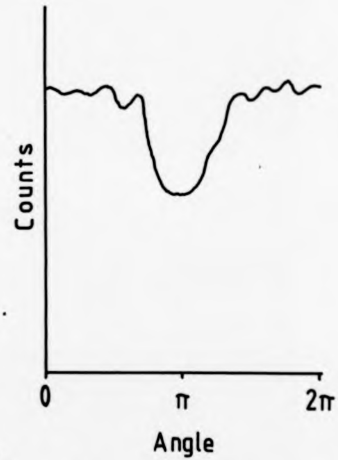

TYPICAL RADIAL PLOT OF THE COUNT DENSITY AROUND A TOMOGRAM

Fig. 6.6(a)

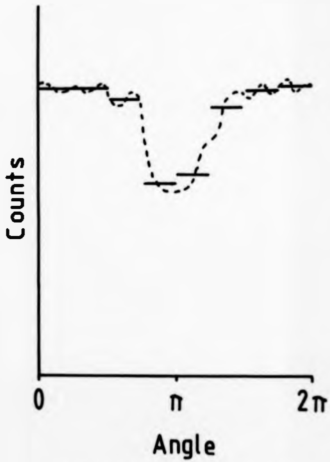

A CRUDELY SMOOTHED RADIAL PLOT OF THE COUNT DENSITY AROUND A TOMOGRAM

Fig. 6.6 (b)

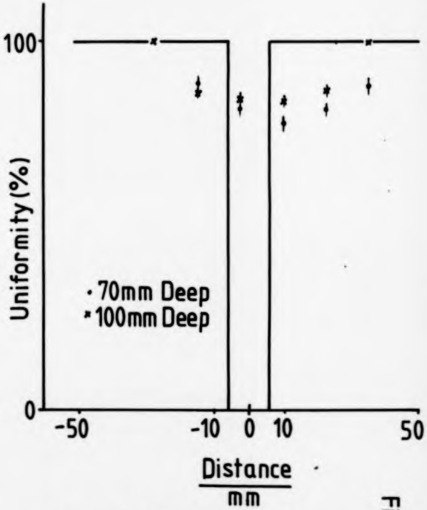

Fig. 6.7

VARIATION IN UNIFORMITY WITH DEPTH AND DEFECT POSITION FOR A TRUE 12mm DEEP, π/2 SECTOR DEFECT

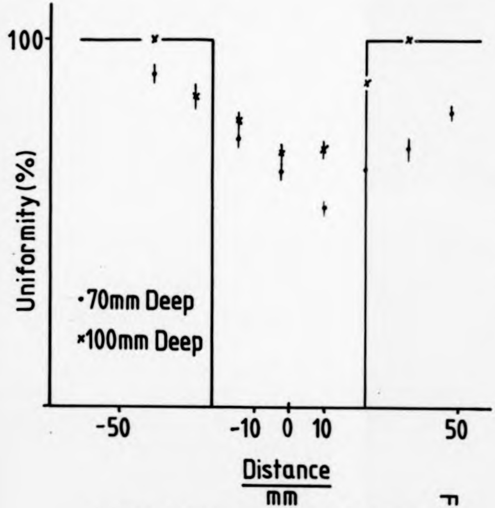

Fig. 6.8

VARIATION IN UNIFORMITY WITH DEPTH AND DEFECT POSITION FOR A TRUE 45mm DEEP, π/2 SECTOR DEFECT

6.5 Variation in Uniformity Due to False Defects in LV Phantom

To assess the variation in uniformity due to false defects, the LV phantom was imaged without any defects present, but with the axis at $\pi/8$ and $\pi/4$ to a line perpendicular to the camera face. Typical images of the resulting false defects are shown in Fig. 6.9. The uniformity variation with distance through the phantom is shown in Fig. 6.10. Also shown in this figure is the relative angular position at which the maximum uniformity variation in each tomogram occured. The maximum uniformity variation changed with the angle between the perpendicular to the camera face and the axis of the phantom. This change is shown in Fig. 6.11 which includes a result for an angle of 10° tilt to the camera axis. These results are similar to that of Hasegawa et al, 1982. From this, it is clear that the uniformity variation for a false defect can be comparable to that for an actual defect.

6.6 Variation in Uniformity Due to False Defects in Ellipsoidal Phantom

To distinguish between the cylindrical and apical sections of the LV phantom and to simulate a left ventricle in a more realistic manner, an ellipsoidal phantom was constructed. This is shown in Fig. 6.12 along with a planar image to demonstrate that the wall can be filled with a radioactive solution. The uniformity variations for angulations of $\pi/8$ and $\pi/4$ are shown in Fig. 6.13. Also shown in this figure is the change in relative angular position of the maximum uniformity variations within each tomogram. This shows that

Fig. 6.9

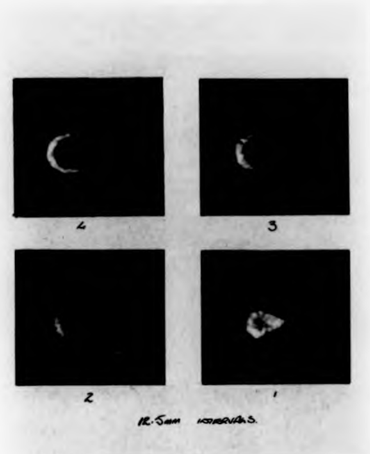

TOMOGRAMS OF TILTED LEFT VENTRICLE PHANTOM SHOWING FALSE DEFECTS

Fig. 6.10

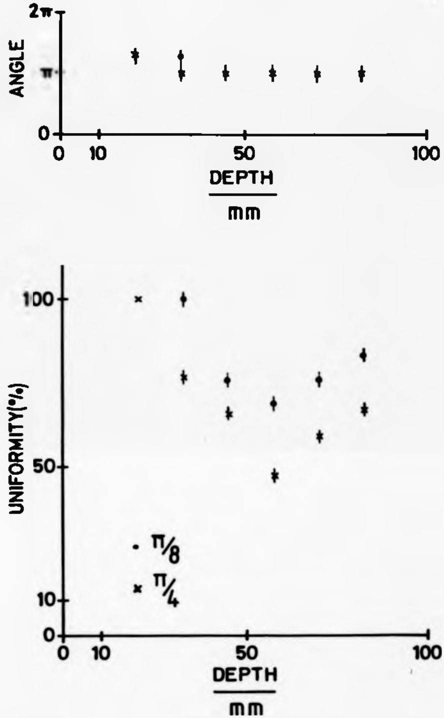

VARIATION IN UNIFORMITY AND DEFECTS ANGULAR POSITION WITH DEPTH AND ANGULATION OF VENTRICLE PHANTOM TO CAMERA

Fig. 6.11

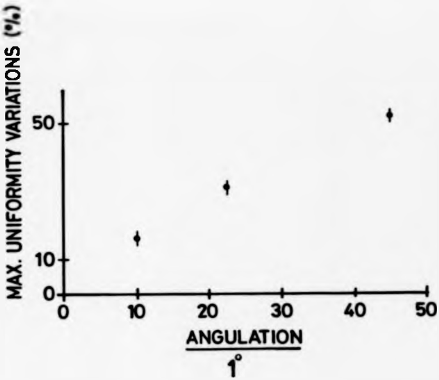

VARIATION IN MAXIMUM UNIFORMITY VARIATION WITH ANGULATION

Fig. 6.12

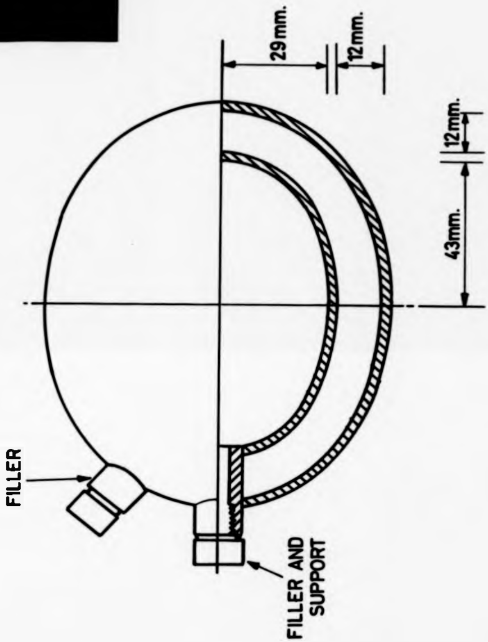

ELLIPSOIDAL PHANTOM

Fig. 6.13

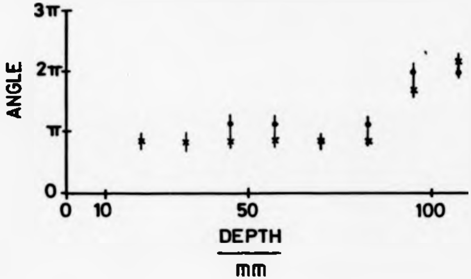

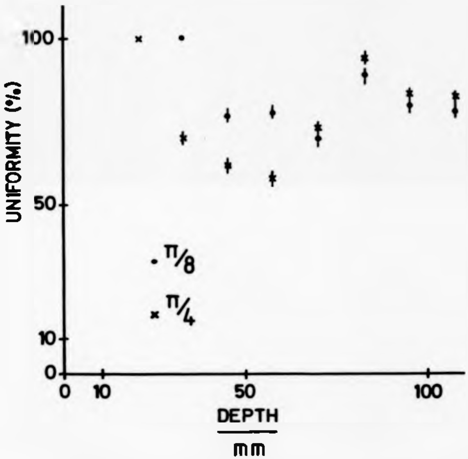

VARIATION IN UNIFORMITY AND DEFECTS ANGULAR POSITION WITH DEPTH AND ANGULATION OF ELLIPSOID PHANTOM TO CAMERA the defect shifts from one side of the phantom to the other and the cross-over point is coincident with the uniformity variation change. This shows that the false defect is associated with curvature.

6.7 Idealised Model and Computer Code to Simulate Reconstruction of Left Ventricle Phantom

A model to represent the LV phantom is shown in Fig. 6.14. This is a grossly simplified object and is angled so that it co-incides with the collimator angle of 26.6°. This simplifies the calculation to obtain the raysums for a four position or QUAD LECT system. Each volume element is given the dimension of 10 x 10 x 10 units and the projections calculated are set equal to the phantom volume intersected. These projections are illustrated in Fig. 6.15.

A reconstruction computer code was written for this QUAD LECT system based on the Iterative Least Squares Reconstruction Technique (ILSRT) as described by Budinger et al. (1974). A listing of this code is given in Appendix 7. Also given in this Appendix is the ideal plane distribution and the plane reconstruction after two iterations.

The ILSRT campares the estimated raysums calculated from the predicted activity distribution A^n (i, j) with the actual views of the object. This is expressed by

$$\Gamma(A) = \sum_{\theta} \sum_{k=1}^{n_\theta} \left(\frac{P_{k\theta} - R_{k\theta}}{\sigma_{k\theta}^2} \right)^2 \qquad - 6.1$$

where	$\sigma_{k\theta}^2$	is the variance of the actual projection
	$P_{k\theta}$	is the actual projection
	$R_{k\theta}$	is the estimated projection
	θ	identifies the view
	k	identifies the projection within a view
	A	is the activity distribution
	i, j	identify the activity element
and	n	is the iteration

Fig. 6.14

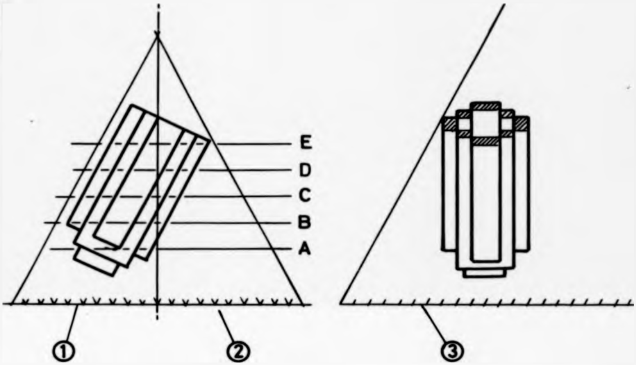

THEORETICAL MODEL OF LEFT VENTRICLE PHANTOM INDICATING POSITION OF RECONSTRUCTED PLANES A TO E

Fig. 6.15

Symmetry about X-X

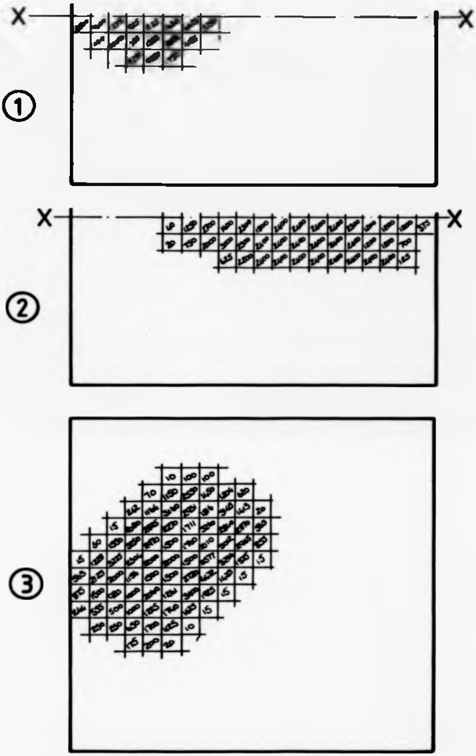

PROJECTIONS OF THEORETICAL MODEL OF LV PHANTOM IN THE DIRECTIONS ① ② and ③

The activity distribution is modified to minimise the difference between the predicted projection and the actual raysum. For the ILSRT this results in the calculation of increments using the equation.

$$\Delta^n A_{i,j} = \left\{ \sum_\theta f_{i,j}^\theta \frac{\left[P_{k\theta} - R_{k\theta}^n \right]}{P_{k\theta}} \right\} \Big/ \sum_\theta \frac{\left[f_{i,j}^\theta \right]^2}{P_{k\theta}} \qquad - 6.2$$

where $\Delta^n A$ is the activity increment,

$f_{i,j}$ accounts for the proportion of the element contributing to the raysum,

and $\sigma_{k\theta}^2$ is taken as being equal to $P_{k\theta}$. The activity increment is added on each iteration using

$$A_{i,j}^{n+1} = A_{i,j}^n + \delta_n \Delta^n A_{i,j} \qquad - 6.3$$

where δ_n is a damping factor, necessary to get convergence of a solution.

The usual method to start iteration is to set all the predicted distribution to zero. This in turn sets all the predicted raysums to zero so that 6.2 becomes

$$\Delta^1 A_{i,j} = \sum_\theta f_{i,j}^\theta \Big/ \sum_\theta \left\{ f_{i,j}^\theta \right\}^2 \Big/ P_{k\theta} \qquad - 6.4$$

In the simple case of $f_{i,j}^\theta$ = 1 for all i, j and θ this gives

$$\Delta^1 A_{i,j} = \frac{N}{\sum_{\theta=1}^{N} 1/P_{k\theta}} \qquad - 6.5$$

Hence, for N = 4, 4 views and δ_1 = 1.0, for the volume element, i, j which has raysums elements k in the 4 views, 6.5

becomes

$$\frac{4}{A_{ij}} = \frac{1}{P_{k1}} + \frac{1}{P_{k2}} + \frac{1}{P_{k3}} + \frac{1}{P_{k4}} \qquad - 6.6$$

This is known as the "impedance operator" and has the effect of minimising the contribution of the most corrupted raysums to the first estimate of a volume element activity. The most corrupted raysum will have the highest numerical value of P_{k1}-P_{k4} and so will make the least contribution to the summation in 6.6.

In order to confirm that studying the idealised LV phantom model and the QUAD reconstruction program would give comparable results to those obtained from the Technicare HEX LECT system, the first approximations were compared. Fig. 6.16 shows two sets of activity profiles taken transversley through the first approximation tomograms from the QUAD LECT system with the idealised LV phantom and from the HEX system with the LV phantom. They have comparable variations in the distribution with defects occurring in the same positions. This demonstrates that the QUAD and LV model phantom suffers the same problem in predicting activity distribution as does the HEX LECT system with the LV phantom.

The first approximation results indicate that defects are introduced in the tomograms from the very start of the reconstruction. Fig. 6.17 shows the profiles which resulted after a varying number of iterations following the first approximation. These show that the distributions remain virtually the same and the iterations make no corrections for the defects. In Fig. 6.18 the variation in the difference between predicted and actual projections as expressed by

$$\sum_{e} (P_e - R_e)^2 \qquad - 6.7$$

Fig. 6.16

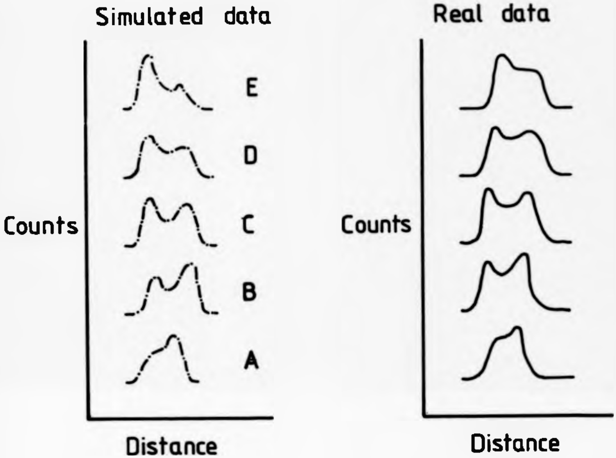

TRANSVERSE PROFILES ACROSS THE FIRST APPROXIMATIONS OBTAINED FROM THE THEORETICAL MODEL OF THE LV WITH A QUAD ITERATIVE LEAST SQUARES RECONSTRUCTION TECHNIQUE AND THOSE FROM REAL IMAGES RECONSTRUCTED ON THE TECHNICARE RSHLECT SYSTEM

TRANSVERSE PROFILES THROUGH THE TOMOGRAMS RECONSTRUCTED FROM THE THEORETICAL LV MODEL FOR 1, 5 AND 6 INTERACTIONS. THE INITIAL DISTRIBUTION WAS OBTAINED USING THE IMPEDANCE OPERATOR AND THE TRUE OR IDEAL TRANSVERSE PROFILE IS SHOWN FOR COMPARISON

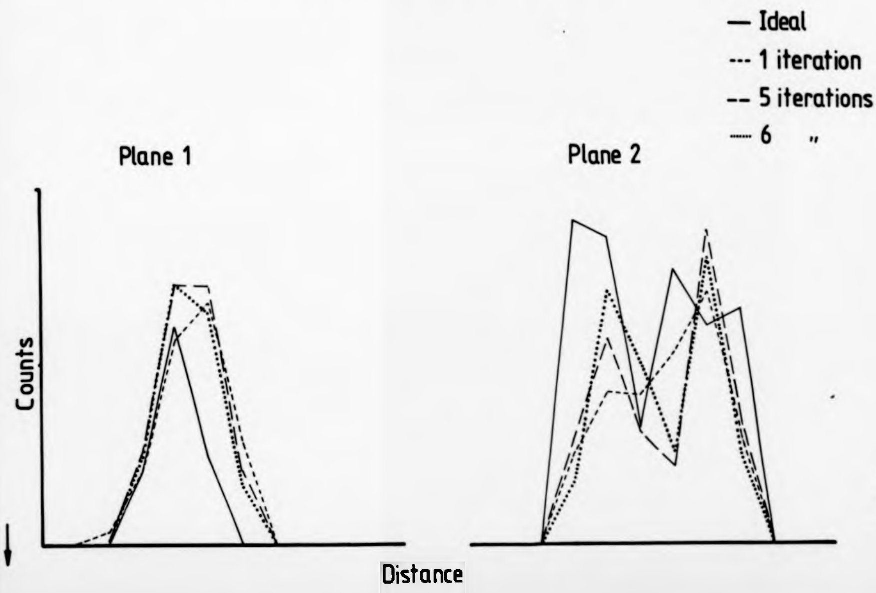

Fig. 6.17

Fig. 6.17 cont.

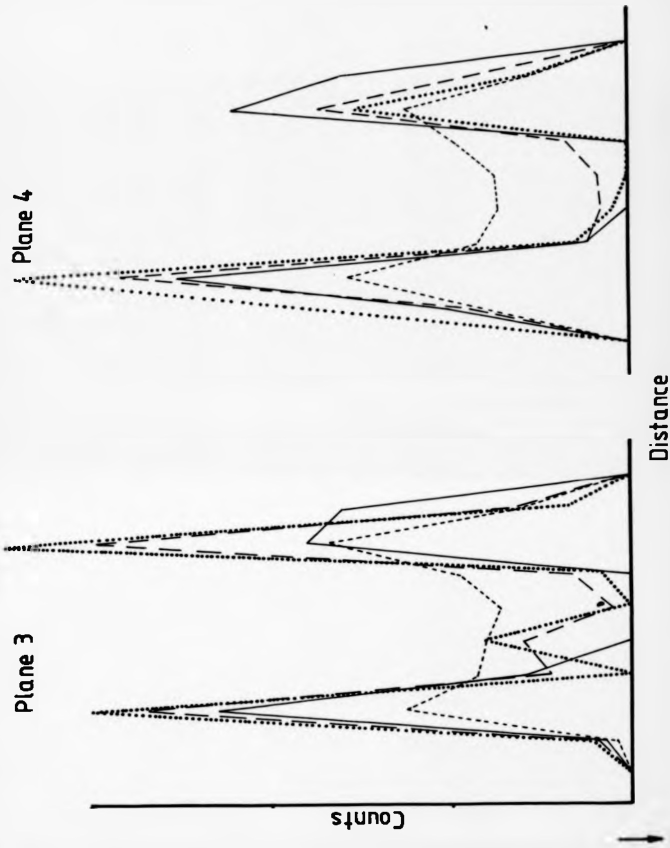

Fig. 6.17cont.

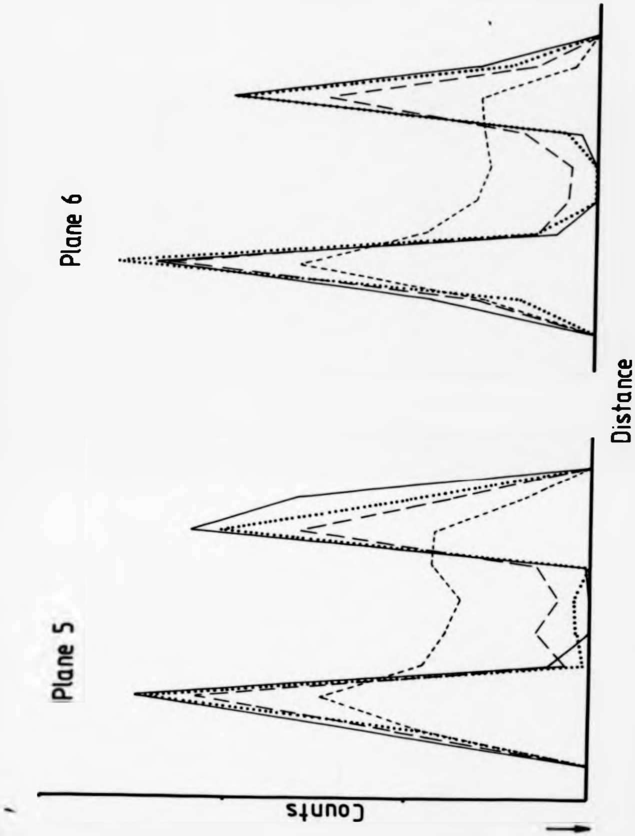

Fig. 6.17cont.

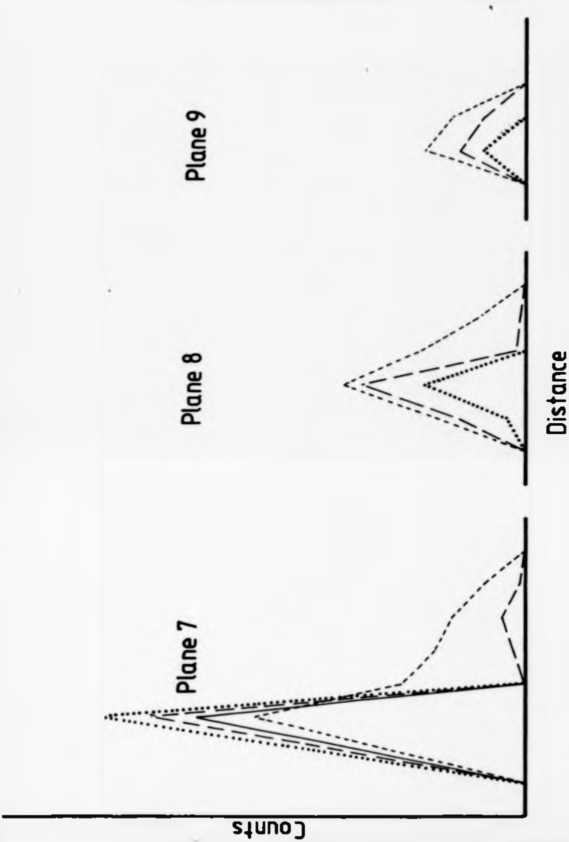

Fig. 6.18

VARIATION IN THE DIFFERENCE BETWEEN PREDICTED AND ACTUAL PROJECTIONS WITH NUMBER OF ITERATIONS

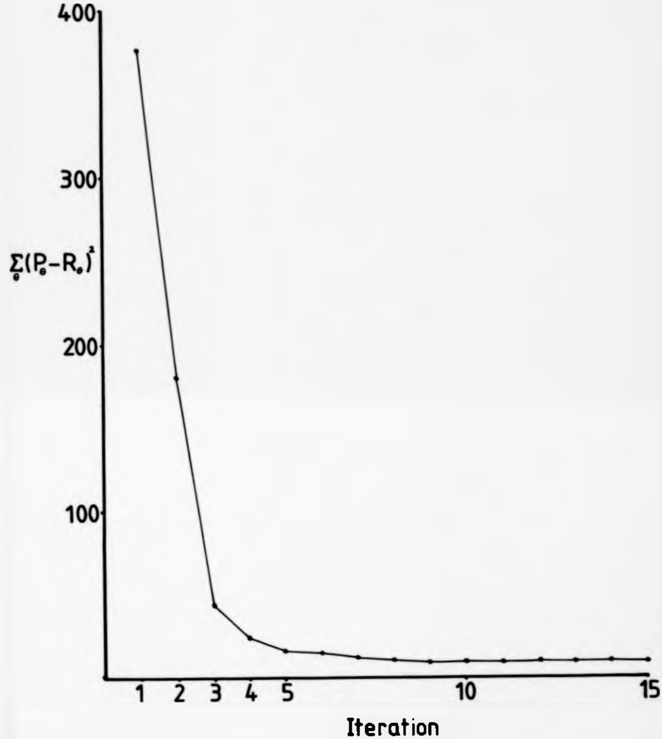

is plotted. It can be seen that a limit has been achieved by about 5 iterations. However, as Fig. 6.17 shows, the predicted distribution does change. Fig. 6.19 shows that up to 5 iterations the relaxation coefficient oscillates in a damped manner towards a final value and beyond this number of iterations it then oscillates. When an ideal activity distribution is used as a first approximation, the subsequent iterations alter this distribution slightly as shown in Fig. 6.20.

The overall conclusion from using this ideal model and the reconstruction code is that false defects are introduced from the very start of the reconstruction and that the subsequent iterations have no effect on their enhancement or their correction.

6.8 Effect of the Relative Size of the Raysums on the Defects Due to the Uniformity Variation

The relative size of the raysums will alter the first approximation to the activity distribution. Fig. 6.21 illustrates the ideal viewing situation with no angulation between the camera and the phantom axis. The approximations which result using the impedance operation are equal and hence

$$\frac{Z_1}{Z_2} = 1 \qquad - 6.8$$

indicating no uniformity variation. Z_1 and Z_2 are the activity predictions shown in Fig. 6.21. Fig. 6.22 illustrates an angled cylinder. The degree of corruption is altered between one side of the cylinder and the other so that the ratio of predicted activities is not equal to unity. This suggests that the ratio would be a function of three variables; attenuation (μ), degree of angulation (θ) and the angle the collimator makes with the horizontal, (ϕ). The ratio may be

Fig. 6.19

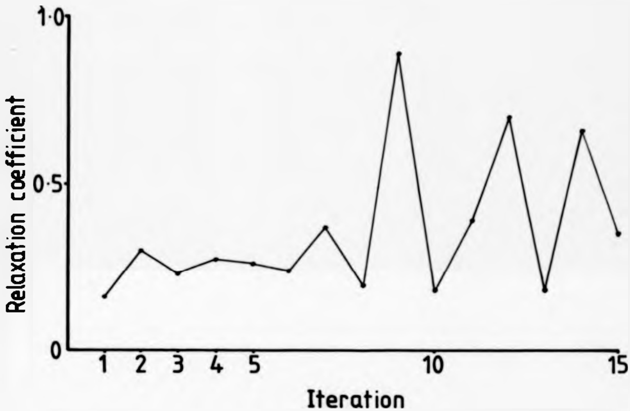

VARIATION OF RELAXATION COEFFICIENT WITH ITERATIONS

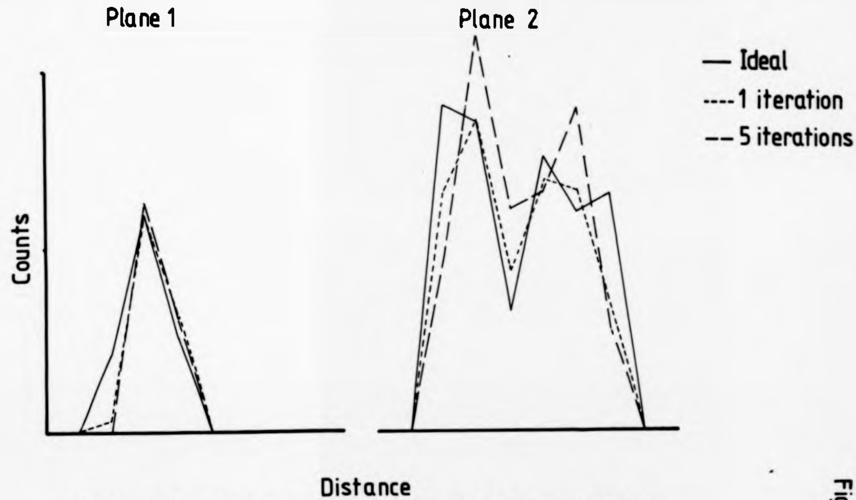

TRANSVERSE PROFILES THROUGH THE TOMOGRAMS RECONSTRUCTED FROM THE THEORETICAL LV MODEL WITH AN INITIAL DISTRIBUTION SET TO THE IDEAL DISTRIBUTION FOR 1, AND 5 ITERATIONS

Fig. 6.20

Fig. 6.20 cont.

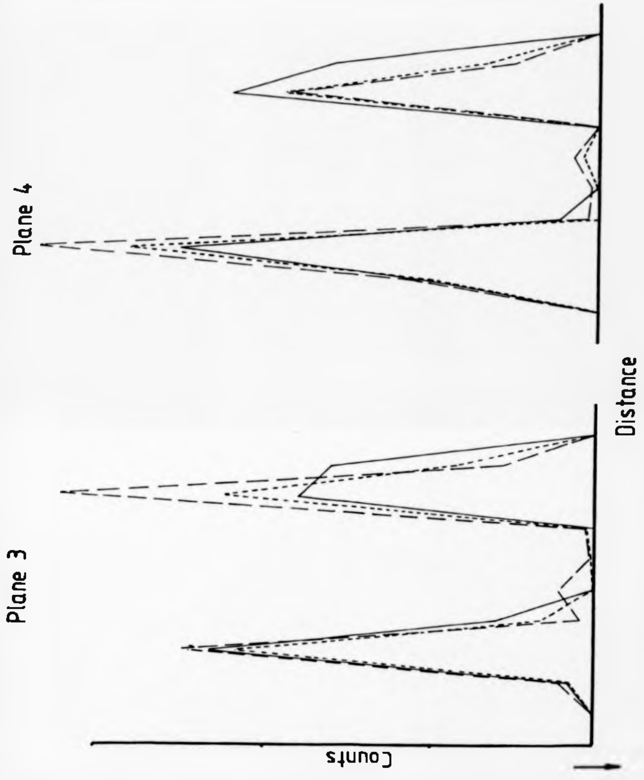

Fig. 6.20 cont.

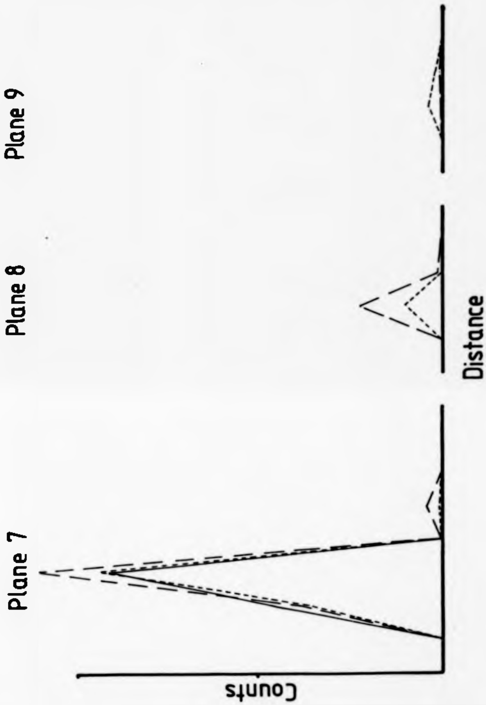

Fig. 6.21

$$Z_2^{-1} = \frac{1}{x} + \frac{1}{y} = Z_1^{-1}$$

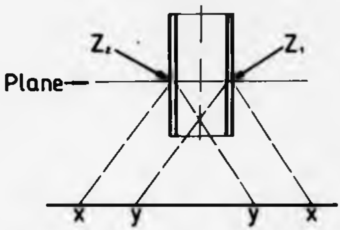

THE RAYSUMS RESULTING FOR AN IDEAL VIEWING DIRECTION ;
NO ANGULATION BETWEEN CAMERA AND LV AXIS

Fig. 6.22

$$Z_1^{-1} = \frac{1}{Y} + \frac{1}{x} \doteq \frac{1}{x}$$

$$Y \gg 1$$

$$Z_2^{-1} = \frac{1}{X} + \frac{1}{y} \doteq \frac{1}{y}$$

$$X \gg 1$$

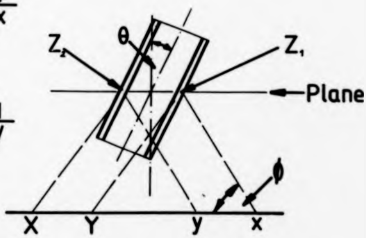

$$\frac{Z_1}{Z_2} = \frac{x}{y}$$

THE RAYSUMS RESULTING FROM A SET OF VIEWING
DIRECTIONS WITH ANGULATION BETWEEN THE CAMERA AND
THE LV AXIS

written as

$$\frac{Z_1}{Z_2} = 1 - \frac{f(\theta, \phi, \mu)}{y} \qquad - 6.9$$

and hence the uniformity variation expressed as a fraction of the maximum value, Z_2 can be written as

$$\frac{Z_2 - Z_1}{Z_2} = \frac{f(\theta, \phi, \mu)}{y} \qquad - 6.10$$

By inspection of fig. 6.22, it can be seen that as the angle Ø decreases, that is the collimator angle increases, the value of $f(\theta, \phi, \mu)$ will increase so that the ratio Z_1/Z_2 will decrease. Likewise, as μ increases $f(\theta, \phi, \mu)$ will increase and again Z_1/Z_2 will decrease. However, as the angulation ϕ is increased, $f(\theta, \phi, \mu)$ will decrease so that the fraction expressed by 6.10 will decrease. However the results shown in fig. 6.11 indicate that the opposite actually occurs with increasing angle of tilt.

To increase the attenuation coefficient, the LV phantom was imaged while surrounded in powder plaster which has a high attenuation coefficient compared to air. Fig. 6.23 shows the variation in uniformity compared to that for air and indicates that there is no difference.

A large feild of view Technicare LECT system was used in order to decrease ϕ. This system has a collimator angle of 35°. The uniformity variation expressed as $\frac{Z_1}{Z_2}$ is shown in fig. 6.24 and indicates that the ratio increases with increasing collimator

Fig. 6.23

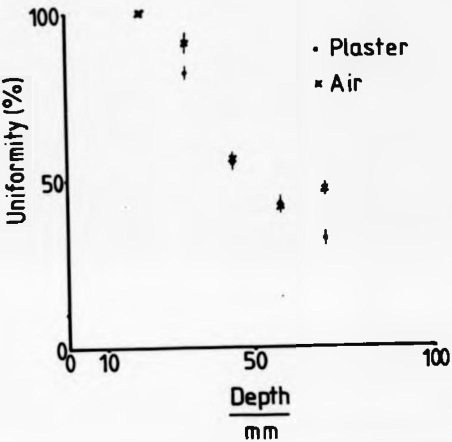

VARIATION OF UNIFORMITY WITH DEPTH AND ATTENUATION COEFFICIENT FOR LV PHANTOM WITH ITS AXIS AT AN ANGLE OF π/4 TO THE CAMERA AXIS

Fig. 6.24

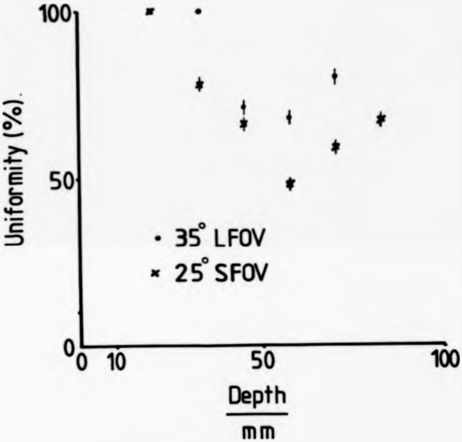

VARIATION IN UNIFORMITY WITH DEPTH AND COLLIMATOR ANGLE FOR LV PHANTOM WITH ITS AXIS AT $\pi/4$ TO THE CAMERA AXIS angle rather than decreasing. These results imply that consideration of the relative size of raysums along is not sufficient to explain the false defect problem.

6.9 Effect of First Approximation Technique on the Uniformity Variation

The first approximation technique used to obtain the distributions studied in the previous sections is the impedance operator. Whatever technique is used, the basic projection data related to any volume element remains the same. A valid technique to obtain a first approximation and satisfy the condition that when a raysum is zero, there is no activity in the volume element, is simply to muliply the raysum values together. Fig. 25 shows

Fig. 6.25

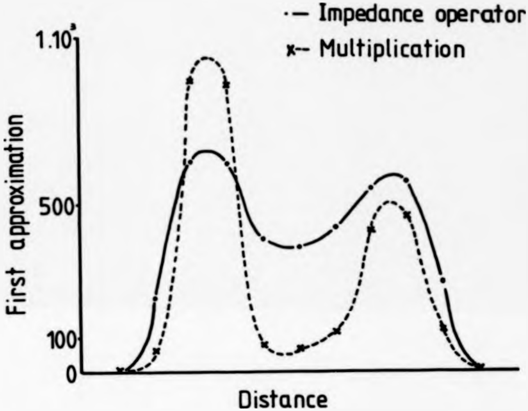

TRANSVERSE PROFILE ACROSS THE FIRST APPROXIMATIONS OF A SINGLE TOMOGRAM OF THE THEORETICAL LV USING THE IMPEDANCE OPERATOR AND MULTIPLICATION TECHNIQUES two profiles for the same tomogram, one obtained using the impedance operator and the other by multiplication of raysums. These show that the relative distribution of activity is not altered. Hence, the basic data available for the first approximation makes the introduction of uniformity variations unavoidable.

6.10 Analysis of the False Defect Problem Using the EVI Technique

The EVI technique identifies the direction in which there is the greatest difference between a plane object and the reconstruction volume. For the RSHLECT system used in the experimental work described above, this direction is at right angles to the camera face (Chapter 3, Pt. 3). For the QUAD LECT system used in the computer simulations described above, it also lies in this direction (Chapter 3, Pt. 2, Table 3.3). This identifies the maximum error volume for both systems as a plane object parallel to the camera face.

The LV phantom can be considered as the summation of separate planes. Each one of these planes will have a reconstruction volume particular to the size and orientation of the plane. If the direction of the planes are parallel to the direction of the maximum EVI, then their reconstruction volume will have the maximum error for that viewing system. Appendix 7 shows that for the impedance operator, the prediction of activity at a point within a stack of planes is equal to the summation of the predictions at that point for the individual planes. Although the activity distribution in the LV is not uniform, the summation of the maximum error volumes will indicate where enhancement from under and overlying planes occur.

Fig. 6.26 shows the LV phantom at an angle to the camera face and divided into a set of planes parallel to the camera face. Likewise, Fig. 6.27 shows an outline of a typical LV also divided into a set of planes parallel to the camera face. The sampling frequency was chosen artbitraly, but large enough to give reasonable resolution of the LV and LV phantom edges. The simulation of the reconstruction of the planes are given in Appendix 6. In the simulation of the reconstruction, an activity value is not given. Since the actual plane activity will vary from object to object, a volume element is merely shown to be set, that is, to have activity.

The overall reconstruction planes resulting from the summation of the individual reconstructions for the LV phantom and the LV are given in Fig. 6.28 and 6.29 respectively. These show clearly an enhancement of predicted activity towards one side of the tomograms for both the LV and the LV phantom. This enhancement on a side of the tomogram results in a false defect on the opposite wall as has been observed experimentally and clinically. Hence, the false defect is a fundamental problem with these LECT systems. It arises in the reconstruction because of the propagation of activity into a volume not occupied by the object. Although this propogation also arises when the LV or LV phantom is symmetrically orientated to the camera it does not produce any enhancement of activity in one side of the wall as compared to the other.

Fig. 6.26

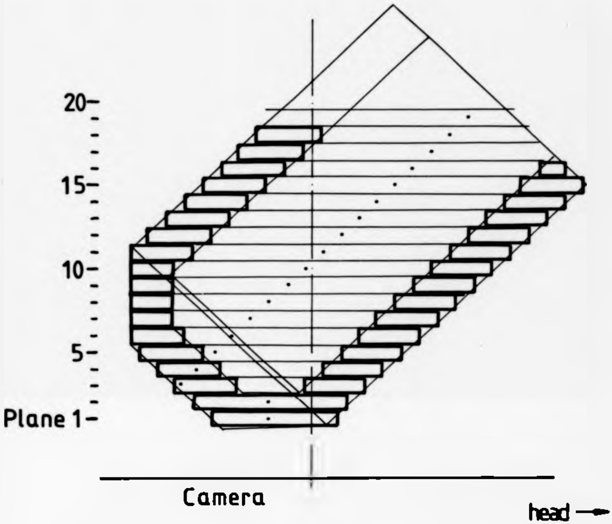

THE LV PHANTOM DIVIDED INTO A SET OF PLANES PARALLEL TO THE CAMERA FACE

Fig. 6.27(a)

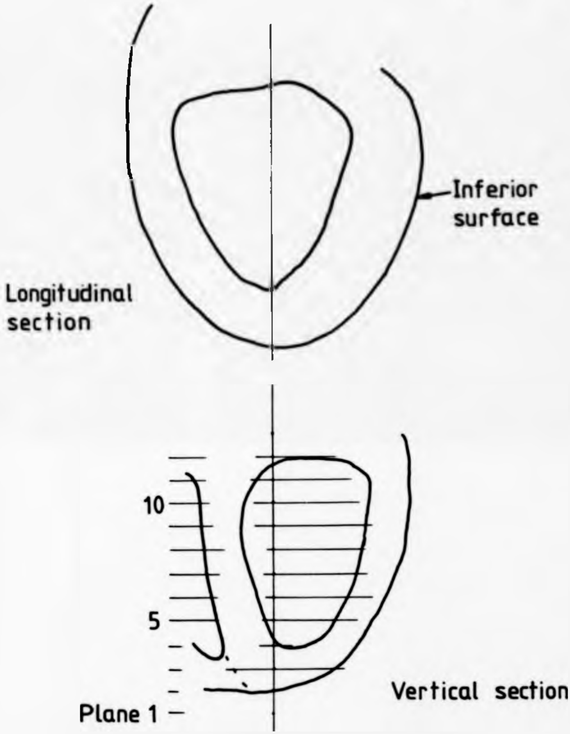

A TYPICAL LV IN CROSS SECTION AND DIVIDED INTO A SET OF PLANES PARALLEL TO THE CAMERA FACE

Fig. 6.27(b)

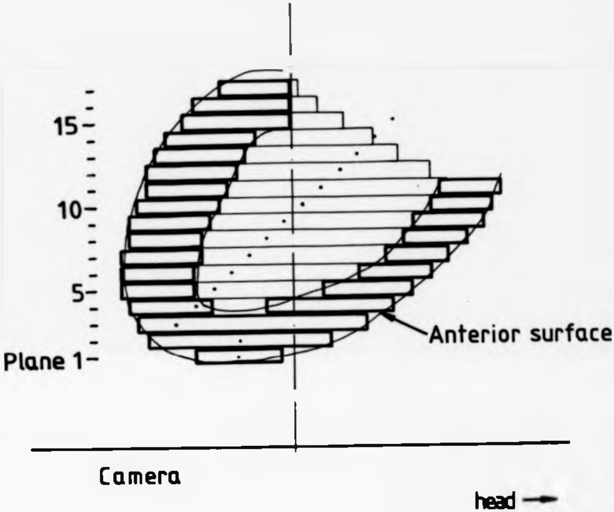

Fig. 6.28

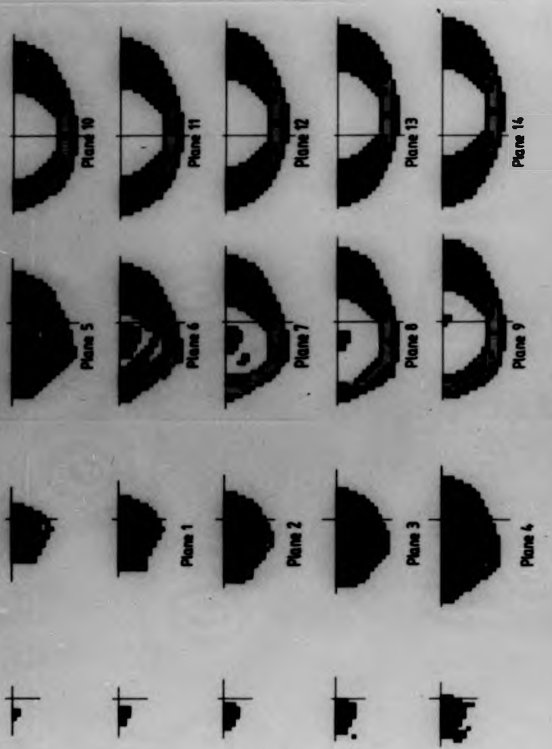

RECONSTRUCTED PLANES OF LV PHANTOM RESULTING FROM THE SUMMATION OF INDIVIDUAL PLANE RECONSTRUCTIONS.

Fig. 6.29

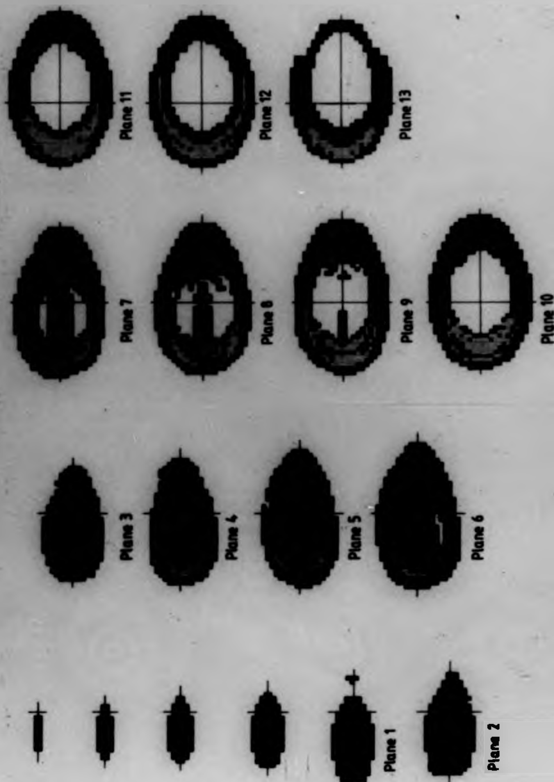

RECONSTRUCTED PLANES OF TYPICAL LV RESULTING FROM THE SUMMATION OF INDIVIDUAL PLANE RECONSTRUCTIONS.

6.11 Explanation of Ellipsoidal Phantom and Increased Collimator Angle Results Using Superposition

In Section 6.6 experimental results with an ellipsoidal phantom were presented. These showed, Fig. 6.15 that with angulation, the false defect showed periodicity with depth and moved from one side of the phantom to the other. Fig. 6.30 shows an angulated ellipsoidal phantom divided into a set of parallel planes. Shown also is the outline of the reconstruction volume for each individual plane. This shows that there is an enhancement on one side of the reconstruction. This enhancement changes to the opposite side with depth and decreases through the vertical plane of the reconstruction showing the periodicity observed in the experimental results.

Fig. 6.24 showed that for an increase of collimator angle the degree of uniformity variation was reduced. The system used to obtain these results was a 35^{o} rotating slant hole LECT system. Using the EVI analysis, the maximum EVI for this system is 0.819 and the maximum reconstruction error volume arises for a plane object parallel to the camera face. The maximum reconstruction error volume takes the form of a double cone, the bases of which are coincident in the plane object and have an included angle of $2.\cos^{-1}$ (EVI) which equals 70^{o}.

Fig. 6.31 illustrates the difference between the maximum reconstruction error volumes for the 25^{o} RSHLECT system and the 35^{o} RSHLECT system, when the same plane object is imaged. It illustrates that the degree of penetration into adjacent planes is reduced by the increased collimator angle system.

Fig. 6.30

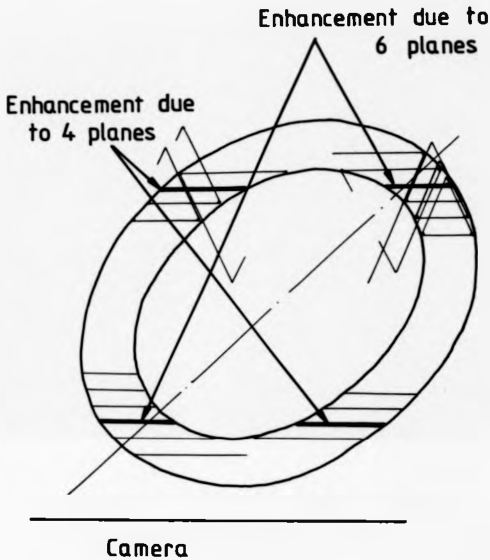

ELLIPSOIDAL PHANTOM WITH ITS AXIS AT AN ANGLE TO THE CAMERA AXIS AND DIVIDED WITH PLANES PARALLEL TO THE CAMERA TO SHOW THE PENETRATION OF ACTIVITY INTO ADJACENT PLANES

Fig. 6.31

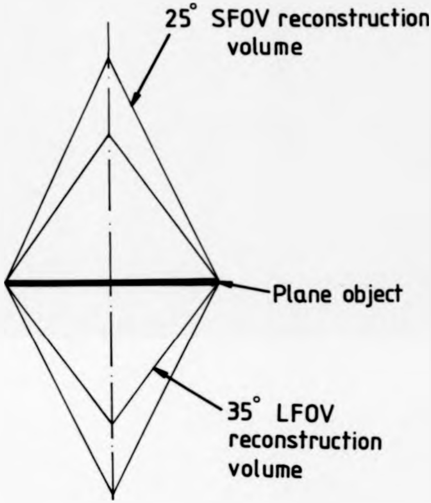

OUTLINE OF MAXIMUM RECONSTRUCTION ERROR VOLUMES FOR A 25° RSHLECT AND 35° RSHLECT SYSTEMS

Hence, the amount of enhancement will be reduced and so will the uniformity variation.

CHAPTER
7

PROBLEMS IN THE USE OF LECT FOR CARDIAC BLOOD POOL IMAGING

7.1 The Cardiac Blood Pool and LECT

The aim in using Tomography of either the rotating head or longitudinal type for cardiac blood pool imaging is to obtain improved visualisation of the inferior and posterior surfaces of the left ventricle (LV). These surfaces cannot be adequately assessed by planar imaging and thus tomography, by removing the over and under lying activity, improves the visualisation of these surfaces. LECT is an attractive technique to develop as a blood pool imaging system because it requires images from only a few directions. Hence, there are fewer images to be acquired compared to a RHECT system. Also, with a 7-pinhole LECT system all the images are acquired simultaneously, making operator intervention between images unnecessary. This reduces the risk of relative motion between the camera and the patient during the acquisition of the images.

The LV blood pool may be considered to approach the shape of a solid ellipsoidal object. The activity is uniformly distributed throughout the volume. Both of these features make the LV blood pool a simple object to image in contrast to say, Thallium-201 perfusion imaging, where a hollow object of non-uniform activity distribution is being imaged. The main problem with a LECT reconstruction of the LV blood pool is the incorrect prediction of object volume giving rise to the propagation of activity into regions where it does not exist. If a correct volume boundary can be generated then, since the blood pool has a uniform activity distribution, the detected activity can be distributed uniformly within that volume.

The direction of the greatest error volume propagation for any LECT system can be determined using the EVI as previously described (Chapter 3). The maximum error volume will be for a plane object with direction parallel to that of the maximum EVI. As previously described, any object can be considered as a summation of planes. The actual extent of the error propagation depends on the size of the plane and on the angle given by $\cos^{-1}$ (EVI). For an object with a curved surface, the indeterminate volume for that object begins to exist when the curvature equals the gradient given by the angle $\cos^{-1}$ (EVI). This can be demonstrated by considering a sphere. The depth d, along the direction of maximum EVI beyond which the reconstruction volume is indeterminate is given by

$$d = R \sin(\cos^{-1}(EVI)) \qquad - 7.1$$

where R is the radius of the sphere, Fig. 7.1. Fig. 7.1 also shows the boundary of the reconstruction of a uniform sphere using a QUAD (26.6°) LECT system for which the maximum EVI is 0.894 in a direction perpendicular to the camera face. The level, or plane at which the error volume for the object begins and the ideal boundary for the object are shown in Fig. 7.1. This chapter examines the relationship between the activity prediction in the error volume and the object shape. An attempt is made to obtain a better approximation to the reconstructed shape for ellipsoidal objects with a uniform activity distribution.

7.2 The Extent of Propagation on a RSHLECT System

As described above , the problem in the use of LECT for cardiac blood pools is the propagation of activity in the reconstruction into regions where there is no activity.

Fig. 7.1

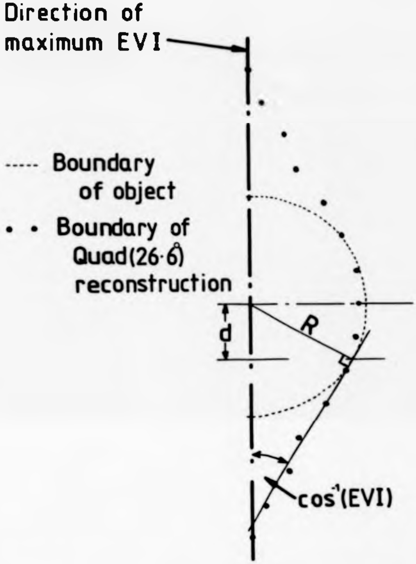

RELATIONSHIP BETWEEN A SPHERE AND ITS INDETERMINATE RECONSTRUCTION VOLUME FOR A QUAD (26.6°) SYSTEM

In order to assess this problem in an actual LECT system, a reconstruction of an ellipsoidal phantom was made with the RSHLECT system described in Chapter 4. The ellipsoidal phantom is shown in Fig. 7.2. The central pool was filled with a uniform solution of Technetium-99m. Three point sources were made by placing minute drops of Technetium-99m solution on absorbent bench paper. These three sources were then placed in a line at regular intervals of 30mm so that they were coincident with the top, bottom and middle of the ellipsoid. The coincidence between the ellipsoid and the point sources is demonstrated by the profiles shown in Fig. 7.3. These profiles were taken from a planar image of the sources and ellipsoid together. The variation in the peak counts for the points is due to slight differences in activity. The variation in the profile counts through the phantom reflects the variation in the cross section of the pool. This was due to the crude construction of the ellipsoid shells, however, the profile does indicate the extent of activity within the pool in the direction which was perpendicular to the camera face during the acquisitions. This direction corresponds to that of the maximum EVI for this system.

Six rotating slant hole images were taken for both the ellipsoid, with its long axis perpendicular to the camera and for the point sources, with their line also at right angles to the camera face. Each image contained a total of approximately 300,000 counts. Reconstructions of both the ellipsoid and the point sources were made with a plane starting depth of 70mm and a 15mm spacing between the planes. Twelve planes and two iterations were used.

The central axis profiles through the resulting reconstructed planes are presented in Fig. 7.4. It is clear that the plane frequency was insufficient to resolve the point sources and they appear as a line source of varying activity.

Fig. 7.2

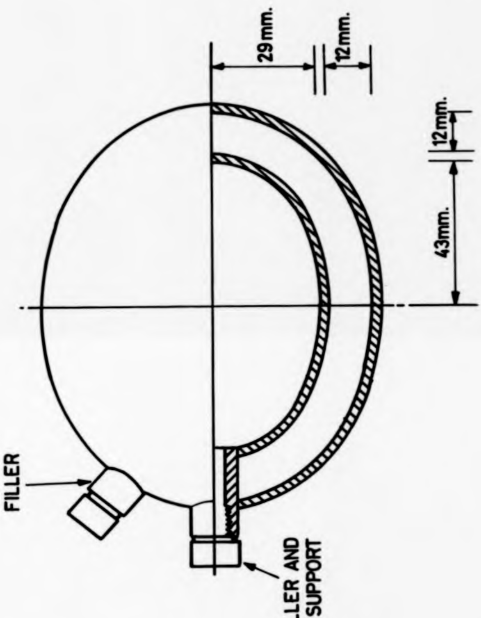

ELLIPSOIDAL PHANTOM

Fig. 7.3

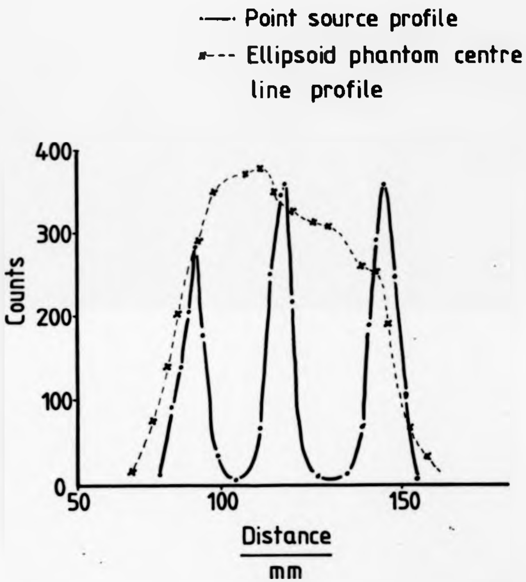

PROFILES THROUGH POINT SOURCES AND ELLIPSOIDAL PHANTOM TO SHOW EXTENT OF OBJECT

Fig. 7.4

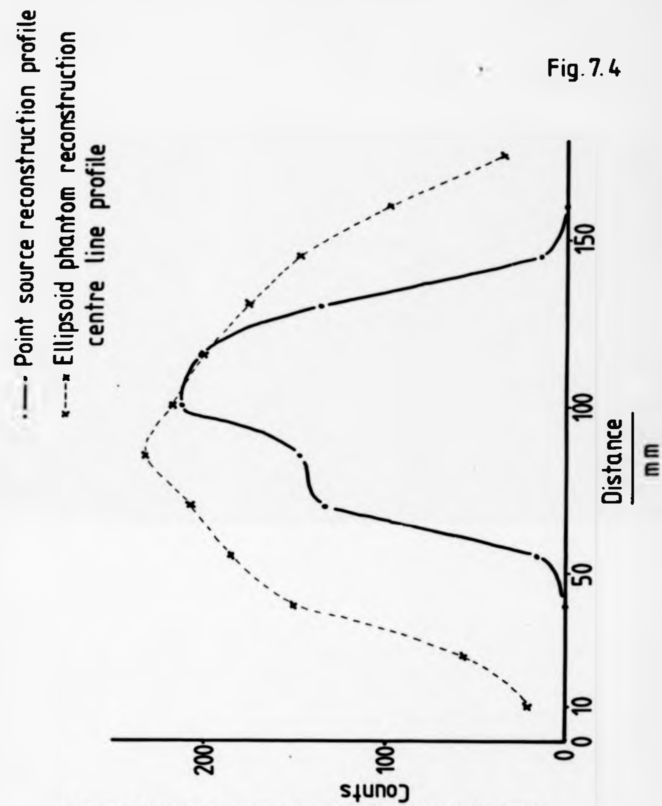

PROFILES THROUGH THE RECONSTRUCTIONS OF THE ELLIPSOIDAL PHANTOM AND POINT SOURCES

However, since for point and line sources their reconstruction volume is correct, the extent of the profile can be taken as correct. In contrast, the extent of the ellipsoid phantom profile exceeds the limit of point sources considerably. It therefore exceeds the boundary of the ellipsoidal object. This demonstrates on a LECT system how there will be a propagation of activity into volumes of the reconstruction which are not occupied by the cardiac blood pool being reconstructed.

7.3 Reconstruction of a Uniform Activity Distribution

In Appendix 7 it is shown that at a point deep within a stack of planes, the predicted activity is equal to the sum of individual predictions at that point for each plane. This is for the impedance operator and holds only for a uniform activity distribution. Although this summation breaks down at the edge of the reconstruction volume, the result suggests that it may be possible to strip activity from the first prediction of an object. In order to do this, the maximum plane width would be found and the penetration associated with this plane calcluated. The prediction would then be corrected by subtracting the activity within the penetration volume. By continuing this process for the adjacent planes the initial prediction would be corrected. To examine this concept, and to eliminate the planes which actually contain no activity a single plane and a stack of three planes are considered. A simplified plane of 5 elements radius is used. This plane is shown in Fig. 7.5a with activity a per element. Also shown is the series of reconstructed planes and the activity values for a QUAD (26.6°) LECT system, Fig. 7.5b. Fig. 7.6. shows the impedance operator prediction and Fig. 7.7., the summation prediction for a stack of three single planes.

It is clear by inspection that although the predicted activity agrees well at a point deep in the stack, there is very poor agreement towards the edge of the reconstruction volume.

Fig. 7.5(a)

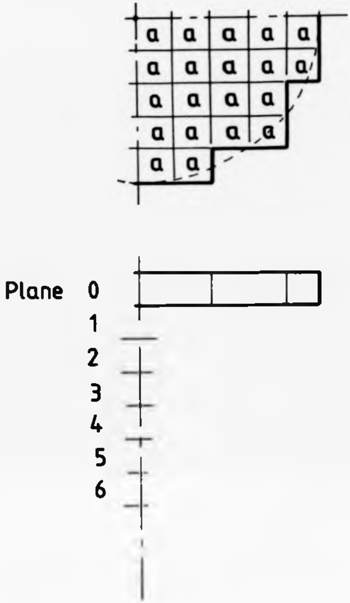

SIMPLIFIED PLANE AND ACTIVITY DISTRIBUTION, ACTIVITY a PER UNIT ELEMENT

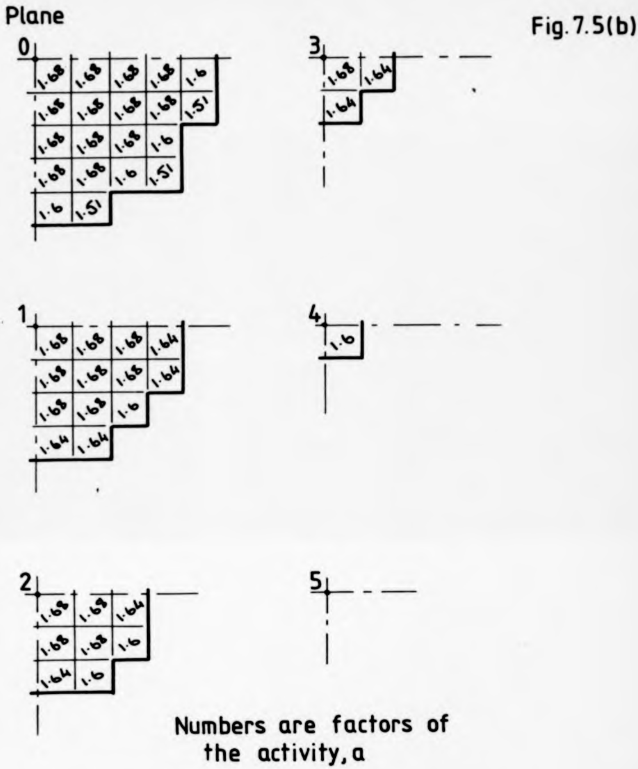

RECONSTRUCTED ACTIVITY DISTRIBUTION OF SIMPLIFIED PLANE WITH A QUAD, (26.6°) LECT SYSTEM

Fig. 7.6

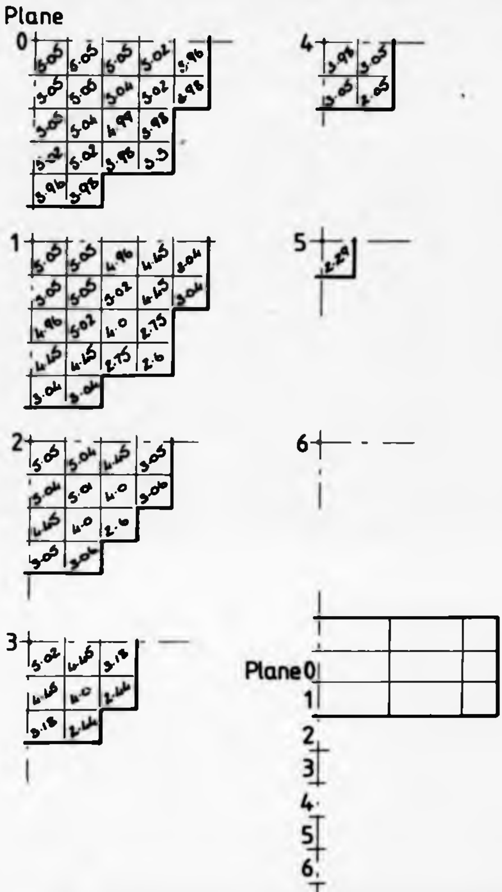

FIRST (IMPEDANCE OPERATOR) PREDICTION OF ACTIVITY FOR A UNIFORMLY DISTRIBUTED THREE PLANE STACK, WITH A QUAD (26.6°) LECT SYSTEM AND THE ILSRT

Fig. 7.7

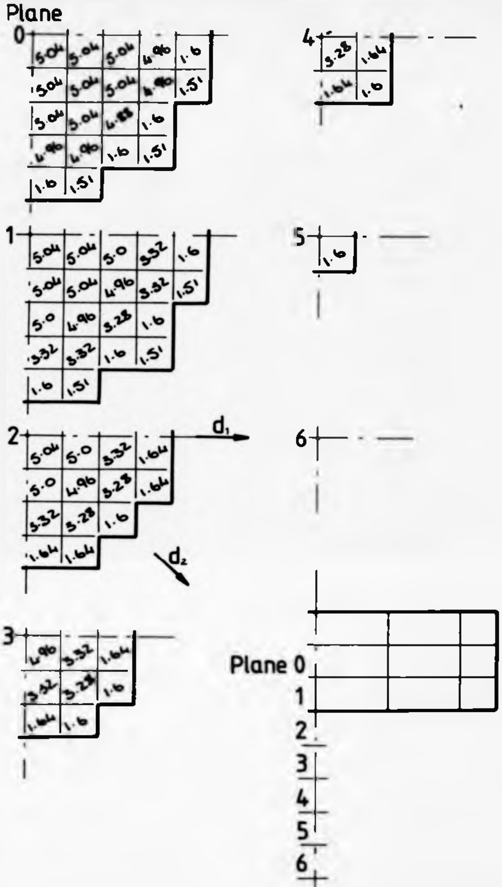

FIRST PREDICTION OF ACTIVITY FOR A UNIFORMLY DISTRIBUTED THREE PLANE STACK USING SUMMATION OF THE SINGLE PLANE RECONSTRUCTION, FIG 7.5 (b)

Fig. 7.8 presents a radial variation of the ratio of the impedance operator prediction to the summation. This shows that at some points the ratio is as great as a factor of 2.0. The good agreement between the summation and the impedance operator prediction at the centre of the stack should allow the number (n) of planes in the stack to be obtained from

$$I = n.1.68.a \qquad - 7.2$$

Where I is the impedance operator prediction and the factor of 1.68 is particular to the QUAD (26.6°) LECT system.

In order to obtain the number of planes n, or indeed to strip a planes propagations from the reconstruction, the activity a has to be obtained. This would have been possible to calculate for a maximum radius plane amongst the stack using

$$a = \frac{E1}{1.6} \qquad - 7.3$$

Where E1 is the impedance operator prediction at the edge of the widest plane and the factor of 1.6 is particular to the QUAD (26.6°) LECT system. However, the large variation at the edges between summation and impedance operator prevents this. The fundamental problem in using the result of Appendix 7 is that to strip activity or to estimate the number of planes in a stack, the density of activity is required. As it is impossible to obtain a sensible estimate of this it is not possible to correct the activity prediction by this means.

7.4 Variation of Central Axis Activity Prediction for Simple Objects and Its Use for Error Volume Correction

The variation of activity along the direction of maximum

Fig.7.8

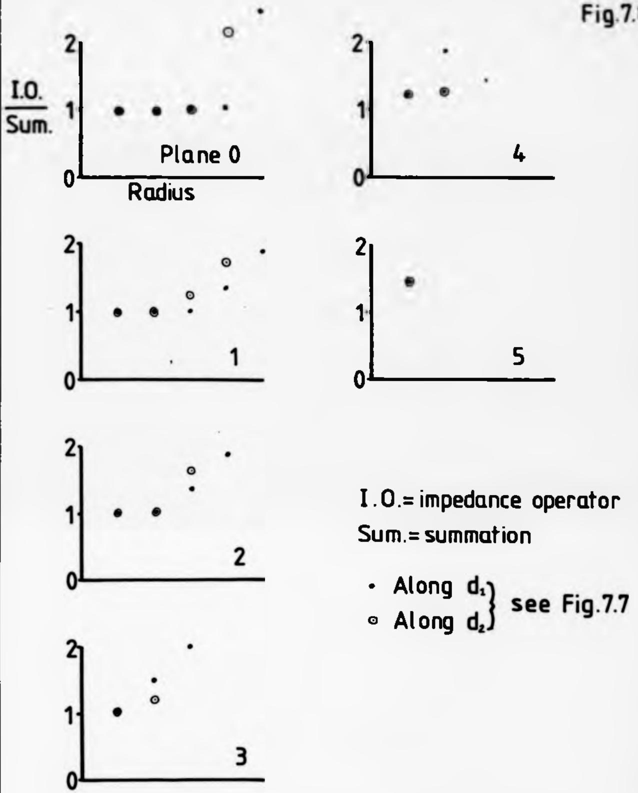

RADIAL VARIATION OF RATIO BETWEEN IMPEDANCE OPERATOR AND SUMMATION TECHNIQUE FOR FIRST PREDICTION FOR THREE PLANE STACK

EVI should contain, for a uniform activity distribution, information about the number of planes which actually contain activity. This may be illustrated simply by considering the range of objects between a single plane and a top which can exist within the maximum error volume for a system.

Fig. 7.9 illustrates the range of symmetrical objects which can crudely be considered to exist in the maximum error volume. Let l be the radius of the central plane.

n the number planes in addition to l/2
and m the number of planes up to l/2

For a QUAD (26.6°) LECT system it is possible to estimate the impedance operator predictions at points A and B; the centre and extremity respectively of the reconstruction volume.

The relationship between an image element and a volume element is illustrated in Fig. 7.10. The predictions at A and B are obtained from

$$E = \frac{3 + n.0.125}{0.75^2\left\{\frac{1}{a_1} + \frac{1}{a_2} + \frac{1}{a_3} + \frac{1}{a_4}\right\} + 0.125^2\left\{\frac{1}{b_1} + \frac{1}{b_2} + \cdots\cdots \frac{1}{bn}\right\}} \qquad - 7.4$$

Where E is the impedance operator prediction

n is the number of adjacent raysums contributing to a volume element activity prediction.

a_1 - a_4 are the direct raysums, while b_1 - b_n are the peripheral contributions.

Fig. 7.9

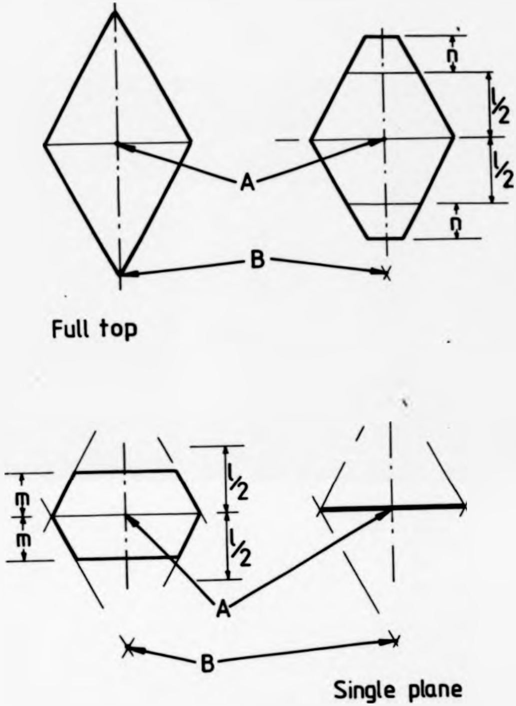

RANGE OF SYMMETRICAL OBJECTS WHICH CAN BE CRUDELY CONSIDERED TO EXIST IN THE MAXIMUM ERROR VOLUME

Fig. 7.10

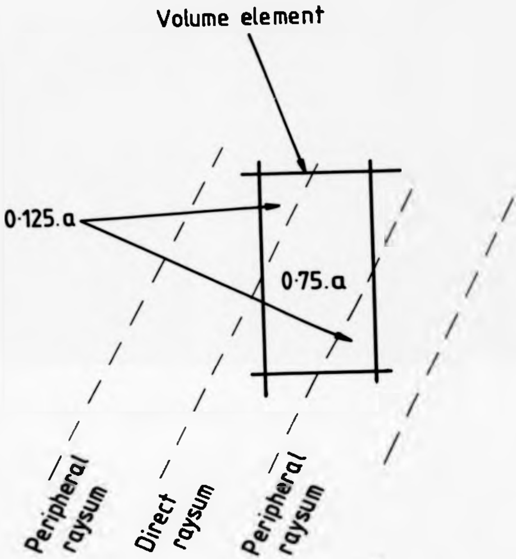

RELATIONSHIP BETWEEN A VOLUME ELEMENT AND IMAGE ELEMENTS

For point A, n = 8 while for point B, n = 6.

Table 7.1 details the ratio (A/B) of the predictions at A and B for the range of objects shown in Fig. 7.9. This illustrates that an object shape can be identified from the A/B ratio and the radius 1.

These are very crude rules derived for ideal distributions of activity with respect to the viewing angle. In reality, and particularly with reference to an ellipsoidal shape, the prediction becomes very different. The problem is again associated with the predictions at the edge of the reconstruction volume, as at points B and C in Fig. 7.11 which illustrates an ellipsoidal object. The value of these predictions is dependent on the amount of intersection between a raysum and the edge of the object.

Since the LV can be considered as ellipsoidal in shape, the variation in the ratio A/B can easily be assessed by considering the prediction and consequent A/B ratio for an ellipse. Fig. 7.11 shows the model used to calculate the ratio and the program for its calculation is given in Appendix 8. Figs. 7.12 and 7.13 show the variation of the ratio with changing ellipsoid and different sized spheres respectively. These show discontinuities in the ratio which would make it impossible to use this ratio to determine the true extent of the object within the reconstruction volume. Fig. 7.13 shows the variation with sphere radius varying through 7 units. This corresponds to the sphere used in the QUAD (26.6°) simulation used previously. The predicted ratio of 6.5 corresponds well to that obtained from the simulated reconstruction of 5.6.
However, the variation of the ratio for a radius of just less than 7 units illustrates how variable this ratio is for small changes in radius.

TABLE 7.1

A/B	OBJECT SHAPE (SEE FIG. 7.9)	COMMENT
1	EITHER SINGLE PLANE	UNLIKELY
	OR FULL TOP	REASONABLE
1 TO 2	EITHER VERY THIN OBJECT	UNLIKELY
	OR TRUNCATED CONE DEPTH 1/2 + n	CALCULATE n USING $\frac{A}{B} = 2.1/\left\{1 + \frac{2n}{p}\right\}$
2	TRUNCATED CONE DEPTH m	TAKE m = p/2 AS THE BEST ESTIMATE

Ratio of the A & B predictions of activity for the objects shown in Fig. 7.9.

Fig. 7.11

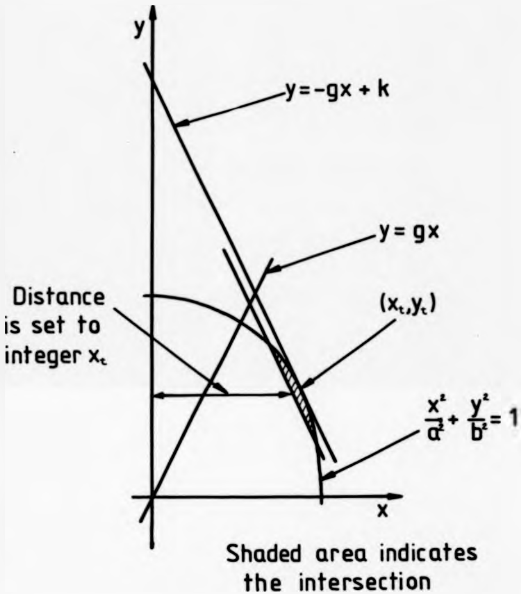

MODEL USED TO CALCULATE THE RATIO A/B FOR AN ELLIPSE

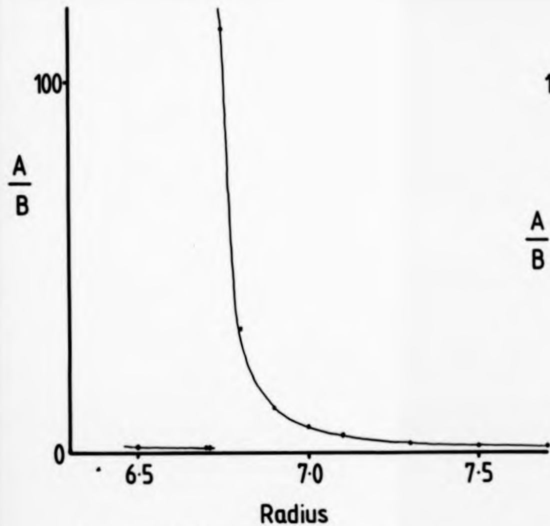

VARIATION OF A/B WITH CHANGE IN SPHERE RADIUS

Fig. 7.13

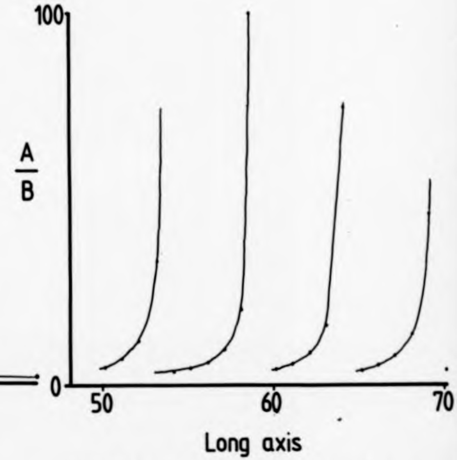

VARIATION OF A/B WITH CHANGES IN THE LONG AXIS WITH A SHORT AXIS OF 50 UNITS

Fig. 7.12

There is a large change in the ratio (A/B) caused by the variation in the intersection between the objects edge and the appropriate raysum. This prevents a simple assessment of the predicted activity being used to estimate the number of planes in the error volume which should be included in the reconstruction.

7.5 Error Volume Correction by Examination of the Reconstruction Volume

In the previous two sections the two obvious techniques to determine the extent of the object in the error volume have been examined. These do not offer a solution to the problem of correcting the reconstruction volume. The activity prediction in the error volume is dependent on the object shape and the prediction technique. With the impedance operator, the is no relation which gives a unique correction to the error volume. On the other hand, for a curved object, the beginning of the error volume can be determined from curvature and viewing angle. Since the object is curved, as for an ellipsoid, the object is known to extend into that error volume, Fig. 7.14, although the amount by which the object extends is unknown. If the LV is assumed to be ellipsoidal, then some reduction in the error volume should improve the reconstruction volume.

The error between the predicted and corrected volume compared to the object volume can be easily calculated for a simple hemi-ellipsoid with a chosen error volume reduction. Using the same ellipsoid model as described in Appendix 8, the co-ordinates of the tangent (X_T, Y_T) to the ellipsoid was obtained along with the distance of the error volumes propagation (Y_I), Fig. 7.14. The extent of this propagation was reduced to Y_R

Where $Y_R = Y_T + (Y_I - Y_T) / f$ - 7.5

Fig. 7.14

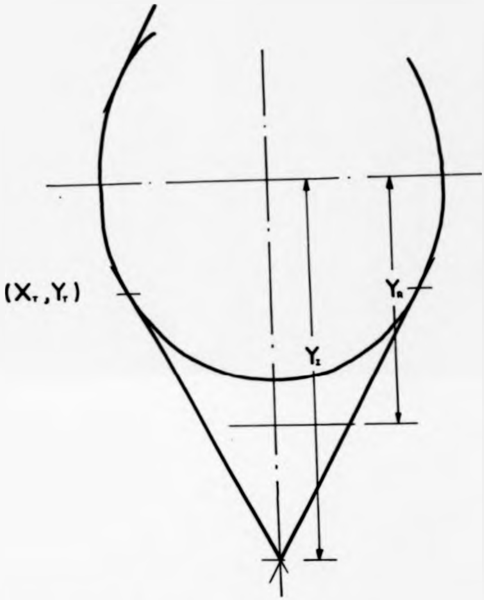

THE ERROR VOLUME ASSOCIATED WITH AN ELLIPSOID OBJECT
FOR A QUAD 26.6° LECT SYSTEM

Where f is an arbitrarily chosen factor. The error between the predicted/corrected and object volume is shown in Fig. 7.15 for a minor axis of 7 and 50 and f = 2. This shows that the volume error decreases quite rapidly from a spherical object and that there is little difference in the error with minor axis.

This reconstruction correction technique would need to be reversed in a reconstruction program. Also, the factor f which was 2 above could be chosen to reduce the error even further over a range of chosen major: minor axis ratios. To reverse the correction technique, the plane with the greatest radius would be obtained. The plane P_I corresponding to the distance of propagation Y_I is then obtained, all by inspection. From the viewing angle, the radius at which a tangent occurs is also found. This radius corresponds to X_T and the plane (P_T) containing the closest radius to X_T will be assumed to lie where the error volume begins. The number of planes in the reconstruction between P_T and P_I is reduced by a preselected number and the reconstruction allowed to continue.

This correction can be built into a renconstruction program. As an example, the QUAD (26.6°) LECT reconstruction program of a sphere was modified to calculate this correction, Appendix 9. The factor f in equation 7.5 was set to 3.2 which decreases the error in reconstruction volume for near spherical objects. The details of the correction are listed in Table 7.2.

Fig 7.16 shows transverse profiles across the tomograms compared to the ideal distribution and the predictions obtained using the standard QUAD (26.6°) system. Although the activity prediction is still incorrect, the distribution of activity is better and the reconstructed volume is improved.

Fig. 7.15

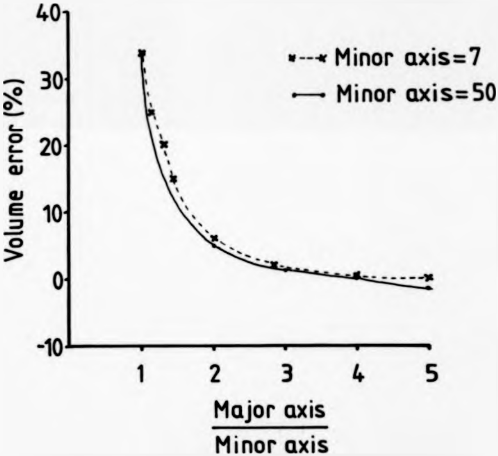

VARIATION IN THE ERROR BETWEEN TRUE AND CORRECTED OBJECT VOLUME, FOR A SIMPLE ERROR VOLUME CORRECTION TECHNIQUE

TABLE 7.2

PLANE	RADIUS	MAX RADIUS	P MAX	P_I	P_T
1	2				
2	3				
3	4				
4	5				
5	6				
6	7	7	6		
7	6				7
8	5				
9	4				
10	3				
11	2				
12	1			12	
13	0				

• $Y_I = 12 - 6 = 6$, $Y_T = 7 - 6 = 1$

• $Y_R = 1 + \dfrac{(6 - 1)}{3.2} = 2.56$

• $P_R = 8$, TO NEAREST PLANE

• USE PLANES 4, 5, 6, 7, 8.

Details of reconstruction volume correction for QUAD (26.6°) LECT reconstruction of a sphere.

Fig. 7.16

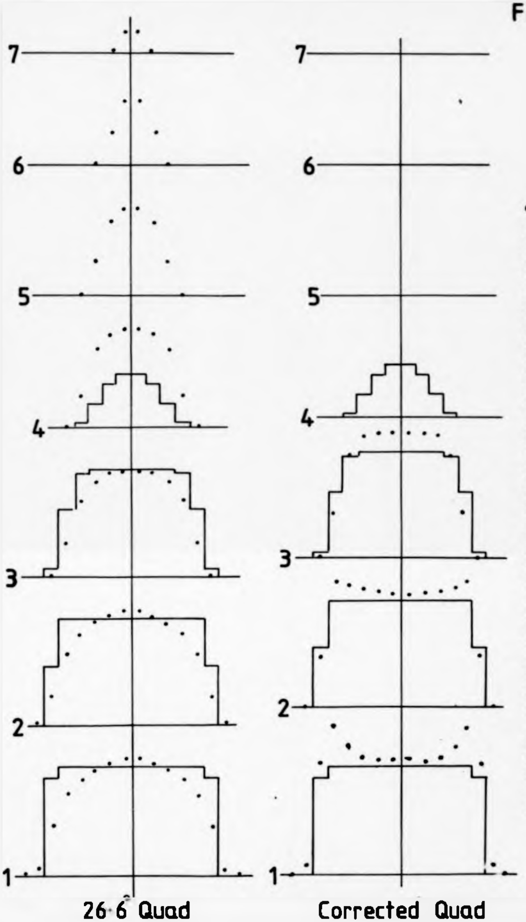

THE PREDICTED ACTIVITY PROFILES ACROSS THE CENTRE OF THE TOMOGRAMS GENERATED BY A 26.6° QUAD LECT SYSTEM AND A 26.6° QUAD LECT SYSTEM WITH A BUILT IN ERROR VOLUME CORRECTION, RECONSTRUCTING A SPHERICAL OBJECT

7.6 Conclusion

Although the LV blood pool is a simply shaped object with uniformly distributed activity, it is not straightforward to correct the reconstructed activity prediction. However, due to its curved shape the pool permits the error volume to be decreased though not entirely elimimated.

Problems in implementing this correction in a real system may arise from the identification of the tomogram boundary. Also, the irregular pool boundary within a tomogram may make radius measurement difficult, particularly with areas of akinesis and diskineses of the wall. Also, the fact that a gated blood pool study will contain several frames of the pool at different extents of ventricle contraction means the correction will need to span a range of shapes. All the reconstructions for a single study will have error volumes associated with them, both before and after correction. The error volume will be reduced, but it may still conceal or inadvertently introduce an abnormality into the scan.

CHAPTER 8
CONCLUSION

Longitudinal emission computed tomography (LECT) appears to suffer from a basic problem: the area of intersection of back projected rays suggests that an object's volume may be exaggerated. A volume external to the true object volume is generated as part of the reconstruction volume and the size and shape of this error volume is dependent on the LECT system and the size of the object. From this the concept of an error volume and an associated error volume index (EVI) arises. This index quantifies the error in a LECT system and permits the intercomparison of systems. The consequences of modifications to systems by the alterations or addition of views can also be assessed using the EVI

The physical performance of LECT systems are very comparable. However, the inter planar resolution and the predicted plane position are very dependent on the frequency (m^{-1}) of planes used in the reconstruction. The plane frequency should be made as high as possible, up to a limit determined by the sampling frequency in the image, and the viewing angle of the system.

In Thallium-201 perfusion imaging, rotating slant hole (RSH) LECT shows no improvement over planar imaging for either infarct detection or ischaemic heart disease detection. The effect of the error volume in the reconstruction is to produce artefacts in the tomograms when there is angulation between the camera and the left ventricle (LV) axis. These artefacts appear as defects in the myocardium and significantly affect the diagnostic performance of the test. In cardiac blood pool imaging, the prediction of activity in the error volume distorts the reconstructed blood pool. It is not possible to correct the reconstruction volume which is generated with the iterative least squares reconstruction technique (ILRST) using the prior knowledge of uniform activity distribution. However, the error volume can be reduced by assuming the LV is an ellipsoid and applying a suitable correction.

Positive opportunities still exist in LECT cardiac imaging. Gated blood pool LECT has still to be evaluated fully and the simple correction mentioned above can be used to reduce the error volume in a clinical trial. The possibility of developing an alternative predicting function which will permit the correction of the reconstruction volume for a uniformly distributed object activity should be examined. In Thallium-201 perfusion, the non-uniform activity distribution is not suitable for correction. There is no point in continuing to use the present types of LECT system in this application, and additional views should be employed to reduce the error volume. The practical advantage of adding views has been demonstrated by Koral (1982, 1984). However, a single additional planar view would be a simpler addition than that of Koral and would give as good a reduction in the error volume. Although the activity prediction will continue to be incorrect, the error volume will be reduced and the clinical consequences of this should be evaluated.

APPENDIX 1

ITERATIVE LEAST SQUARES RECONSTRUCTION TECHNIQUE (ILSRT) PROGRAM FOR A (26.6°) QUAD LECT SYSTEM WITH SIMULATED 28 x 28 MATRIX VIEW DATA OF A SPHERE

```
FILE: SQUIRT02 FORTRAN  A    ** UNIVERSITY OF WARWICK **                PAGE 001

 $RESET FREE
C      THIS PROGRAM IS FOR A QUAD SYSTEM ONLY
C      QUADRANT PROJECTION ITERATIVE RECONSTRUCTION TECHNIQUE
FILE   12(KIND=DISK,TITLE='JAM01/RESULT.',MAXRECSIZE=20,NEWFILE)
FILE   4(KIND=DISK,TITLE='JAM01/RSDAT.',FILETYPE=7)
FILE   3(KIND=DISK,TITLE='JAM01/LSDAT.',FILETYPE=7)
       REAL NUM
       DIMENSION P(3136),R(3136),A(3276),DA(3276),ILST(50),IX(4,2),
      CIY(4,2),IRA(28)
       EQUIVALENCE(IX(1),ILST(1)),(IY(1),ILST(31))
       DATA (ILST(I),I=1,48)/1,0,1,2,0,1,2,1,28,13,0,0,1,0,7*1,9*0,
      C1,0,1,0,0,1,0,1,2*0,-1,0,1,0,0,-1,0,1/
       WRITE(6,2000)
1      READ(5,/)ILST(17)
       IF(ILST(17).LT.1.OR.ILST(17).GT.2) GOTO 1
       IF(ILST(17).EQ.2) GOTO 30
C      READS IN INITIAL PLANE DISTRIBUTION
       WRITE(6,2010)
       READ(3,/)(A(I),I=1,3276)
       DO 20 I=1,3276
       DA(I)=0.0
20     CONTINUE
       GOTO 40
30     DO 40 I=1,3276
       A(I)=0.0
       DA(I)=0.0
40     CONTINUE
       WRITE(6,2020)
       READ(5,/)ILST(12)
       WRITE(6,2030)
       READ(5,/)ILST(15)
       WRITE(6,2040)
       READ(5,/)ILST(16)
C      READS IN PROJECTION DATA
       WRITE(6,2080)
       READ(4,/)(P(I),I=1,3136)
 10    CONTINUE
C      CALCULATION OF RAYSUMS AND PLANE INCREMENTS
       WRITE(6,3000)
       DO 100 IT=1,4
       KA=(IT-1)*ILST(9)**2
       DO 110 L=1,ILST(9)
       KB=(L-1)*ILST(9)
       DO 120 K=1,ILST(9)
       IZ=K+KA+KB
       IV=0
       CT=0
       DO 130 N=1,ILST(10)
       NW=ILST(9)-2*N
       KK=K-IX(IT,2)*N
       IF(KK.LT.1.OR.KK.GT.NW) GOTO 130
       LL=L-IX(IT,1)*N
       IF(LL.LT.1.OR.LL.GT.NW) GOTO 130
       IW=IV+(LL-1)*NW+KK
       IWP=IW+IY(IT,2)*NW+IY(IT,1)
```

```
      IWM=IW-IY(IT,2)*NW-IY(IT,1)
      CT=CT+A(IW)*0.75
      IF(IT.EQ.2.OR.IT.EQ.4) GOTO 135
      IF(KK.GT.1) CT=CT+A(IWM)*0.125
      IF(KK.LT.NW) CT=CT+A(IWP)*0.125
      GOTO 145
135   IF(LL.GT.1) CT=CT+A(IWM)*0.125
      IF(LL.LT.NW) CT=CT+A(IWP)*0.125
145   CONTINUE
      IV=IV+NW**2
130   CONTINUE
      R(IZ)=CT
120   CONTINUE
110   CONTINUE
100   CONTINUE
C     CALCULATES THE INCREMENTS
      WRITE(6,3100)
      IV=0
      DO 200 N=1,ILST(10)
      NLT=ILST(9)-2*N
      DO 210 J=1,NLT
      DO 220 I=1,NLT
      IV=IV+1
      NUM=0
      DEN=0
      DO 240 IT=1,4
      II=I+IX(IT,2)*N
      JJ=J+IX(IT,1)*N
      IZ=II+(JJ-1)*ILST(9)+(IT-1)*ILST(9)**2
      IF(P(IZ).EQ.0) GOTO 250
      NUM=NUM+0.75*(P(IZ)-R(IZ))/P(IZ)
      DEN=DEN+0.75**2/P(IZ)
      IZP=IZ+IY(IT,2)*ILST(9)+IY(IT,1)
      IZM=IZ-IY(IT,2)*ILST(9)-IY(IT,1)
      IF(IT.EQ.2.OR.IT.EQ.4) GOTO 260
      IF(II.EQ.1) GOTO 270
      IF(P(IZM).EQ.0.0) GOTO 270
      NUM=NUM+(P(IZM)-R(IZM))/P(IZM)*0.125
      DEN=DEN+0.125**2/P(IZM)
270   IF(II.EQ.ILST(9)) GOTO 240
      IF(P(IZP).EQ.0.0) GOTO 240
      NUM=NUM+0.125*(P(IZP)-R(IZP))/P(IZP)
      DEN=DEN+0.125**2/P(IZP)
      GOTO 240
260   IF(JJ.EQ.1) GOTO 290
      IF(P(IZM).EQ.0.0) GOTO 290
      NUM=NUM+(P(IZM)-R(IZM))/P(IZM)*0.125
      DEN=DEN+0.125**2/P(IZM)
290   IF(JJ.EQ.ILST(9)) GOTO 240
      IF(P(IZP).EQ.0.0) GOTO 240
      NUM=NUM+(P(IZP)-R(IZP))/P(IZP)*0.125
      DEN=DEN+0.125**2/P(IZP)
240   CONTINUE
      DA(IV)=NUM/DEN
      GOTO 220
```

```
 250  A(IV)=0
      DA(IV)=0
 220  CONTINUE
 210  CONTINUE
 200  CONTINUE
C     CALCULATES THE DELTA FACTOR
      WRITE(6,3200)
      NUM=0
      DEN=0
      DO 400 IT=1,4
      KA=(IT-1)*ILST(9)**2
      DO 410 L=1,ILST(9)
      KB=(L-1)*ILST(9)
      DO 420 K=1,ILST(9)
      IZ=K+KA+KB
      IF(P(IZ).EQ.0.0) GOTO 420
      ZCOM=0
      IV=0
      DO 430 N=1,ILST(10)
      NW=ILST(9)-2*N
      KK=K-IX(IT,2)*N
      IF(KK.LT.1.OR.KK.GT.NW) GOTO 430
      LL=L-IX(IT,1)*N
      IF(LL.LT.1.OR.LL.GT.NW) GOTO 430
      IW=IV+KK+(LL-1)*NW
      IWP=IW+IY(IT,2)*NW+IY(IT,1)
      IWM=IW-IY(IT,2)*NW-IY(IT,1)
      ZCOM=ZCOM+DA(IW)*0.75
      IF(IT.EQ.2.OR.IT.EQ.4) GOTO 440
      IF(KK.GT.1) ZCOM=ZCOM+DA(IWM)*0.125
      IF(KK.LT.NW) ZCOM=ZCOM+DA(IWP)*0.125
      GOTO 450
 440  IF(LL.GT.1) ZCOM=ZCOM+DA(IWM)*0.125
      IF(LL.LT.NW) ZCOM=ZCOM+DA(IWP)*0.125
 450  CONTINUE
      IV=IV+NW**2
 430  CONTINUE
      NUM=NUM+(P(IZ)-R(IZ))/P(IZ)*ZCOM
      DEN=DEN+ZCOM**2/P(IZ)
 420  CONTINUE
 410  CONTINUE
 400  CONTINUE
      WRITE(6,/) NUM,DEN
      D=NUM/DEN
      WRITE(12,1040)
      WRITE(6,/) D
C     CORRECTS THE PLANE DISTRIBUTIONS
      WRITE(6,3300)
      IV=0
      DO 500 N=1,ILST(10)
      NLT=ILST(9)-2*N
      DO 510 J=1,NLT
      DO 520 I=1,NLT
      IV=IV+1
      A(IV)=A(IV)+D*DA(IV)
```

```
      IF(A(IV).LE.0.0) A(IV)=0.0
 520  CONTINUE
 510  CONTINUE
 500  CONTINUE
C     PRINT ROUTINE FOR PLANES AND RAYSUMS
      WRITE(12,1000) ILST(13)
      IF(ILST(15).NE.1) GOTO 900
C     PRINT RAYSUMS
      WRITE(6,2050)
      DO 910 IT=1,4
      WRITE(12,1010)IT
      KA=(IT-1)*ILST(9)**2
      DO 920 L=1,ILST(9)
      KB=(L-1)*ILST(9)
      DO 930 K=1,ILST(9)
      IZ=K+KA+KB
      IRA(K)=R(IZ)
 930  CONTINUE
      WRITE(12,1020)(IRA(N),N=1,ILST(9))
 920  CONTINUE
 910  CONTINUE
 900  IF(ILST(16).NE.2.AND.ILST(13).NE.ILST(12)) GOTO 990
C     PRINT PLANES
      WRITE(6,2060)
      IV=0
      DO 940 N=1,ILST(10)
      WRITE(12,1030)N
      NW=ILST(9)-2*N
      DO 950 I=1,NW
      DO 960 J=1,NW
      IV=IV+1
      IRA(J)=A(IV)
 960  CONTINUE
      WRITE(12,1020)(IRA(K),K=1,NW)
 950  CONTINUE
 940  CONTINUE
 990  IF(ILST(13).EQ.ILST(12)) GOTO 995
      ILST(13)=ILST(13)+1
      GOTO 10
 995  WRITE(6,2070)
1000  FORMAT(1H ,6X,10HITERATION ,I3/1HO)
1010  FORMAT(1H ,6X,7HRAYSUM ,I2/1HO)
1020  FORMAT(1H ,14(1X,I6)/1H ,14(1X,I6))
1030  FORMAT(1H ,5X,6HPLANE ,I3/1HO)
1040  FORMAT(5X,8HDELTA = ,1PE12.4)
2000  FORMAT(1H ,5X,35HINPUT THE FIRST APPROXIMATION INDEX/
     C1H ,22X,8H1. IDEAL/1H ,22X,21H2. IMPEDANCE OPERATOR/1H /
     C1H ,22X,11HINPUT 1-2  )
2010  FORMAT(1HO,5X,36HNOW INPUTING THE FIRST APPROXIMATION)
2020  FORMAT(1HO,5X,41HINPUT THE NUMBER OF ITERATIONS REQUIRED  )
2030  FORMAT(1HO,5X,44HDO YOU WISH THE RAYSUMS PRINTED 1-YES,2-NO  )
2040  FORMAT(1HO,5X,26HDO YOU WISH PLANES PRINTED/
     C1H ,22X,24H1. AFTER FINAL ITERATION/
     C1H ,22X,23H2. AFTER EACH ITERATION/1H /
     C1H ,22X,11HINPUT 1-2  )
```

```
2050  FORMAT(1H0,5X,20HNOW PRINTING RAYSUMS)
2060  FORMAT(1H0,5X,32HNOW PRINTING PLANE DISTRIBUTIONS)
2070  FORMAT(1H0,15X,11H*** END ***)
2080  FORMAT(1H0,5X,28HNOW INPUTING THE PROJECTIONS)
3000  FORMAT(1H0,5X,23HNOW CALCULATING RAYSUMS)
3100  FORMAT(1H0,5X,26HNOW CALCULATING INCREMENTS)
3200  FORMAT(1H0,5X,21HNOW CALCULATING DELTA)
3300  FORMAT(1H0,5X,25HNOW CORRECTING THE PLANES)
      LOCK(12)
      STOP
      END
```

APPENDIX 2

PROGRAM TO DETERMINE MAXIMUM ERROR VOLUME DIRECTIONS AND ERROR VOLUME INDEX (EVI) FOR UP TO 15 VIEWING DIRECTIONS.

```
LIST

6  REM    PROGRAM TO CALCULATE MAX ERROR
8  REM    VOLUME DIRECTIONS AND EVI'S
10  REM  FOR UP TO 15 VIEWS
12  HOME
15  DIM X(16),Y(16),Z(16),P(4,120),M(4,120)
18  DEF  FN TRK(I) = ( INT (I * 1E3)) / 1E3
20  INPUT "INPUT NO. OF VECTORS ";N: PRINT
25  FOR J = 1 TO N
30  INPUT "X,Y,Z        ";X(J),Y(J),Z(J)
35  NEXT J
38 K = 1
40  FOR I = 1 TO N - 1
45  FOR J = I + 1 TO N
47 D1 = X(I) + X(J):D2 = Y(I) + Y(J):D3 = Z(I) + Z(J)
50 D =  SQR (D1 ^ 2 + D2 ^ 2 + D3 ^ 2)
60 P(1,K) = D1 / D:P(2,K) = D2 / D:P(3,K) = D3 / D
70 D1 = X(I) - X(J):D2 = Y(I) - Y(J):D3 = Z(I) - Z(J)
80 D =  SQR (D1 ^ 2 + D2 ^ 2 + D3 ^ 2)
120 M(1,K) = D1 / D:M(2,K) = D2 / D:M(3,K) = D3 / D
130 K = K + 1
140  NEXT J
150  NEXT I
160 K9 = K - 1
200  FOR K = 1 TO K9
210 P5 = 10:M5 = 10
220  FOR J = 1 TO N
230 C5 = P(1,K) * X(J) + P(2,K) * Y(J) + P(3,K) * Z(J)
240 C5 =  ABS (C5)
250  IF C5 < P5 THEN P5 = C5
260 C5 = M(1,K) * X(J) + M(2,K) * Y(J) + M(3,K) * Z(J)
270 C5 =  ABS (C5)
280  IF C5 < M5 THEN M5 = C5
290  NEXT J
300 P(4,K) =  FN TRK(P5):M(4,K) =  FN TRK(M5)
310  NEXT K
400  PR# 1: TEXT : PRINT
410  PRINT "  MAX ERROR VOL DIRECTIONS AND EVI": PRINT
420  PRINT  TAB( 11)"DIRECTION"
430  PRINT  TAB( 63)"EVI"
440  PRINT "   X              Y                   Z"
450  PRINT
460  FOR K = 1 TO K9
470  PRINT  FN TRK(P(1,K)), FN TRK(P(2,K)), FN TRK(P(3,K)), TAB( 32)P(4,K
     )
490  PRINT  FN TRK(M(1,K)), FN TRK(M(2,K)), FN TRK(M(3,K)), TAB( 32)M(4,K
     )
500  NEXT K
510  PRINT "       END"
550  PR# 0
600  END
```

APPENDIX 3

ILSRT PROGRAM FOR A (26.6°) QUAD PLUS ONE PLANAR (+1) VIEW LECT SYSTEM


```
$RESET FREE
C      THIS PROGRAM IS FOR QUAD+1 PLANAR VIEW
FILE  12(KIND=DISK,TITLE='JAM01/RESULT.',MAXRECSIZE=20,NEWFILE)
FILE  4(KIND=DISK,TITLE='JAM01/RSDAT.',FILETYPE=7)
FILE  3(KIND=DISK,TITLE='JAM01/LSDAT.',FILETYPE=7)
FILE  2(KIND=DISK,TITLE='JAM01/PRSDAT.',FILETYPE=7)
       REAL NUM
       DIMENSION P(3920),R(3920),A(3276),DA(3276),ILST(50),IX(4,2),
      CIY(4,2),IRA(28)
       EQUIVALENCE(IX(1),ILST(1)),(IY(1),ILST(31))
       DATA (ILST(I),I=1,48)/1,0,1,2,0,1,2,1,28,13,0,0,1,4,381,
      C3,381,980,1,0,1,0,0,1,0,1,280,-1,0,1,0,0,-1,0,1/
       WRITE(6,2000)
1      READ(5,/)ILST(17)
       IF(ILST(17).LT.1.OR.ILST(17).GT.2) GOTO 1
       IF(ILST(17).EQ.2) GOTO 30
C      READS IN INITIAL PLANE DISTRIBUTION
       WRITE(6,2010)
       READ(3,/)(A(I),I=1,3276)
       DO 20 I=1,3276
       DA(I)=0.0
20     CONTINUE
       GOTO 40
30     DO 40 I=1,3276
       A(I)=0.0
       DA(I)=0.0
40     CONTINUE
       WRITE(6,2020)
       READ(5,/)ILST(12)
       WRITE(6,2030)
       READ(5,/)ILST(15)
       WRITE(6,2040)
       READ(5,/)ILST(16)
C      READS IN PROJECTION DATA
       WRITE(6,2090)
       READ(5,/) ILST(14)
       WRITE(6,2080)
       READ(4,/)(P(I),I=1,3136)
       IF(ILST(14).LE.4) GOTO 10
       READ(2,/)(P(I),I=3137,3920)
 10    CONTINUE
C      CALCULATION OF RAYSUMS AND PLANE INCREMENTS
       WRITE(6,3000)
       DO 100 IT=1,ILST(14)
       KA=(IT-1)*ILST(9)**2
       IW=0
       DO 110 L=1,ILST(9)
       KB=(L-1)*ILST(9)
       DO 120 K=1,ILST(9)
       IZ=K+KA+KB
       IV=0
       CT=0
       IF(IT.LE.4) GOTO 140
       IF(L.LE.ILST(18)) GOTO 110
       NP=INT((L-ILST(18))/2+0.5)
```

```
      NW=ILST(9)-2*NP
      IF(L.LE.(ILST(18)+2)) GOTO 160
      IF(K.NE.1) GOTO 160
      MW=INT((ILST(18)+2*NP-L)/2+0.5)
      IW=IW+MW*(NW+2)**2
  160 IF(K.LE.NP.OR.K.GT.(NP+NW)) GOTO 120
      IV=IW+K
      DO 150 KP=1,NW
      CT=CT+A(IV+(KP-1)*NW)*0.5
  150 CONTINUE
      GOTO 130
  140 CONTINUE
      DO 130 N=1,ILST(10)
      NW=ILST(9)-2*N
      KK=K-IX(IT,2)*N
      IF(KK.LT.1.OR.KK.GT.NW) GOTO 130
      LL=L-IX(IT,1)*N
      IF(LL.LT.1.OR.LL.GT.NW) GOTO 130
      IW=IV+(LL-1)*NW+KK
      IWP=IW+IY(IT,2)*NW+IY(IT,1)
      IWM=IW-IY(IT,2)*NW-IY(IT,1)
      CT=CT+A(IW)*0.75
      IF(IT.EQ.2.OR.IT.EQ.4) GOTO 135
      IF(KK.GT.1) CT=CT+A(IWM)*0.125
      IF(KK.LT.NW) CT=CT+A(IWP)*0.125
      GOTO 145
  135 IF(LL.GT.1) CT=CT+A(IWM)*0.125
      IF(LL.LT.NW) CT=CT+A(IWP)*0.125
  145 CONTINUE
      IV=IV+NW**2
  130 CONTINUE
      R(IZ)=CT
  120 CONTINUE
  110 CONTINUE
  100 CONTINUE
C     CALCULATES THE INCREMENTS
      WRITE(6,3100)
      IV=0
      DO 200 N=1,ILST(10)
      NLT=ILST(9)-2*N
      DO 210 J=1,NLT
      DO 220 I=1,NLT
      IV=IV+1
      NUM=0
      DEN=0
      DO 240 IT=1,ILST(14)
      IF(IT.LE.4) GOTO 230
      IE=(2*(N-1)+ILST(18))*ILST(9)+I+N+3136
      IF(P(IE).EQ.0.0.AND.P(IE+ILST(9)).EQ.0.0) GOTO 250
      DO 280 IS=1,2
      IE=IE+(IS-1)*ILST(9)
      IF(P(IE).EQ.0.0) GOTO 280
      NUM=NUM+0.5*(P(IE)-R(IE))/P(IE)
      DEN=DEN+0.5**2/P(IE)
  280 CONTINUE
```

```
      GOTO 240
 230  CONTINUE
      II=I+IX(IT,2)*M
      JJ=J+IX(IT,1)*M
      IZ=II+(JJ-1)*ILST(9)+(IT-1)*ILST(9)**2
      IF(P(IZ).EQ.0) GOTO 250
      NUM=NUM+0.75*(P(IZ)-R(IZ))/P(IZ)
      DEN=DEN+0.75**2/P(IZ)
      IZP=IZ+IY(IT,2)*ILST(9)+IY(IT,1)
      IZM=IZ-IY(IT,2)*ILST(9)-IY(IT,1)
      IF(IT.EQ.2.OR.IT.EQ.4) GOTO 260
      IF(II.EQ.1) GOTO 270
      IF(P(IZM).EQ.0.0) GOTO 270
      NUM=NUM+(P(IZM)-R(IZM))/P(IZM)*0.125
      DEN=DEN+0.125**2/P(IZM)
 270  IF(II.EQ.ILST(9)) GOTO 240
      IF(P(IZP).EQ.0.0) GOTO 240
      NUM=NUM+0.125*(P(IZP)-R(IZP))/P(IZP)
      DEN=DEN+0.125**2/P(IZP)
      GOTO 240
 260  IF(JJ.EQ.1) GOTO 290
      IF(P(IZM).EQ.0.0) GOTO 290
      NUM=NUM+(P(IZM)-R(IZM))/P(IZM)*0.125
      DEN=DEN+0.125**2/P(IZM)
 290  IF(JJ.EQ.ILST(9)) GOTO 240
      IF(P(IZP).EQ.0.0) GOTO 240
      NUM=NUM+(P(IZP)-R(IZP))/P(IZP)*0.125
      DEN=DEN+0.125**2/P(IZP)
 240  CONTINUE
      DA(IV)=NUM/DEN
      GOTO 220
 250  A(IV)=0
      DA(IV)=0
 220  CONTINUE
 210  CONTINUE
 200  CONTINUE
C     CALCULATES THE DELTA FACTOR
      WRITE(6,3200)
      NUM=0
      DEN=0
      DO 400 IT=1,ILST(14)
      KA=(IT-1)*ILST(9)**2
      IW=0
      DO 410 L=1,ILST(9)
      KB=(L-1)*ILST(9)
      DO 420 K=1,ILST(9)
      IZ=K+KA+KB
      IF(P(IZ).EQ.0.0) GOTO 420
      ZCOM=0
      IV=0
      IF(IT.LE.4) GOTO 460
      IF(L.LE.ILST(18)) GOTO 410
      NP=INT((L-ILST(18))/2+0.5)
      NW=ILST(9)-2*NP
      IF(L.LE.(ILST(18)+2)) GOTO 470
```

```
      IF(K.NE.1) GOTO 470
      MW=INT((ILST(18)+2*NP-L)/2+0.5)
      IW=IW+MW*(NW+2)**2
  470 IF(K.LE.NP.OR.K.GT.(NP+NW)) GOTO 420
      IV=IW+K
      DO 480 KP=1,NW
      ZCOM=ZCOM+DA(IV+(KP-1)*NW)*0.5
  480 CONTINUE
      GOTO 430
  460 CONTINUE
      DO 430 N=1,ILST(10)
      NW=ILST(9)-2*N
      KK=K-IX(IT,2)*N
      IF(KK.LT.1.OR.KK.GT.NW) GOTO 430
      LL=L-IX(IT,1)*N
      IF(LL.LT.1.OR.LL.GT.NW) GOTO 430
      IW=IV+KK+(LL-1)*NW
      IWP=IW+IY(IT,2)*NW+IY(IT,1)
      IWM=IW-IY(IT,2)*NW-IY(IT,1)
      ZCOM=ZCOM+DA(IW)*0.75
      IF(IT.EQ.2.OR.IT.EQ.4) GOTO 440
      IF(KK.GT.1) ZCOM=ZCOM+DA(IWM)*0.125
      IF(KK.LT.NW) ZCOM=ZCOM+DA(IWP)*0.125
      GOTO 450
  440 IF(LL.GT.1) ZCOM=ZCOM+DA(IWM)*0.125
      IF(LL.LT.NW) ZCOM=ZCOM+DA(IWP)*0.125
  450 CONTINUE
      IV=IV+NW**2
  430 CONTINUE
      NUM=NUM+(P(IZ)-R(IZ))/P(IZ)*ZCOM
      DEN=DEN+ZCOM**2/P(IZ)
  420 CONTINUE
  410 CONTINUE
  400 CONTINUE
      WRITE(6,/) NUM,DEN
      D=NUM/DEN
      WRITE(12,1040)
      WRITE(6,/) D
C     CORRECTS THE PLANE DISTRIBUTIONS
      WRITE(6,3300)
      IV=0
      DO 500 N=1,ILST(10)
      NLT=ILST(9)-2*N
      DO 510 J=1,NLT
      DO 520 I=1,NLT
      IV=IV+1
      A(IV)=A(IV)+D*DA(IV)
      IF(A(IV).LE.0.0) A(IV)=0.0
  520 CONTINUE
  510 CONTINUE
  500 CONTINUE
C     PRINT ROUTINE FOR PLANES AND RAYSUMS
      WRITE(12,1000) ILST(13)
      IF(ILST(15).NE.1) GOTO 900
C     PRINT RAYSUMS
```

```
      WRITE(6,2050)
      DO 910 IT=1,ILST(14)
      WRITE(12,1010)IT
      KA=(IT-1)*ILST(9)**2
      DO 920 L=1,ILST(9)
      KB=(L-1)*ILST(9)
      DO 930 K=1,ILST(9)
      IZ=K+KA+KB
      IRA(K)=R(IZ)
 930  CONTINUE
      WRITE(12,1020)(IRA(N),N=1,ILST(9))
 920  CONTINUE
 910  CONTINUE
 900  IF(ILST(16).NE.2.AND.ILST(13).NE.ILST(12)) GOTO 990
C     PRINT PLANES
      WRITE(6,2060)
      IV=0
      DO 940 N=1,ILST(10)
      WRITE(12,1030)N
      NW=ILST(9)-2*N
      DO 950 I=1,NW
      DO 960 J=1,NW
      IV=IV+1
      IRA(J)=A(IV)
 960  CONTINUE
      WRITE(12,1020)(IRA(K),K=1,NW)
 950  CONTINUE
 940  CONTINUE
 990  IF(ILST(13).EQ.ILST(12)) GOTO 995
      ILST(13)=ILST(13)+1
      GOTO 10
 995  WRITE(6,2070)
1000  FORMAT(1H ,6X,10HITERATION ,I3/1H0)
1010  FORMAT(1H ,6X,7HRAYSUM ,I2/1H0)
1020  FORMAT(1H ,14(1X,I6)/1H ,14(1X,I6))
1030  FORMAT(1H ,5X,6HPLANE ,I3/1H0)
1040  FORMAT(5X,8HDELTA = ,1PE12.4)
2000  FORMAT(1H ,5X,35HINPUT THE FIRST APPROXIMATION INDEX/
     C1H ,22X,8H1. IDEAL/1H ,22X,21H2. IMPEDANCE OPERATOR/1H /
     C1H ,22X,11HINPUT 1-2  )
2010  FORMAT(1H0,5X,36HNOW INPUTING THE FIRST APPROXIMATION)
2020  FORMAT(1H0,5X,41HINPUT THE NUMBER OF ITERATIONS REQUIRED  )
2030  FORMAT(1H0,5X,44HDO YOU WISH THE RAYSUMS PRINTED 1-YES,2-NO  )
2040  FORMAT(1H0,5X,26HDO YOU WISH PLANES PRINTED/
     C1H ,22X,24H1. AFTER FINAL ITERATION/
     C1H ,22X,23H2. AFTER EACH ITERATION/1H /
     C1H ,22X,11HINPUT 1-2  )
2050  FORMAT(1H0,5X,20HNOW PRINTING RAYSUMS)
2060  FORMAT(1H0,5X,32HNOW PRINTING PLANE DISTRIBUTIONS)
2070  FORMAT(1H0,15X,11H*** END ***)
2080  FORMAT(1H0,5X,28HNOW INPUTING THE PROJECTIONS)
2090  FORMAT(1H0,5X,33HINPUT THE NUMBER OF PROJECTIONS  )
3000  FORMAT(1H0,5X,23HNOW CALCULATING RAYSUMS)
3100  FORMAT(1H0,5X,26HNOW CALCULATING INCREMENTS)
3200  FORMAT(1H0,5X,21HNOW CALCULATING DELTA)
```

```
3300  FORMAT(1H0,5X,25HNOW CORRECTING THE PLANES)                   00027600
      LOCK(12)                                                      00027700
      STOP                                                          00027800
      END                                                           00027900
```

APPENDIX 4

ILSRT PROGRAM FOR A DOUBLE (2x) (26.6°) QUAD LECT SYSTEM


```
$RESET FREE
C     THIS PROGRAM IS FOR A DOUBLE QUAD SYSTEM
C     QUADRANT PROJECTION ITERATIVE RECONSTRUCTION TECHNIQUE
FILE  12(KIND=DISK,TITLE="JAM01/RESULT.",MAXRECSIZE=20,NEWFILE)
FILE  4(KIND=DISK,TITLE="JAM01/RSDAT.",FILETYPE=7)
FILE  3(KIND=DISK,TITLE="JAM01/LSDAT.",FILETYPE=7)
FILE  2(KIND=DISK,TITLE="JAM01/OSDAT.",FILETYPE=7)
      REAL NUM
      DIMENSION P(6272),R(6272),A(3276),DA(3276),ILST(50),IX(4,2),
     CIY(4,2),IRA(20),RF(4)
      EQUIVALENCE(IX(1),ILST(1)),(IY(1),ILST(31))
      DATA (ILST(I),I=1,40)/1,0,1,2,0,1,2,1,20,13,0,0,1,4,381,
     C3,381,980,1,0,1,0,0,1,0,1,280,-1,0,1,0,0,-1,0,1/
      DATA (RF(I),I=1,4)/0.375,0.5,0.5,0.375/
      WRITE(6,2000)
1     READ(5,/)ILST(17)
      IF(ILST(17).LT.1.OR.ILST(17).GT.2) GOTO 1
      IF(ILST(17).EQ.2) GOTO 30
C     READS IN INITIAL PLANE DISTRIBUTION
      WRITE(6,2010)
      READ(3,/)(A(I),I=1,3276)
      DO 20 I=1,3276
      DA(I)=0.0
20    CONTINUE
      GOTO 40
30    DO 40 I=1,3276
      A(I)=0.0
      DA(I)=0.0
40    CONTINUE
      WRITE(6,2020)
      READ(5,/)ILST(12)
      WRITE(6,2030)
      READ(5,/)ILST(15)
      WRITE(6,2040)
      READ(5,/)ILST(16)
C     READS IN PROJECTION DATA
      WRITE(6,2090)
      READ(5,/) ILST(14)
      WRITE(6,2080)
      READ(4,/)(P(I),I=1,3136)
      IF(ILST(14).LE.4) GOTO 10
      READ(2,/)(P(I),I=3137,6272)
 10   CONTINUE
C     CALCULATION OF RAYSUMS AND PLANE INCREMENTS
      LNT=2*ILST(10)
      WRITE(6,3000)
      DO 100 IT=1,ILST(14)
      WRITE(6,5000)IT
 5000 FORMAT(1H ,4H5000,I3)
      KA=(IT-1)*ILST(9)**2
      IW=0
      DO 110 L=1,ILST(9)
      KB=(L-1)*ILST(9)
      DO 120 K=1,ILST(9)
      IZ=K+KA+KB
```

```
      IV=0
      CT=0
      IF(IT.LE.4) GOTO 140
      IF(IT.EQ.5.OR.IT.EQ.7) GOTO 600
      IF(L.LE.ILST(18).AND.IT.EQ.8) GOTO 110
      DO 150 N=1,LMT
      BR=L-ILST(18)+N*(7-IT)+IT-6
      NP=INT(BR/2)
      NP=NP+(IT-7)*2
      NW=ILST(9)-2*NP
      IF(N.NE.1) GOTO 160
      BR=L-ILST(18)-(NP-1)*2
      IEX=INT(BR/2)
      IS=2
      IF(IEX.EQ.1.AND.IT.EQ.6)IS=4
      IF(IEX.EQ.0.AND.IT.EQ.8)IS=4
 160  CONTINUE
      IF(NP.LT.1.OR.NP.GT.ILST(10)) GOTO 170
      IF(K.LE.NP.OR.K.GT.(NP+NW)) GOTO 170
      IF(N.LE.(NP-2)) GOTO 170
      IF(N.GT.(NP+NW-2)) GOTO 130
      IW=0
      IF(NP.EQ.1) GOTO 180
      DO 180 NIP=1,(NP-1)
      IIP=ILST(9)-2*NIP
      IW=IW+IIP**2
 180  CONTINUE
      IV=IW+(N-NP+1)*NW+K-NP
      CT=CT+RF(IS)*A(IV)
      NC=N-NP+2
      KC=K-NP
      IF(IS.EQ.4.AND.IT.EQ.6.AND.NC.EQ.(NW-1)) CT=CT+
     C0.125*A(IV+NW)
      IF(IS.EQ.1.AND.IT.EQ.8.AND.NC.EQ.2) CT=CT+
     C0.125*A(IV-NW)
      IF(NP.EQ.1) GOTO 185
      IF(IS.EQ.3.AND.IT.EQ.8.AND.NC.EQ.NW) CT=CT+
     C0.125*A(IW-ILST(9)+K+NP-1)
      IF(IS.EQ.2.AND.IT.EQ.6.AND.NC.EQ.1) CT=CT+
     C0.125*A(IW-(NW+2)**2+K-NP+1)
 185  CONTINUE
      IF(IS.EQ.2.OR.IS.EQ.3) GOTO 170
      IF(IT.EQ.8) GOTO 165
      IF(NC.EQ.1.AND.IS.EQ.4) GOTO 170
      IF(NC.EQ.NW.AND.IS.EQ.4) GOTO 170
 165  IF(IT.EQ.6.AND.IS.EQ.4) GOTO 190
      IF(IT.EQ.8.AND.IS.EQ.1) GOTO 190
      IF(NP.EQ.1) GOTO 170
      IWA=IW-(NW+2)**2+(N-NP+2)*(NW+2)+K-NP+1
      GOTO 195
 190  IF(NP.EQ.ILST(10).OR.KC.EQ.1.OR.KC.EQ.NW) GOTO 170
      IWA=IW+NW**2+(N-NP)*(NW-2)+K-NP-1
 195  CONTINUE
      CT=CT+0.125*A(IWA)
 170  CONTINUE
```

```
      IS=IS+1
      IF(IS.EQ.5)IS=1
150   CONTINUE
      GOTO 130
600   IF(L.LE.ILST(18)) GOTO 110
      BR=L-ILST(18)
      NP=INT(BR/2+0.5)
      IW=0
      IF(NP.EQ.1) GOTO 605
      DO 605 NIP=1,(NP-1)
      IIP=ILST(9)-2*NIP
      IW=IW+IIP**2
605   CONTINUE
      NW=ILST(9)-2*NP
      DO 610 N=1,(NW+NP-2)
      BR=N-1
      KK=INT(BR/2+0.5)
      IF(N.LE.(NP-2)) GOTO 610
      KT=K+(6-IT)*KK
      IF(KT.LE.NP.OR.KT.GT.(NP+NW)) GOTO 610
      IV=IW+(N-NP+1)*NW+KT-NP
      CT=CT+0.375*A(IV)
      BR=N+(7-IT)/2
      ID=(-1)**BR
      NC=N-NP+2
      IF(KT.EQ.(NP+1).AND.ID.EQ.-1) GOTO 620
      IF(KT.EQ.(NP+NW).AND.ID.EQ.1) GOTO 630
      CT=CT+0.125*A(IV+ID)
      GOTO 610
620   IF(IT.EQ.5.AND.NC.EQ.1) GOTO 610
      IF(IT.EQ.7.AND.NC.EQ.NW) GOTO 610
      IF(IT.EQ.5) CT=CT+0.125*A(IV-NW)
      IF(IT.EQ.7) CT=CT+0.125*A(IV+NW)
      GOTO 610
630   IF(IT.EQ.5.AND.NC.EQ.NW) GOTO 610
      IF(IT.EQ.7.AND.NC.EQ.1) GOTO 610
      IF(IT.EQ.5) CT=CT+0.125*A(IV+NW)
      IF(IT.EQ.7) CT=CT+0.125*A(IV-NW)
610   CONTINUE
      GOTO 130
140   CONTINUE
      DO 130 N=1,ILST(10)
      NW=ILST(9)-2*N
      KK=K-IX(IT,2)*N
      IF(KK.LT.1.OR.KK.GT.NW) GOTO 130
      LL=L-IX(IT,1)*N
      IF(LL.LT.1.OR.LL.GT.NW) GOTO 130
      IW=IV+(LL-1)*NW+KK
      IWP=IW+IY(IT,2)*NW+IY(IT,1)
      IWM=IW-IY(IT,2)*NW-IY(IT,1)
      CT=CT+A(IW)*0.75
      IF(IT.EQ.2.OR.IT.EQ.4) GOTO 135
      IF(KK.GT.1) CT=CT+A(IWM)*0.125
      IF(KK.LT.NW) CT=CT+A(IWP)*0.125
      GOTO 145
```

```
135   IF(LL.GT.1) CT=CT+A(IWM)*0.125
      IF(LL.LT.NW) CT=CT+A(IWP)*0.125
145   CONTINUE
      IV=IV+NW**2
130   CONTINUE
      R(IZ)=CT
120   CONTINUE
110   CONTINUE
100   CONTINUE
105   CONTINUE
C     CALCULATES THE INCREMENTS
      WRITE(6,3100)
      IV=0
      DO 200 N=1,ILST(10)
      NLT=ILST(9)-2*N
      DO 210 J=1,NLT
      DO 220 I=1,NLT
      IV=IV+1
      NUM=0
      DEN=0
      DO 240 IT=1,ILST(14)
      IF(IT.LE.4) GOTO 230
      IZT=0
      IZC=0
      IF(IT.EQ.5.OR.IT.EQ.7) GOTO 750
      BR=N-2+J
      LL=INT(BR/2+0.5)
      LL=ILST(10)+2*(N-1)+1+(IT-7)*LL
      IF(IT.EQ.6)LL=LL+1
      IF(LL.GT.ILST(9).OR.LL.LT.1) GOTO 240
      IZ=I+N+(LL-1)*ILST(9)+(IT-1)*ILST(9)**2
      IZC=IZC+1
      IF(P(IZ).EQ.0.0) GOTO 700
      NUM=NUM+0.5*(P(IZ)-R(IZ))/P(IZ)
      DEN=DEN+0.5**2/P(IZ)
      GOTO 705
700   IZT=IZT+1
705   RD=J+N-2+(IT-6)/2
      TST=RD-2*INT(RD/2)
      IF(TST.EQ.0)ID=1
      IF(TST.GT.0)ID=-1
      IF(LL.EQ.1.AND.ID.EQ.-1) GOTO 715
      IF(LL.EQ.ILST(9).AND.ID.EQ.1) GOTO 715
      IZL=IZ+ID*ILST(9)
      IZC=IZC+1
      IF(P(IZL).EQ.0.0) GOTO 710
      NUM=NUM+0.375*(P(IZL)-R(IZL))/P(IZL)
      DEN=DEN+0.375**2/P(IZL)
      GOTO 715
710   IZT=IZT+1
715   IF(LL.EQ.1.AND.ID.EQ.1) GOTO 725
      IF(LL.EQ.ILST(9).AND.ID.EQ.-1) GOTO 725
      IZS=IZ-ID*ILST(9)
      IZC=IZC+1
      IF(P(IZS).EQ.0.0) GOTO 720
```

```
      NUM=NUM+0.125*(P(IZS)-R(IZS))/P(IZS)
      DEN=DEN+0.125**2/P(IZS)
      GOTO 240
 720  IZT=IZT+1
 725  IF(IZT.EQ.IZC) GOTO 250
      GOTO 240
 750  LL=ILST(10)+2*(N-1)
      BR=J+N-2
      KK=INT(BR/2)
      NC=J+N-2
      RD=NC+(IT-7)/2+1
      TST=RD-2*INT(RD/2)
      IF(TST.EQ.0)ID=1
      IF(TST.GT.0)ID=-1
      KK=I+N+(IT-6)*KK
      IF(KK.LT.1.OR.KK.GT.ILST(9)) GOTO 240
      IZ=KK+LL*ILST(9)+(IT-1)*ILST(9)**2
      IDB=1
 780  IZC=IZC+1
      IF(P(IZ).EQ.0.0) GOTO 760
      NUM=NUM+0.375*(P(IZ)-R(IZ))/P(IZ)
      DEN=DEN+0.375**2/P(IZ)
      GOTO 765
 760  IZT=IZT+1
 765  IF(KK.EQ.1.AND.ID.EQ.-1) GOTO 775
      IF(KK.EQ.ILST(9).AND.ID.EQ.1) GOTO 775
      IZC=IZC+1
      IF(P(IZ+ID).EQ.0.0) GOTO 770
      NUM=NUM+0.125*(P(IZ+ID)-R(IZ+ID))/P(IZ+ID)
      DEN=DEN+0.125**2/P(IZ+ID)
      GOTO 775
 770  IZT=IZT+1
 775  IF(N.EQ.ILST(10).OR.IDB.EQ.2) GOTO 790
      IZ=IZ+ILST(9)
      IDB=2
      GOTO 780
 790  IF(IZT.EQ.IZC) GOTO 250
      GOTO 240
 230  CONTINUE
      II=I+IX(IT,2)*N
      JJ=J+IX(IT,1)*N
      IZ=II+(JJ-1)*ILST(9)+(IT-1)*ILST(9)**2
      IF(P(IZ).EQ.0) GOTO 250
      NUM=NUM+0.75*(P(IZ)-R(IZ))/P(IZ)
      DEN=DEN+0.75**2/P(IZ)
      IZP=IZ+IY(IT,2)*ILST(9)+IY(IT,1)
      IZM=IZ-IY(IT,2)*ILST(9)-IY(IT,1)
      IF(IT.EQ.2.OR.IT.EQ.4) GOTO 260
      IF(II.EQ.1) GOTO 270
      IF(P(IZM).EQ.0.0) GOTO 270
      NUM=NUM+(P(IZM)-R(IZM))/P(IZM)*0.125
      DEN=DEN+0.125**2/P(IZM)
 270  IF(II.EQ.ILST(9)) GOTO 240
      IF(P(IZP).EQ.0.0) GOTO 240
      NUM=NUM+0.125*(P(IZP)-R(IZP))/P(IZP)
```

```
      DEN=DEN+0.125**2/P(IZP)
      GOTO 240
260   IF(JJ.EQ.1) GOTO 290
      IF(P(IZM).EQ.0.0) GOTO 290
      NUM=NUM+(P(IZM)-R(IZM))/P(IZM)*0.125
      DEN=DEN+0.125**2/P(IZM)
290   IF(JJ.EQ.ILST(9)) GOTO 240
      IF(P(IZP).EQ.0.0) GOTO 240
      NUM=NUM+(P(IZP)-R(IZP))/P(IZP)*0.125
      DEN=DEN+0.125**2/P(IZP)
240   CONTINUE
      DA(IV)=NUM/DEN
      GOTO 220
250   A(IV)=0
      DA(IV)=0
220   CONTINUE
210   CONTINUE
200   CONTINUE
C     CALCULATES THE DELTA FACTOR
      WRITE(6,3200)
      NUM=0
      DEN=0
      DO 400 IT=1,ILST(14)
      WRITE(6,5100)IT
5100  FORMAT(1H ,4HS100,I3)
      KA=(IT-1)*ILST(9)**2
      IW=0
      DO 410 L=1,ILST(9)
      KB=(L-1)*ILST(9)
      DO 420 K=1,ILST(9)
      IZ=K+KA+KB
      IF(P(IZ).EQ.0.0) GOTO 420
      ZCOM=0
      IV=0
      IF(IT.LE.4) GOTO 460
      IF(IT.EQ.5.OR.IT.EQ.7) GOTO 800
      IF(L.LE.ILST(18).AND.IT.EQ.8) GOTO 410
      DO 470 N=1,LMT
      BR=L-ILST(18)+N*(7-IT)+IT-6
      NP=INT(BR/2)
      NP=NP+(IT-7)*2
      NW=ILST(9)-2*NP
      IF(N.NE.1) GOTO 480
      BR=L-ILST(18)-(NP-1)*2
      IEX=INT(BR/2)
      IS=2
      IF(IEX.EQ.1.AND.IT.EQ.6) IS=4
      IF(IEX.EQ.0.AND.IT.EQ.8) IS=4
480   CONTINUE
      IF(NP.LT.1.OR.NP.GT.ILST(10)) GOTO 490
      IF(K.LE.NP.OR.K.GT.(NP+NW)) GOTO 490
      IF(N.LE.(NP-2)) GOTO 490
      IF(N.GT.(NP+NW-2)) GOTO 430
      IW=0
      IF(NP.EQ.1) GOTO 485
```

```
      DO 485 NIP=1,(NP-1)
      IIP=ILST(9)-2*NIP
      IW=IW+IIP**2
485   CONTINUE
      IV=IW+(N-NP+1)*NW+K-NP
      ZCOM=ZCOM+RF(IS)*DA(IV)
      NC=N-NP+2
      KC=K-NP
      IF(IS.EQ.4.AND.IT.EQ.6.AND.NC.EQ.(NW-1))ZCOM=ZCOM+
     C0.125*DA(IV+NW)
      IF(IS.EQ.1.AND.IT.EQ.8.AND.NC.EQ.2)ZCOM=ZCOM+
     C0.125*DA(IV-NW)
      IF(NP.EQ.1) GOTO 495
      IF(IS.EQ.3.AND.IT.EQ.8.AND.NC.EQ.NW)ZCOM=ZCOM+
     C0.125*DA(IW-ILST(9)+K+NP-1)
      IF(IS.EQ.2.AND.IT.EQ.6.AND.NC.EQ.1)ZCOM=ZCOM+
     C0.125*DA(IW-(NW+2)**2+K-NP+1)
495   CONTINUE
      IF(IS.EQ.3.OR.IS.EQ.2) GOTO 490
      IF(IT.EQ.8) GOTO 455
      IF(NC.EQ.1.AND.IS.EQ.4) GOTO 490
      IF(NC.EQ.NW.AND.IS.EQ.4) GOTO 490
455   IF(IT.EQ.6.AND.IS.EQ.4) GOTO 475
      IF(IT.EQ.8.AND.IS.EQ.1) GOTO 475
      IF(NP.EQ.1) GOTO 490
      IWA=IW-(NW+2)**2+(N-NP+2)*(NW+2)+K-NP+1
      GOTO 465
475   IF(NP.EQ.ILST(10).OR.KC.EQ.1.OR.KC.EQ.NW) GOTO 490
      IWA=IW+NW**2+(N-NP)*(NW-2)+K-NP-1
465   CONTINUE
      ZCOM=ZCOM+0.125*DA(IWA)
490   CONTINUE
      IS=IS+1
      IF(IS.EQ.5)IS=1
470   CONTINUE
      GOTO 430
800   IF(L.LE.ILST(18)) GOTO 410
      BR=L-ILST(18)
      NP=INT(BR/2+0.5)
      IW=0
      IF(NP.EQ.1) GOTO 805
      DO 805 NIP=1,(NP-1)
      IIP=ILST(9)-2*NIP
      IW=IW+IIP**2
805   CONTINUE
      NW=ILST(9)-2*NP
      DO 810 N=1,(NW+NP-2)
      BR=N-1
      KK=INT(BR/2+0.5)
      IF(N.LE.(NP-2)) GOTO 810
      KT=K+(6-IT)*KK
      IF(KT.LE.NP.OR.KT.GT.(NP+NW)) GOTO 810
      IV=IW+(N-NP+1)*NW+KT-NP
      ZCOM=ZCOM+0.375*DA(IV)
      BR=N+(7-IT)/2
```

```
      ID=(-1)**DR
      NC=N-NP+2
      IF(KT.EQ.(NP+1).AND.ID.EQ.-1) GOTO 820
      IF(KT.EQ.(NP+NW).AND.ID.EQ.1) GOTO 830
      ZCOM=ZCOM+0.125*DA(IV+ID)
      GOTO 810
820   IF(IT.EQ.5.AND.NC.EQ.1) GOTO 810
      IF(IT.EQ.7.AND.NC.EQ.NW) GOTO 810
      IF(IT.EQ.5)ZCOM=ZCOM+0.125*DA(IV-NW)
      IF(IT.EQ.7)ZCOM=ZCOM+0.125*DA(IV+NW)
      GOTO 810
830   IF(IT.EQ.5.AND.NC.EQ.NW) GOTO 810
      IF(IT.EQ.7.AND.NC.EQ.1) GOTO 810
      IF(IT.EQ.5)ZCOM=ZCOM+0.125*DA(IV+NW)
      IF(IT.EQ.7)ZCOM=ZCOM+0.125*DA(IV-NW)
810   CONTINUE
      GOTO 430
460   CONTINUE
      DO 430 N=1,ILST(10)
      NW=ILST(9)-2*N
      KK=K-IX(IT,2)*N
      IF(KK.LT.1.OR.KK.GT.NW) GOTO 430
      LL=L-IX(IT,1)*N
      IF(LL.LT.1.OR.LL.GT.NW) GOTO 430
      IW=IV+KK+(LL-1)*NW
      IWP=IW+IY(IT,2)*NW+IY(IT,1)
      IWM=IW-IY(IT,2)*NW-IY(IT,1)
      ZCOM=ZCOM+DA(IW)*0.75
      IF(IT.EQ.2.OR.IT.EQ.4) GOTO 440
      IF(KK.GT.1) ZCOM=ZCOM+DA(IWM)*0.125
      IF(KK.LT.NW) ZCOM=ZCOM+DA(IWP)*0.125
      GOTO 450
440   IF(LL.GT.1) ZCOM=ZCOM+DA(IWM)*0.125
      IF(LL.LT.NW) ZCOM=ZCOM+DA(IWP)*0.125
450   CONTINUE
      IV=IV+NW**2
430   CONTINUE
      NUM=NUM+(P(IZ)-R(IZ))/P(IZ)*ZCOM
      DEN=DEN+ZCOM**2/P(IZ)
420   CONTINUE
410   CONTINUE
400   CONTINUE
      WRITE(6,/) NUM,DEN
      D=NUM/DEN
      WRITE(12,1040)
      WRITE(6,/) D
C     CORRECTS THE PLANE DISTRIBUTIONS
      WRITE(6,3300)
      IV=0
      DO 500 N=1,ILST(10)
      NLT=ILST(9)-2*N
      DO 510 J=1,NLT
      DO 520 I=1,NLT
      IV=IV+1
      A(IV)=A(IV)+D*DA(IV)
```

```
      IF(A(IV).LE.0.0) A(IV)=0.0
  520 CONTINUE
  510 CONTINUE
  500 CONTINUE
C     PRINT ROUTINE FOR PLANES AND RAYSUMS
      WRITE(12,1000) ILST(13)
      IF(ILST(15).NE.1) GOTO 900
C     PRINT RAYSUMS
      WRITE(6,2050)
      DO 910 IT=1,ILST(14)
      WRITE(12,1010)IT
      KA=(IT-1)*ILST(9)**2
      DO 920 L=1,ILST(9)
      KB=(L-1)*ILST(9)
      DO 930 K=1,ILST(9)
      IZ=K+KA+KB
      IRA(K)=R(IZ)
  930 CONTINUE
      WRITE(12,1020)(IRA(N),N=1,ILST(9))
  920 CONTINUE
  910 CONTINUE
  900 IF(ILST(16).NE.2.AND.ILST(13).NE.ILST(12)) GOTO 990
C     PRINT PLANES
      WRITE(6,2060)
      IV=0
      DO 940 N=1,ILST(10)
      WRITE(12,1030)N
      NW=ILST(9)-2*N
      DO 950 I=1,NW
      DO 960 J=1,NW
      IV=IV+1
      IRA(J)=A(IV)
  960 CONTINUE
      WRITE(12,1020)(IRA(K),K=1,NW)
  950 CONTINUE
  940 CONTINUE
  990 IF(ILST(13).EQ.ILST(12)) GOTO 995
      ILST(13)=ILST(13)+1
      GOTO 10
  995 WRITE(6,2070)
 1000 FORMAT(1H ,6X,10HITERATION ,I3/1H0)
 1010 FORMAT(1H ,6X,7HRAYSUM ,I2/1H0)
 1020 FORMAT(1H ,14(1X,I6)/1H ,14(1X,I6))
 1030 FORMAT(1H ,5X,6HPLANE ,I3/1H0)
 1040 FORMAT(5X,8HDELTA = ,1PE12.4)
 2000 FORMAT(1H ,5X,35HINPUT THE FIRST APPROXIMATION INDEX/
     C1H ,22X,8H1. IDEAL/1H ,22X,21H2. IMPEDANCE OPERATOR/1H /
     C1H ,22X,11HINPUT 1-2  )
 2010 FORMAT(1H0,5X,36HNOW INPUTING THE FIRST APPROXIMATION)
 2020 FORMAT(1H0,5X,41HINPUT THE NUMBER OF ITERATIONS REQUIRED  )
 2030 FORMAT(1H0,5X,44HDO YOU WISH THE RAYSUMS PRINTED 1-YES,2-NO  )
 2040 FORMAT(1H0,5X,26HDO YOU WISH PLANES PRINTED/
     C1H ,22X,24H1. AFTER FINAL ITERATION/
     C1H ,22X,23H2. AFTER EACH ITERATION/1H /
     C1H ,22X,11HINPUT 1-2  )
```

```
2050  FORMAT(1H0,5X,20HNOW PRINTING RAYSUMS)
2060  FORMAT(1H0,5X,32HNOW PRINTING PLANE DISTRIBUTIONS)
2070  FORMAT(1H0,15X,11H*** END ***)
2080  FORMAT(1H0,5X,28HNOW INPUTING THE PROJECTIONS)
2090  FORMAT(1H0,5X,33HINPUT THE NUMBER OF PROJECTIONS  )
3000  FORMAT(1H0,5X,23HNOW CALCULATING RAYSUMS)
3100  FORMAT(1H0,5X,26HNOW CALCULATING INCREMENTS)
3200  FORMAT(1H0,5X,21HNOW CALCULATING DELTA)
3300  FORMAT(1H0,5X,25HNOW CORRECTING THE PLANES)
      LOCK(12)
      STOP
      END
```

APPENDIX 5

ILSRT PROGRAM FOR A (26.6°) QUAD LECT SYSTEM WITH SIMULATED 14 x 14 MATRIX VIEW DATA FOR A LEFT VENTRICLE (LV) PHANTOM

```
      JANIS - PROGRAM FOR TOMOGRAPHIC RECONSTRUCTION #1
      COMMON/BUFF/P(1000),ILST(256)
      DIMENSION IPR(256)
      DATA P(1)/14*0.0,3*0.0,2*9250.0,1750.0,14*0.0,
     C 0.0,1100.0,10090.0,2*1383.0,9859.0,4125.0,13*0.0,
     C 2500.0,7500.0,1275.0,2*925.0,1530.0,5625.0,3750.0,12*0.0,
     C 2500.0,7500.0,1275.0,2*925.0,1530.0,5625.0,3750.0,12*0.0,
     C 0.0,1100.0,10090.0,2*1333.0,9858.0,4125.0,13*0.0,
     C 3*0.0,2*9250.0,1750.0,14*0.0,140*0.0,
     C 3*0.0,19.0,693.0,1076.0,300.0,8*0.0,
     C 7*0.0,37.0,1493.0,2614.0,1345.0,693.0,308.0,7*0.0,
     C 6*0.0,19.0,1907.0,3957.0,2460.0,1132.0,615.0,309.0,7*0.0,
     C 5*0.0,293.0,2558.0,3993.0,2834.0,1422.0,2*1230.0,800.0,215.0,6*0.0,
     C 4*0.0,96.0,1432.0,3475.0,3653.0,2460.0,1345.0,2534.0,1507.0,
     C 2091.0,246.0,6*0.0,
     C 3*0.0,12.0,1415.0,3847.0,2792.0,1845.0,2460.0,1845.0,1551.0,
     C 2140.0,1384.0,25.0,6*0.0,
     C 3*0.0,123.0,3137.0,3605.0,2135.0,2165.0,1345.0,3346.0,4132.0,
     C 1999.0,12.0,7*0.0,
     C 3*0.0,123.0,1794.0,2234.0,4010.0,2595.0,3170.0,5501.0,2368.0,
     C 19.0,8*0.0,
     C 4*0.0,1431.0,3863.0,3473.0,3705.0,4017.0,1753.0,19.0,9*0.0,
     C 4*0.0,763.0,1738.0,3530.0,3622.0,1691.0,19.0,10*0.0,
     C 5*0.0,25.0,695.0,1052.0,19.0,11*0.0,180*0.0,
     C 140*0.0,9*0.0,625.0,2200.0,8*2400.0,125.0,0.0,
     C 5*0.0,20.0,750.0,2000.0,3000.0,2300.0,6*2400.0,1300.0,1200.0,700.0,
     C 6*0.0,40.0,1250.0,2700.0,1600.0,2300.0,1300.0,4*2400.0,2300.0,
     C 3*1200.0,375.0,
     C 5*0.0,40.0,1250.0,2700.0,1600.0,2300.0,1300.0,4*2400.0,2300.0,
     C 3*1200.0,375.0,
     C 5*0.0,20.0,750.0,2000.0,3000.0,2300.0,6*2400.0,1300.0,1200.0,700.0,
     C 9*0.0,625.0,2200.0,8*2400.0,125.0,0.0,140*0.0,
     C 180*0.0,5*0.0,25.0,695.0,1052.0,19.0,11*0.0,
     C 4*0.0,763.0,1738.0,3530.0,3622.0,1591.0,19.0,10*0.0,
     C 4*0.0,1431.0,3863.0,3473.0,3705.0,4017.0,1753.0,19.0,9*0.0,
     C 3*0.0,123.0,1794.0,2234.0,4010.0,2595.0,3170.0,5301.0,2368.0,
     C 19.0,8*0.0,
     C 3*0.0,123.0,3137.0,3605.0,2135.0,2165.0,1845.0,3346.0,4132.0,
     C 1999.0,12.0,7*0.0,
     C 3*0.0,12.0,1415.0,3837.0,2792.0,1845.0,2460.0,1845.0,1551.0,
     C 2140.0,1384.0,25.0,6*0.0,
     C 4*0.0,96.0,1432.0,3475.0,3653.0,2450.0,1345.0,2534.0,1507.0,2091.0,
     C 246.0,6*0.0,
     C 5*0.0,293.0,2558.0,3993.0,2834.0,1422.0,2*1230.0,800.0,215.0,6*0.0,
     C 6*0.0,19.0,1907.0,3967.0,2460.0,1132.0,615.0,308.0,7*0.0,
     C 7*0.0,37.0,1493.0,2614.0,1345.0,683.0,303.0,7*0.0,
     C 3*0.0,19.0,673.0,1076.0,300.0,8*0.0/
      DATA ILST(1)/1,0,1,2,0,1,2,1,20,9,2*0,1,0,7*1,9*0,
     C 1,0,1,0,0,1,0,1,2*0,-1,0,1,0,0,-1,0,1/
      TYPE" INPUT THE FIRST APPROXIMATION INDEX      "
      TYPE"                         1. IDEAL"
      TYPE"                         2. IMPEDANCE OPERATOR"
      TYPE
1     ACCEPT"                                    INPUT 1-2    ",ILST(17)
      IF(ILST(17).LT.1.OR.ILST(17).GT.2) GOTO 1
      TYPE
      TYPE" INPUT THE RELAXATION COEFFICIENT INDEX"
      TYPE"                         1. GLOBAL"
      TYPE"                         2. LOCAL"
      TYPE
5     ACCEPT"                                    INPUT 1-2    ",ILST(23)
      IF(ILST(23).LT.1.OR.ILST(23).GT.2) GOTO 5
      TYPE
```

```
      WRITE(12,1000)ILST(17),ILST(22)
1000  FORMAT(1H ,6X,29HINITIAL DISTRIBUTION INDEX   ,I2/1H ,6X,
     C 29HRELAXATION INDEX            = ,I2)
      ACCEPT" INPUT THE NUMBER OF ITERATIONS REQUIRED   ",ILST(17)
      TYPE
      ACCEPT" DO YOU WISH RAYSUMMS PRINTED(1-YES,2-NO)  ",ILST(15)
      TYPE
      TYPE" DO YOU WISH PLANES PRINTED"
      TYPE"                  1.AFTER FINAL ITERATION ONLY"
      TYPE"                  2.AFTER EACH ITERATION"
      TYPE
      ACCEPT"                                  INPUT 1-2   ",ILST(16)
      TYPE
      CALL DIR("DP0",IER)
      IF(IER.NE.1) TYPE"FAILED AT DIR,IER = ",IER
      CALL CFILW("RECDAT",3,34,IER)
      IF(IER.NE.1) TYPE"FAILED AT CFILW,IER = ",IER
      CALL OPEN(5,"RECDAT",2,IER)
      IF(IER.NE.1) TYPE"FAILED AT OPEN,IER = ",IER
      HI=0
      DO 10 I=1,1600
      IF(P(I).GT.HI) HI=P(I)
10    CONTINUE
      ST=16383/HI
      ST=ST*1000
      IF(ST.GT.16383) ST=16383
      ILST(18)=ST
      ST=ILST(18)
      IV=0
      DO 20 IBLK=0,6
      DO 40 J=1,256
      IV=IV+1
      IPR(J)=ST/1000.0*P(IV)
      IF(IV.EQ.1600) GOTO 60
40    CONTINUE
60    CALL WRBLK(5,IBLK,IPR,1,IER)
      IF(IER.NE.1)TYPE"FAILED IN 1ST WRBLK,IER= ",IER," IBLK= ",IBLK
20    CONTINUE
      CALL WRBLK(5,24,ILST,1,IER)
      IF(IER.NE.1) TYPE"FAILED AT 2ND WRBLK,IER = ",IER
      CALL CLOSE(5,IER)
      IF(IER.NE.1) TYPE"FAILED AT CLOSE,IER = ",IER
      TYPE"      EXIT JAM15"
      CALL FCHAN("PLANRA.SV")
      END
```

```
C       PLANRA -  INITIAL APPROXIMATION OF PLANE ACTIVITY
        COMMON/BUFF/A(1140,2),ILST(256),IAR(255)
        DIMENSION P(1600),IX(4,2),IW(4,2),IP(4)
        EQUIVALENCE (IX(1),ILST(1)),(IW(1),ILST(41))
        DATA A(1)/126*0.0,4*0.0,1000.0,3000.0,1965.0,11*0.0,
     C  4*0.0,2000.0,6000.0,2525.0,11*0.0,4*0.0,2000.0,6000.0,2525.0,11*0.0,
     C  4*0.0,1000.0,3000.0,1965.0,11*0.0,126*0.0,
     C  30*0.0,3*0.0,500.0,4000.0,3400.0,10*0.0,
     C  2*0.0,6250.0,6100.0,15000.0,11500.0,7000.0,9*0.0,
     C  2*0.0,9000.0,8500.0,3200.0,7600.0,6000.0,6500.0,3*0.0,
     C  2*0.0,9000.0,8500.0,3200.0,7600.0,6000.0,6500.0,3*0.0,
     C  2*0.0,6250.0,6100.0,15000.0,11500.0,7000.0,9*0.0,
     C  3*0.0,500.0,4000.0,3400.0,10*0.0,80*0.0,
     C  56*0.0,2*0.0,2000.0,14000.0,15500.0,4500.0,8*0.0,
     C  0.0,3750.0,12500.0,2000.0,1125.0,11000.0,6500.0,7*0.0,
     C  750.0,11500.0,3000.0,3*0.0,9000.0,8000.0,6*0.0,750.0,11500.0,3000.0,
     C  3*0.0,9000.0,8000.0,6*0.0,
     C  0.0,3750.0,12500.0,2000.0,1125.0,11000.0,6500.0,7*0.0,
     C  2*0.0,2000.0,14000.0,15500.0,4500.0,9*0.0,56*0.0,
     C  36*0.0,2*0.0,2000.0,14000.0,15500.0,4500.0,6*0.0,
     C  0.0,3000.0,13000.0,2000.0,280.0,11500.0,6000.0,5*0.0,
     C  5000.0,12500.0,1125.0,3*0.0,11000.0,8000.0,4*0.0,
     C  5000.0,12500.0,1125.0,3*0.0,11000.0,8000.0,4*0.0,
     C  0.0,3000.0,13000.0,2000.0,280.0,11500.0,6000.0,5*0.0,
     C  2*0.0,2000.0,14000.0,15500.0,4500.0,6*0.0,36*0.0,
     C  20*0.0,2*0.0,2000.0,14000.0,15500.0,5000.0,4*0.0,
     C  0.0,3750.0,13000.0,2000.0,500.0,11000.0,5000.0,3*0.0,
     C  5000.0,12500.0,1125.0,2*0.0,125.0,11000.0,8000.0,2*0.0,
     C  5000.0,12500.0,1125.0,2*0.0,125.0,11000.0,8000.0,2*0.0,
     C  0.0,3750.0,13000.0,2000.0,500.0,11000.0,5000.0,3*0.0,
     C  2*0.0,2000.0,14000.0,15500.0,5000.0,4*0.0,20*0.0,
     C  3*0.0,2*0.0,2000.0,14000.0,15500.0,2750.0,2*0.0,
     C  0.0,3750.0,13000.0,2000.0,500.0,12250.0,2000.0,0.0,4500.0,12000.0,
     C  1125.0,2*0.0,500.0,10000.0,3300.0,
     C  4500.0,12000.0,1125.0,2*0.0,500.0,10000.0,3300.0,0.0,3750.0,13000.0,
     C  2000.0,500.0,12250.0,2000.0,0.0,
     C  2*0.0,2000.0,14000.0,15500.0,2750.0,2*0.0,3*0.0,
     C  2*0.0,2500.0,6000.0,2000.0,0.0,0.0,3400.0,7500.0,3*0.0,
     C  4600.0,9000.0,4*0.0,4600.0,9000.0,4*0.0,
     C  0.0,3400.0,7500.0,3*0.0,2*0.0,2500.0,6000.0,2000.0,0.0,
     C  16*0.0,4*0.0,1140*0.0/
        TYPE"       NOW INPUTING FIRST APPROXIMATION"
        TYPE
        CALL DIR("DP0",IER)
        IF(IER.NE.1) TYPE"FAILED IN DIR,IER = ",IER
        CALL OPEN(5,"RECDAT",2,IER)
        IF(IER.NE.1) TYPE"FAILED IN OPEN,IER = ",IER
        CALL RDBLK(5,24,ILST,1,IER)
        IF(IER.NE.1) TYPE"FAILED IN 1ST RDBLK,IER = ",IER
        ID=ILST(17)
        IF(ID.EQ.1.OR.ID.EQ.2) GOTO 500
C       OTHER TECHNIQUES
        TYPE"       NOT AVAILABLE YET"
        TYPE"       IMPEDANCE OPERATOR SUBSTITUTED"
        ID=2
500     HI=0
        RT=1.0
        DO 510 J=1,1140
        IF(A(J,ID).GT.HI) HI=A(J,ID)
510     CONTINUE
        IF(HI.NE.0.0) GOTO 515
        ST=1.0
        RT=0.0
```

```
      GOTO 525
515   ST=16383/HI
      ST=ST*1000
      IF(ST.GT.16383) ST=16383
      ILST(20)=ST
      ST=ILST(20)
525   II=0
      DO 520 IBLK=14,18
      DO 540 N=1,256
      II=II+1
      IAR(N)=ST/1000.0*A(II,ID)+RT
      IF(II.EQ.1140) GOTO 560
540   CONTINUE
560   CALL WRBLK(5,IBLK,IAR,1,IER)
      IF(IER.NE.1) TYPE"FAILED IN 1ST WRBLK,IER = ",IER,"IBLK = ",IBLK
520   CONTINUE
      IF(ILST(23).NE.2) GOTO 630
      ILST(22)=1000
      II=0
      DO 620 IBLK=25,33
      DO 640 N=1,256
      II=II+1
      IAR(N)=1000
      IF(II.EQ.2280) GOTO 660
640   CONTINUE
660   CALL WRBLK(5,IBLK,IAR,1,IER)
      IF(IER.NE.1) TYPE"FAILED IN 2ND WRBLK,IER = ",IER
620   CONTINUE
630   CONTINUE
      CALL WRBLK(5,24,ILST,1,IER)
      IF(IER.NE.1) TYPE"FAILED IN 3RD WRBLK,IER = ",IER
      CALL CLOSE(5,IER)
      IF(IER.NE.1) TYPE"FAILED IN CLOSE,IER = ",IER
      CALL FCHAN("PADINC.SV")
      END
```

```
C       PADINC - PROGRAM TO CALCULATE RAYSUMS AND PLANE INCREMENTS
        COMMON/DUFF/ILST(256),PX(90),RX(90)
        DIMENSION P(1600),R(1600),AR(2280),IX(4,2),IY(4,2),IAR(256)
        EQUIVALENCE (IX(1),ILST(1)),(IY(1),ILST(31))
        REAL NUM
        DATA PX(1)/4*0.0,750.0,2063.0,234.0,11*0.0,
      C 2*0.0,3656.0,7000.0,4875.0,6000.0,3000.0,1313.0,8*0.0,
      C 234.0,3906.0,4188.0,3*4000.0,3375.0,1641.0,6*0.0,
      C 1422.0,6*4000.0,2000.0,4*0.0,
      C 1219.0,6*4000.0,2000.0,2*0.0,
      C 1125.0,5*4000.0,3500.0,938.0,
      C 1125.0,3375.0,2625.0,1500.0,500.0,0.0,
      C 6*0.0/
        CALL DIR("DPO",IER)
        IF(IER.NE.1) TYPE"FAILED IN DIR,IER = ",IER
        CALL OPEN(5,"RECDAT",2,IER)
        IF(IER.NE.1) TYPE"FAILED IN OPEN,IER = ",IER
        CALL RDBLK(5,24,ILST,1,IER)
        IF(IER.NE.1) TYPE"FAILED IN 1ST RDBLK,IER = ",IER
        NP=ILST(10)
        M=ILST(9)
        ST=ILST(18)
        ST=ST/1000.0
        IV=0
        DO 10 IBLK=0,6
        CALL RDBLK(5,IBLK,IAR,1,IER)
        IF(IER.NE.1) TYPE"FAILED IN 2ND RDBLK,IER = ",IER
        DO 20 J=1,256
        IV=IV+1
        PP=IAR(J)
        PP=PP/ST
        IP=PP
        P(IV)=IP
        IF(IV.EQ.1600) GOTO 10
20      CONTINUE
10      CONTINUE
        ST=ILST(20)
        ST=ST/1000.0
        IV=0
        DO 30 IBLK=14,18
        CALL RDBLK(5,IBLK,IAR,1,IER)
        IF(IER.NE.1) TYPE"FAILED IN 3RD RDBLK,IER = ",IER
        DO 40 J=1,256
        IV=IV+1
        AR(IV)=IAR(J)
        AR(IV)=AR(IV)/ST
        IF(IV.EQ.1140) GOTO 30
40      CONTINUE
30      CONTINUE
        TYPE"      NOW CALCULATING RAYSUMS"
        TYPE
        RSUM=0.0
        GOTO 15
        IVX=0
        IVV=0
        DO 13 N=1,NP
        NW=M-2*N
        DO 16 NX=1,NW
        IVX=IVX+1
        XUM=0.0
        DO 14 NY=1,NW
        IW=IVV+(NY-1)*NW+NX
        XUM=XUM+AR(IW)
```

```
14      CONTINUE
        RX(IVX)=XUM
16      CONTINUE
        IVV=IVV+NW**2
13      CONTINUE
        TYPE" DONE THE EXTRA"
15      CONTINUE
        DO 110 IT=1,4
        DO 120 L=1,M
        DO 140 K=1,M
        IZ=K+(L-1)*M+(IT-1)*M**2
        IV=0
        CT=0
        DO 150 N=1,NP
        NW=M-2*N
        KK=K-IX(IT,2)*N
        IF(KK.LT.1.OR.KK.GT.NW) GOTO 160
        LL=L-IX(IT,1)*N
        IF(LL.LT.1.OR.LL.GT.NW) GOTO 160
        IW=IV+(LL-1)*NW+KK
        IWP=IW+IY(IT,2)*NW+IY(IT,1)
        IWM=IW-IY(IT,2)*NW-IY(IT,1)
        CT=CT+AR(IW)/8.0*0.75
        IF(IT.EQ.2.OR.IT.EQ.4) GOTO 165
        IF(KK.GT.1) CT=CT+AR(IWM)/8.0*0.125
        IF(KK.LT.NW) CT=CT+AR(IWP)/8.0*0.125
        GOTO 175
165     IF(LL.GT.1) CT=CT+AR(IWM)/8.0*0.125
        IF(LL.LT.NW) CT=CT+AR(IWP)/8.0*0.125
175     CONTINUE
        IV=IV+NW**2
160     CONTINUE
        R(IZ)=CT
        RSUM=RSUM+(P(IZ)-R(IZ))**2
140     CONTINUE
120     CONTINUE
110     CONTINUE
        WRITE(12,1000) RSUM
1000    FORMAT(6X,7HRSUM = ,1PE12.4)
        TYPE"I AM HERE ",RSUM
        HI=0
        RT=1.0
        DO 170 J=1,1600
        IF(ABS(R(J)).GT.HI) HI=ABS(R(J))
170     CONTINUE
        IF(HI.NE.0.0) GOTO 174
        ST=1
        RT=0.0
        GOTO 185
174     ST=16383.0/HI
        ST=ST*1000.0
        IF(ST.GT.16383) ST=16383
        ILST(19)=ST
        ST=ILST(19)
185     IV=0
        DO 180 IBLK=7,13
        DO 190 J=1,256
        IV=IV+1
        IAR(J)=ST/1000.0*R(IV)*RT
        IF(IV.EQ.1600) GOTO 195
190     CONTINUE
195     CALL WRBLK(5,IBLK,IAR,1,IER)
        IF(IER.NE.1) TYPE"FAILED IN 1ST WRBLK,IER = ",IER
```

```
130   CONTINUE
      TYPE"      NOW CALCULATING INCREMENTS"
      TYPE
      IVV=0
      IV=1140
      DO 210 N=1,NP
      NLT=M-2*N
      DO 220 J=1,NLT
      DO 240 I=1,NLT
      IV=IV+1
      NUM=0
      DEN=0
      DO 260 IT=1,4
      II=I+IX(IT,2)*N
      JJ=J+IX(IT,1)*N
      IZ=II+(JJ-1)*M+(IT-1)*M**2
      IF(N.EQ.1.AND.I.EQ.6.AND.J.EQ.9)TYPE "IZ",P(IZ)
      IF(P(IZ).EQ.0) GOTO 250
      NUM=NUM+0.75*(P(IZ)-R(IZ))/P(IZ)
      DEN=DEN+0.75**2/P(IZ)
      IZP=IZ+IY(IT,2)*M+IY(IT,1)
      IZM=IZ-IY(IT,2)*M-IY(IT,1)
      IF(IT.EQ.2.OR.IT.EQ.4) GOTO 200
      IF(II.EQ.1) GOTO 255
      IF(N.EQ.1.AND.I.EQ.6.AND.J.EQ.9)TYPE"IZM",P(IZM)
      IF(P(IZM).EQ.0.0) GOTO 255
      NUM=NUM+(P(IZM)-R(IZM))/P(IZM)*0.125
      DEN=DEN+0.125**2/P(IZM)
255   IF(II.EQ.M) GOTO 260
      IF(N.EQ.1.AND.I.EQ.6.AND.J.EQ.9)TYPE"IZP",P(IZP)
      IF(P(IZP).EQ.0.0) GOTO 260
      NUM=NUM+0.125*(P(IZP)-R(IZP))/P(IZP)
      DEN=DEN+0.125**2/P(IZP)
      GOTO 260
200   IF(JJ.EQ.1) GOTO 265
      IF(N.EQ.1.AND.I.EQ.6.AND.J.EQ.9)TYPE"IZM",P(IZM)
      IF(P(IZM).EQ.0.0) GOTO 265
      NUM=NUM+(P(IZM)-R(IZM))/P(IZM)*0.125
      DEN=DEN+0.125**2/P(IZM)
265   IF(JJ.EQ.M) GOTO 260
      IF(N.EQ.1.AND.I.EQ.6.AND.J.EQ.9)TYPE"IZP",P(IZP)
      IF(P(IZP).EQ.0.0) GOTO 260
      NUM=NUM+(P(IZP)-R(IZP))/P(IZP)*0.125
      DEN=DEN+0.125**2/P(IZP)
260   CONTINUE
      GOTO 215
      IVX=IVV+I
      IF(N.EQ.1.AND.I.EQ.6.AND.J.EQ.9)TYPE"IVX",PX(IVX)
      IF(PX(IVX).EQ.0.0) GOTO 250
      NUM=NUM+(PX(IVX)-RX(IVX))/PX(IVX)
      DEN=DEN+1.0/PX(IVX)
215   CONTINUE
      AR(IV)=NUM/DEN*8.0
      IF(N.EQ.1.AND.I.EQ.6.AND.J.EQ.9)TYPE"AR",AR(IV)
      GOTO 240
250   AR(IV)=0
      AR(IV-1140)=0
240   CONTINUE
220   CONTINUE
      IVV=IVV+NLT
210   CONTINUE
      MI=0
      DO 270 J=1141,2280
```

```
      IF(ABS(AR(J)).GT.HI) HI=ABS(AR(J))
270   CONTINUE
      ST=16383.0/HI
      ST=ST*1000.0
      IF(ST.GT.16383) ST=16383
      ILST(21)=ST
      ST=ILST(21)
      IV=1140
      DO 280 IBLK=19,23
      DO 290 J=1,256
      IV=IV+1
      IAR(J)=ST/1000.0*AR(IV)
      IF(IV.EQ.1280) TYPE"IAR ",IAR(J),ST
      IF(IV.EQ.2280) GOTO 295
290   CONTINUE
295   CALL WRBLK(5,IBLK,IAR,1,IER)
      IF(IER.NE.1) TYPE"FAILED IN 2ND WRBLK,IER = ",IER
280   CONTINUE
      HI=0
      DO 310 J=1,1140
      IF(ABS(AR(J)).GT.HI) HI=ABS(AR(J))
310   CONTINUE
      IF(HI.NE.0.0) GOTO 315
      ST=1.0
      RT=0.0
      GOTO 325
315   ST=16383/HI
      ST=ST*1000.0
      IF(ST.GT.16383) ST=16383
      ILST(20)=ST
      ST=ILST(20)
325   IV=0
      DO 320 IBLK=14,18
      DO 330 J=1,256
      IV=IV+1
      IAR(J)=ST/1000.0*AR(IV)+RT
      IF(IV.EQ.1140) GOTO 335
330   CONTINUE
335   CALL WRBLK(5,IBLK,IAR,1,IER)
      IF(IER.NE.1)TYPE"FAILED IN 3RD WRBLK,IER = ",IER
320   CONTINUE
      CALL WRBLK(5,24,ILST,1,IER)
      IF(IER.NE.1) TYPE"FAILED IN 4TH WRBLK,IER = ",IER
      CALL CLOSE(5,IER)
      IF(IER.NE.1) TYPE"FAILED IN CLOSE,IER = ",IER
      TYPE"       EXIT PADINC"
      CALL FCHAN("DELCOR.SV")
      END
```

```
C       DELCOR - PROGRAM TO CALCULATE DELTA AND CORRECT PLANES
        COMMON/BUFF/ ILST(256)
        DIMENSION P(1600),R(1600),AR(2280),IX(4,2),IY(4,2),IAP(256),E(2280)
        EQUIVALENCE (IX(1),ILST(1)),(IY(1),ILST(31))
        REAL NUM
        CALL DIR("DP0",IER)
        IF(IER.NE.1) TYPE"FAILED  IN DIR,IER = ",IER
        CALL OPEN(5,"RECDAT",2,IER)
        IF(IER.NE.1) TYPE"FAILED IN OPEN,IER = ",IER
        CALL RDBLK(5,24,ILST,1,IER)
        IF(IER.NE.1) TYPE"FAILED IN 1ST RDBLK,IER = ",IER
        NP=ILST(10)
        M=ILST(9)
        ST=ILST(18)
        ST=ST/1000.0
        IV=0
        DO 10 IBLK=0,6
        CALL RDBLK(5,IBLK,IAR,1,IER)
        IF(IER.NE.1) TYPE"FAILED IN 2ND RDBLK,IER = ",IER
        DO 20 J=1,256
        IV=IV+1
        PP=IAR(J)
        P(IV)=PP/ST
        IF(IV.EQ.1600) GOTO 10
20      CONTINUE
10      CONTINUE
        ST=ILST(19)
        ST=ST/1000.0
        IV=0
        DO 30 IBLK=7,13
        CALL RDBLK(5,IBLK,IAR,1,IER)
        IF(IER.NE.1) TYPE"FAILED IN 3RD RDBLK,IER = ",IER
        DO 40 J=1,256
        IV=IV+1
        PP=IAR(J)
        R(IV)=PP/ST
        IF(IV.EQ.1600) GOTO 30
40      CONTINUE
30      CONTINUE
        ST=ILST(20)
        ST=ST/1000.0
        IV=0
        DO 50 IBLK=14,18
        CALL RDBLK(5,IBLK,IAR,1,IER)
        IF(IER.NE.1) TYPE"FAILED IN 4TH RDBLK,IER = ",IER
        DO 60 J=1,256
        IV=IV+1
        PP=IAR(J)
        AR(IV)=PP/ST
        IF(IV.EQ.1140) GOTO 50
60      CONTINUE
50      CONTINUE
        ST=ILST(21)
        ST=ST/1000.0
        IV=1140
        DO 70 IBLK=19,23
        CALL RDBLK(5,IBLK,IAR,1,IER)
        IF(IER.NE.1) TYPE"FAILED IN 5TH RDBLK,IER = ",IER
        DO 80 J=1,256
        IV=IV+1
        PP=IAR(J)
        AR(IV)=PP/ST
        IF(IV.EQ.1290) TYPE"AR ",AR(IV),IAR(J),ST,PP
```

```
      IF(IV.EQ.2280) GOTO 70
80    CONTINUE
70    CONTINUE
      IF(ILST(23).NE.2) GOTO 95
      ST=ILST(22)
      TYPE"  ONE ",ILST(22),ST
      IV=0
      DO 90 IBLK=25,33
      CALL RDBLK(5,IBLK,IAR,1,IER)
      IF(IER.NE.1) TYPE"FAILED IN 5TH RDBLK,IER = ",IER,IBLK
      DO 100 J=1,256
      IV=IV+1
      PP=IAR(J)
      E(IV)=PP/ST
      IF(IV.EQ.2280) GOTO 90
100   CONTINUE
90    CONTINUE
95    CONTINUE
      TYPE"        NOW CALCULATING DELTA"
      IF(ILST(23).NE.2)  GOTO 105
      TYPE"        LOCALLY"
      IV=0
      DO 500 N=1,NP
      NLT=M-2*N
      DO 520 J=1,NLT
      DO 540 I=1,NLT
      IV=IV+1
      NUM=0.0
      DO 560 IT=1,4
      II=I+IX(IT,2)*N
      JJ=J+IX(IT,1)*N
      IZ=II+(JJ-1)*M+(IT-1)*M**2
      IF(P(IZ).EQ.0.0) GOTO 630
      IVV=0
      ZIG=0.0
      DO 580 NN=1,NP
      NW=M-2*NN
      KK=II-IX(IT,2)*NN
      IF(KK.LT.1.OR.KK.GT.NW) GOTO 580
      LL=JJ-IX(IT,1)*NN
      IF(LL.LT.1.OR.LL.GT.NW) GOTO 580
      IW=IVV+(LL-1)*NW+KK
      IWP=IW+IY(IT,2)*NW+IY(IT,1)
      IWM=IW-IY(IT,2)*NW-IY(IT,1)
      ZIG=ZIG+E(IW)*0.75*AR(IW+1140)/8.0
      IF(IT.EQ.2.OR.IT.EQ.4) GOTO 610
      IF(KK.GT.1) ZIG=ZIG+E(IWM)*0.125*AR(IWM+1140)/8.0
      IF(KK.LT.NW) ZIG=ZIG+E(IWP)*0.125*AR(IWP+1140)/8.0
      GOTO 620
610   IF(LL.GT.1) ZIG=ZIG+E(IWM)*0.125*AR(IWM+1140)/8.0
      IF(LL.LT.NW) ZIG=ZIG+E(IWP)*0.125*AR(IWP+1140)/8.0
620   CONTINUE
      IVV=IVV+NW**2
580   CONTINUE
      NUM=NUM+P(IZ)-R(IZ)-ZIG
560   CONTINUE
      NUM=NUM+4.0*E(IV)*0.75*AR(1140+IV)/8.0
      E(1140+IV)=NUM/4.0/0.75/AR(1140+IV)*8.0
      GOTO 540
630   E(1140+IV)=1.0
540   CONTINUE
520   CONTINUE
500   CONTINUE
```

```
      DO 2310 I=1,114
      JS=(I-1)*10+1141
      JF=I+10
      WRITE(12,2300)(E(J),J=JS,JF)
2300  FORMAT(6X,10(1PE10.4,1X))
2310  CONTINUE
      DO 640 I=1,1140
      E(I)=E(1140+I)
640   CONTINUE
      GOTO 190
130   NUM=0
      DEN=0
      TYPE"      GLOBALLY"
      DO 110 IT=1,4
      TYPE "THREE ",NUM,DEN
      DO 120 L=1,M
      DO 140 K=1,M
      IZ=K+(L-1)*M+(IT-1)*M**2
      IF(P(IZ).EQ.0) GOTO 140
      ZCOM=0
      IV=1140
      DO 160 N=1,NP
      NW=M-2*N
      KK=K-IX(IT,2)*N
      IF(KK.LT.1.OR.KK.GT.NW) GOTO 160
      LL=L-IX(IT,1)*N
      IF(LL.LT.1.OR.LL.GT.NW) GOTO 160
      IW=IV+KK+(LL-1)*NW
      IWP=IW+IY(IT,2)*NW+IY(IT,1)
      IWM=IW-IY(IT,2)*NW-IY(IT,1)
      ZCOM=ZCOM+AR(IW)/8.0*0.75
      IF(IT.EQ.2.OR.IT.EQ.4) GOTO 165
      IF(KK.GT.1) ZCOM=ZCOM+AR(IWM)/8.0*0.125
      IF(KK.LT.NW) ZCOM=ZCOM+AR(IWP)/8.0*0.125
      GOTO 175
165   IF(LL.GT.1) ZCOM=ZCOM+AR(IWM)/8.0*0.125
      IF(LL.LT.NW) ZCOM=ZCOM+AR(IWP)/8.0*0.125
175   CONTINUE
      IV=IV+NW**2
160   CONTINUE
      IF(IT.EQ.1.AND.K.EQ.4.AND.L.EQ.8)TYPE "FIVE ",NUM,DEN
      NUM=NUM+(P(IZ)-R(IZ))/P(IZ)*ZCOM
      DEN=DEN+ZCOM**2/P(IZ)
      IF(IT.EQ.1.AND.K.EQ.4.AND.L.EQ.8)TYPE "FOUR ",NUM,DEN,ZCOM,P(IZ),R(IZ)
      IF(IT.EQ.1.AND.K.EQ.6.AND.L.EQ.10)TYPE "ONE",P(IZ),R(IZ),ZCOM
140   CONTINUE
120   CONTINUE
110   CONTINUE
      TYPE"TWO",NUM,DEN
      D=NUM/DEN
      DO 150 I=1,1140
      E(I)=D
150   CONTINUE
      WRITE(12,1000) E
1000  FORMAT(1H ,6X,10HDELTA = ,1PE10.4)
      TYPE
      TYPE"      DELTA = ",D
190   TYPE
      TYPE"      NOW CORRECTING PLANES"
      TYPE
      IV=0
      DO 210 N=1,NP
      TOT=0
```

```
      NLT=M-2*N
      DO 220 J=1,NLT
      DO 240 I=1,NLT
      IV=IV+1
      IVV=IV+1140
      AR(IV)=AR(IV)+E(IV)*AR(IVV)
      IF(AR(IV).LE.0.0) AR(IV)=0.0
      IF(IV.EQ.150) TYPE"ARP ",AR(IV)
240   CONTINUE
220   CONTINUE
210   CONTINUE
      HI=0
      DO 310 J=1,1140
      IF(ABS(AR(J)).GT.HI) HI=ABS(AR(J))
310   CONTINUE
      ST=16383.0/HI
      ST=ST*1000.0
      IF(ST.GT.16383)ST=16383
      ILST(20)=ST
      ST=ILST(20)
      IV=0
      DO 320 IBLK=14,19
      DO 340 J=1,256
      IV=IV+1
      IAR(J)=ST/1000.0*AR(IV)
      IF(IV.EQ.1140) GOTO 345
340   CONTINUE
345   CALL WRBLK(5,IBLK,IAR,1,IER)
      IF(IER.NE.1) TYPE"FAILED IN 1ST WRBLK,IER = ",IER
320   CONTINUE
      IF(ILST(23).NE.2) GOTO 425
      IV=0
      DO 420 IBLK=25,33
      DO 430 J=1,256
      IV=IV+1
      IAR(J)=1000.0*E(IV)
      IF(IAR(J).GT.16383)IAR(J)=16383
      IF(IV.EQ.2280) GOTO 440
430   CONTINUE
440   CALL WRBLK(5,IBLK,IAR,1,IER)
      IF(IER.NE.1) TYPE"FAILED IN 2ND WRBLK,IER = ",IER
420   CONTINUE
425   CONTINUE
      CALL WRBLK(5,24,ILST,1,IER)
      IF(IER.NE.1) TYPE"FAILED IN 3RD WRBLK,IER = ",IER
      CALL CLOSE(5,IER)
      IF(IER.NE.1) TYPE"FAILED IN CLOSE,IER = ",IER
      CALL FCHAN("PRARS.SV")
      END
```

```
C       PRAPS - PROGRAM TO PRINT PLANE AND RAYSUM DISTRIBUTIONS
        DIMENSION R(1600),DA(1140),ILST(256),IAR(256),IRA(20)
        TYPE"       NOW IN PRINT AND ITERATION CHECK"
        TYPE
        CALL DIR("DP0",IER)
        IF(IER.NE.1) TYPE"FAILED IN DIR,IER = ",IER
        CALL OPEN(5,"RECDAT",2,IER)
        IF(IER.NE.1) TYPE"FAILED IN OPEN,IER = ",IER
        CALL RDBLK(5,24,ILST,1,IER)
        IF(IER.NE.1) TYPE"FAILED IN 1ST RDBLK,IER = ",IER
        IPRS=ILST(15)
        IPAS=ILST(16)
        ITER=ILST(12)
        ITC=ILST(17)
        NP=ILST(10)
        M=ILST(9)
        IF(IPRS.NE.1) GOTO 100
        TYPE"       NOW PRINTING RAYSUMS"
        TYPE
        IV=0
        ST=ILST(19)
        ST=ST/1000.0
        DO 10 IBLK=7,13
        CALL RDBLK(5,IBLK,IAR,1,IER)
        IF(IER.NE.1) TYPE"FAILED IN 2ND RDBLK,IER= ",IER
        DO 15 J=1,256
        IV=IV+1
        R(IV)=IAR(J)
        R(IV)=R(IV)/ST
        IF(IV.EQ.1600) GOTO 10
15      CONTINUE
10      CONTINUE
        WRITE(12,1000) ILST(13)
        DO 20  IT=1,4
        WRITE(12,1010)IT
        DO 40 L=1,M
        DO 60 K=1,M
        IZ=K+(L-1)*M+(IT-1)*M**2
        IRA(K)=R(IZ)
60      CONTINUE
        WRITE(12,1020)(IRA(N),N=1,M)
40      CONTINUE
20      CONTINUE
100     IF(IPAS.NE.2.AND.ITC.NE.ITER) GOTO 200
        TYPE"       NOW PRINTING PLANE DISTRIBUTIONS"
        TYPE
        IV=0
        ST=ILST(20)
        ST=ST/1000
        DO 110 IBLK=14,18
        CALL RDBLK(5,IBLK,IAR,1,IER)
        IF(IER.NE.1) TYPE"FAILED IN 3RD RDBLK,IER= ",IER
        DO 115 J=1,256
        IV=IV+1
        DA(IV)=IAR(J)
        DA(IV)=DA(IV)/ST
        IF(IV.EQ.1140) GOTO 110
115     CONTINUE
110     CONTINUE
        IV=0
        DO 120 N=1,NP
        WRITE(12,1030)N
        NW=M-2*N
```

```
      DO 140 I=1,NW
      DO 160 J=1,NW
      IV=IV+1
      IRA(J)=DA(IV)
160   CONTINUE
      WRITE(12,1020)(IRA(K),K=1,NW)
140   CONTINUE
120   CONTINUE
200   IF(ITC.EQ.ITER) GOTO 210
      ILST(15)=ILST(15)+1
      CALL WRBLK(5,24,ILST,1,IER)
      IF(IER.NE.1) TYPE"FAILED IN WRBLK,IER = ",IER
      CALL CLOSE(5,IER)
      IF(IER.NE.1) TYPE"FAILED IN CLOSE,IER = ",IER
      CALL FCHAN("PADINC.SV")
210   CALL CLOSE(5,IER)
      IF(IER.NE.1) TYPE"FAILED IN CLOSE,IER = ",IER
      CALL DFILW("RECDAT",IER)
      IF(IER.NE.1) TYPE"FAILED IN DFILW,IER = ",IER
1000  FORMAT(1H0,6X,10HITERATION ,I3/1H0)
1010  FORMAT(1H0,5X,7HRAYSUM ,I2/1H0)
1020  FORMAT(6X,20(I5,1X))
1030  FORMAT(1H0,5X,6HPLANE ,I3/1H0)
      STOP
      END
```

APPENDIX

6

RECONSTRUCTION OF INDIVIDUAL PLANES FROM LV PHANTOM AND LV SHOWN IN FIG. 6.26 AND FIG. 6.27 (b) RESPECTIVELY

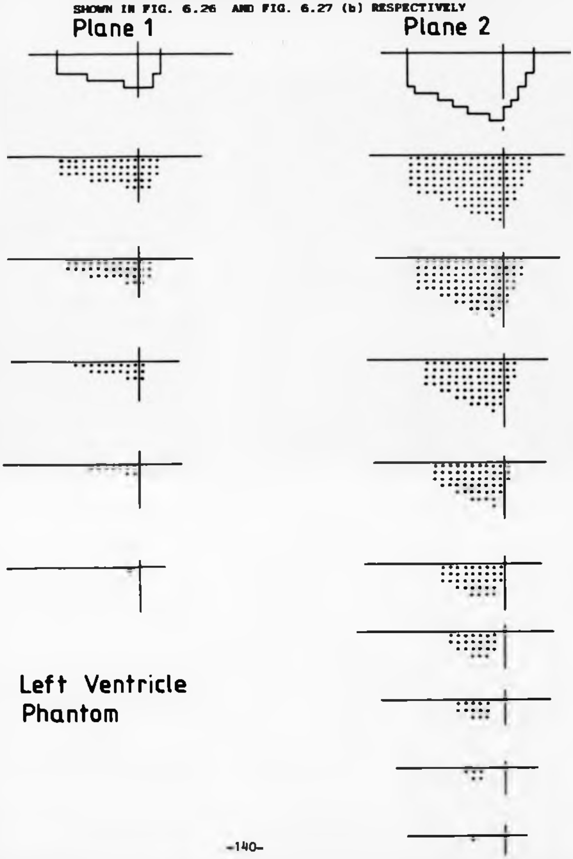

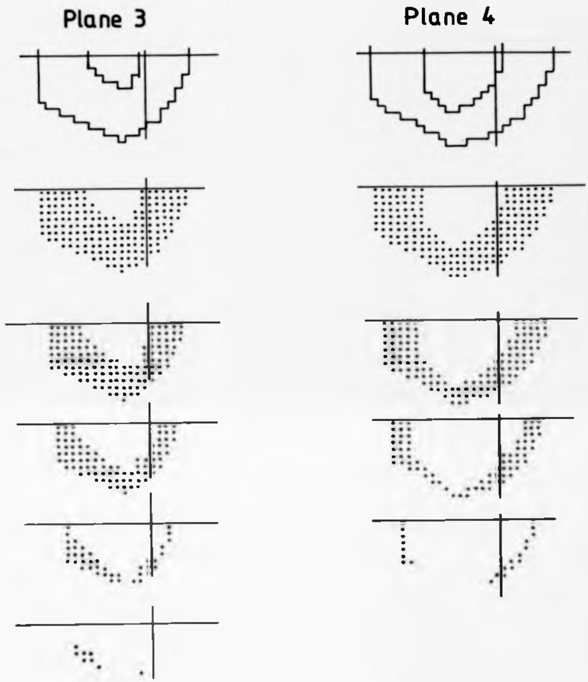
Plane 3
Plane 4

Plane 5

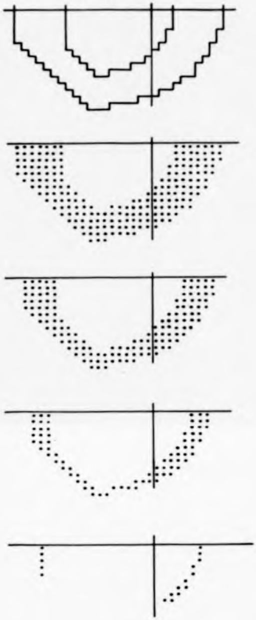

Plane 6

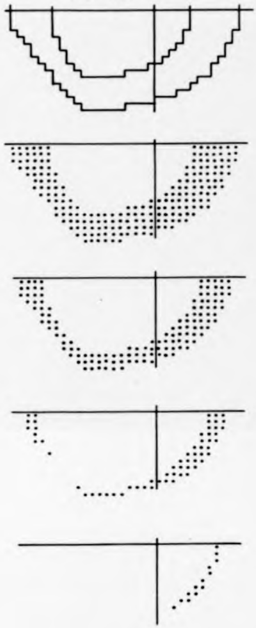

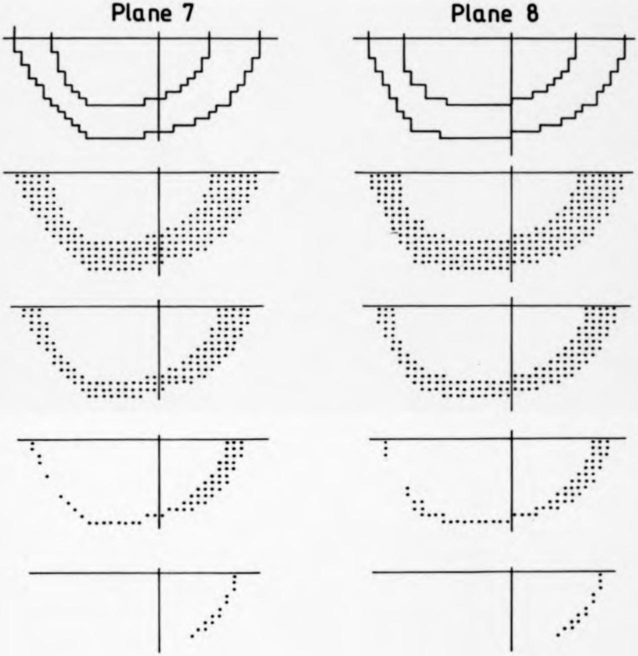
Plane 7
Plane 8

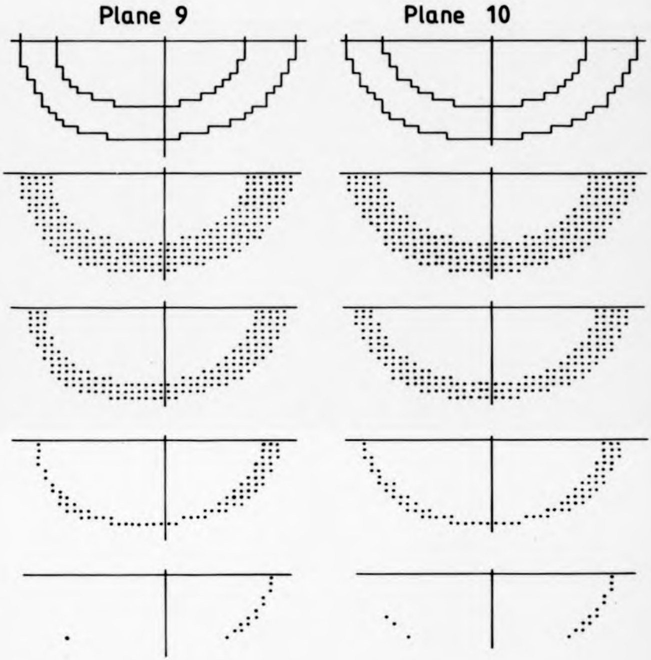
Plane 9
Plane 10

Planes 11 to 15

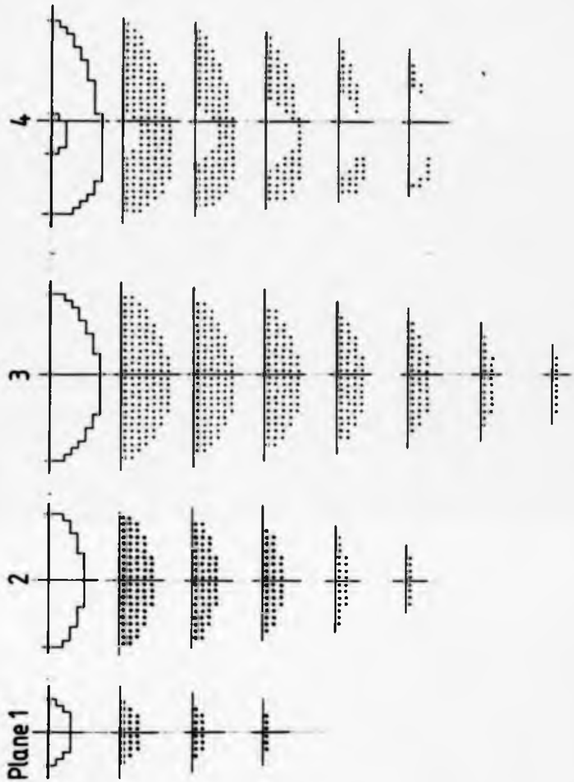

Left Ventricle

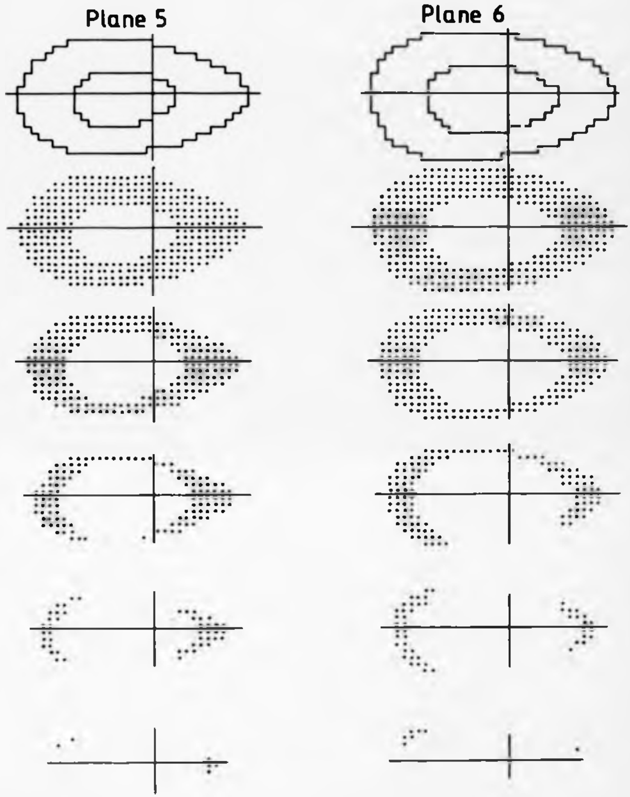
Plane 5
Plane 6

Plane 7

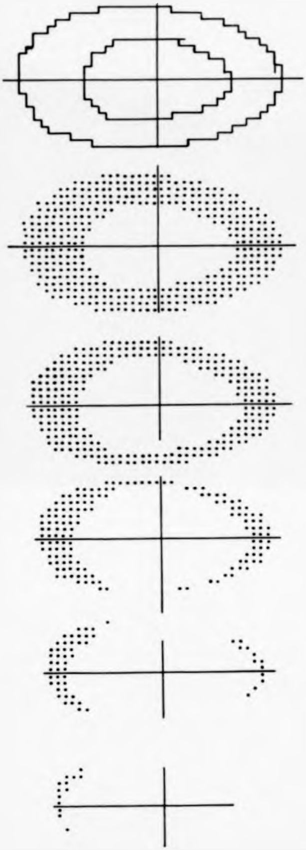

Plane 8

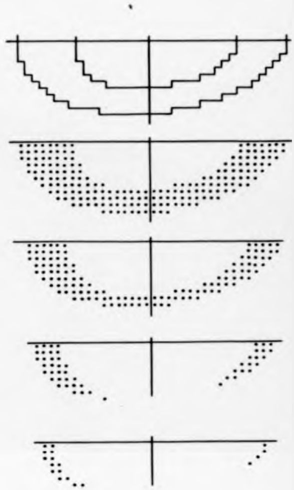

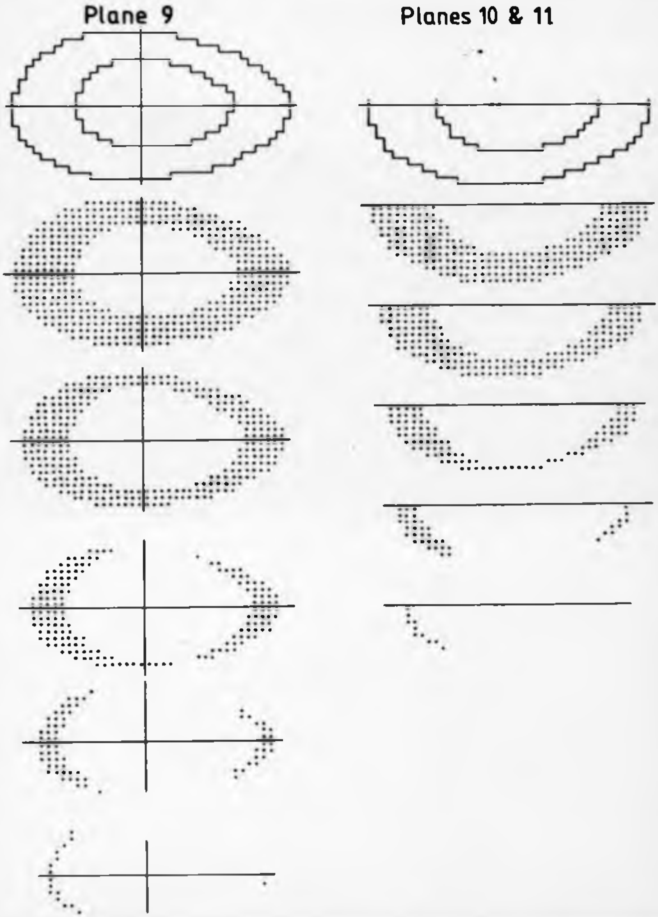

Plane 9
Planes 10 & 11

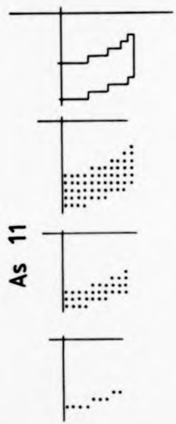

Plane 12

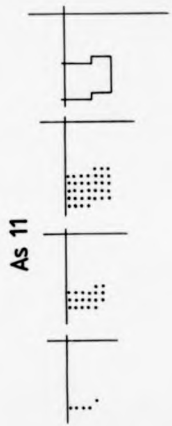

Plane 13

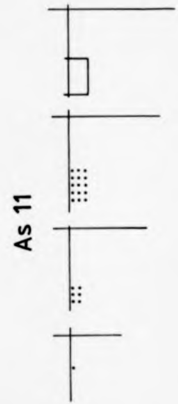

Plane 14

APPENDIX

7

FIRST PREDICTION USING IRLST FOR SINGLE AND MULTIPLE PLANES.

Fig. A10.1 shows a summation of planes all containing uniform activity distribution.

From the IRLST, Budinger 1974, the first prediction for the single plane and for a number of planes is given by

$$a_{ij} = \sum_{\theta} f_{ij} \Big/ \sum_{\theta} \left\{ f_{ij}^2 / P_{k\theta} \right\}$$

and

$$p_{ij} = \sum_{\theta} f_{ij} \Big/ \sum_{\theta} \left\{ f_{ij}^2 / \eta_{k\theta} \right\}$$

where a_{ij} and p_{ij} are the predictions for the summation and single plane respectively.

$P_{k\theta}$ and $\eta_{k\theta}$ are the raysums appropriate to the summation and single plane respectively.

θ identifies the view and k the pixel.
and f_{ij} is the factor associated with any voxels.

The summation of the activity at the point i,j is given by $a''_{ij} = \sum_{n} p_{ij\,m}$
where m identifies plane

$$\Rightarrow \quad a''_{ij} = \sum_{n} \left[\sum_{\theta} f_{ij} \Big/ \sum_{\theta} \left\{ f_{ij}^2 / \eta_{k\theta} \right\} \right]$$

if $P_{k\theta} = n.\eta_{k\theta}$ then

$$a'_{ij} = \sum_{\theta} f_{ij} \Big/ \sum_{\theta} \left\{ f_{ij} / n.\eta_{k\theta} \right\} = n \left[\sum_{\theta} f_{ij} \Big/ \sum_{\theta} \left\{ f_{ij}^2 / \eta_{k\theta} \right\} \right]$$

$$\Rightarrow \quad a^*_{ij} = a_{ij} = n\, p_{ij}$$

This is the case for volume elements close to the central axis in a regular object, e.g. a cylinder. However, towards the periphery, the relation $P_{k\theta} = n\,\eta_{k\theta}$ does not hold and $P_{k\theta} = n_{k\theta} \cdot \eta_{k\theta}$

$$a^*_{ij} = \sum_{n} \left[\sum_{\theta} f_{ij} \Big/ \sum_{\theta} \left\{ f^*_{ij} \cdot n_{k\theta} / P_{k\theta} \right\} \right]$$

$$= \sum_{\theta} f_{ij} \cdot \sum_{n} \left[\sum_{\theta} \left\{ f^*_{ij} \cdot n_{k\theta} / P_{k\theta} \right\}^{-1} \right]$$

$$\frac{a^*_{ij}}{a_{ij}} = \sum_{\theta} \left\{ f^*_{ij} / P_{k\theta} \right\} \sum_{n} \left[\sum_{\theta} \left\{ f^*_{ij}\, n_{k\theta} / P_{k\theta} \right\}^{-1} \right]$$

and only if $n_{k\theta} = n$ does $\dfrac{a^*_{ij}}{a_{ij}} = 1.$

Thus the summation holds at the centre of the object volume but not at the periphery of the object volume.

Fig. A10.1

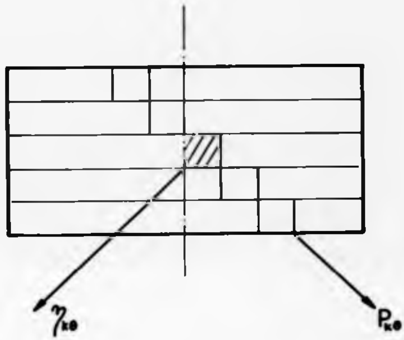

ELEVATION OF SUMMATION OF PLANES WITH UNIFORM ACTIVITY. EACH PLANE IS DIVIDED INTO DISCRETE VOLUME ELEMENTS

APPENDIX

8

CALCULATION OF THE RAYSUMS THROUGH THE CENTRE OF AND AT THE TANGENT TO A HEMI-ELLIPSOID

Fig. A11.1 shows the cross section of an object, composed of two hemi-ellipsoids with points at which predicted activity can easily be located. Point A is at centre of maximum plane radius. Point C and B are at the extremities of the reconstruction volume.

A11.1 Use of Ratios to Estimate Object Volume

$$AL = AL_1 + AL_2 \qquad \rho_1 = \frac{AL_1}{B} \text{ and } \rho_2 = \frac{AL_2}{C}$$

$$\rho_b = \frac{AL_1 + AL_2}{B} \quad \text{and} \quad \rho_c = \frac{AL_1 + AL_2}{C}$$

where AL, AL_1 and AL_1 are the predictions based on the lengths L, L_1 and L_2 shown in Fig. A11.1

B and C are the predictions at points B and C

ρ_1 and ρ_2 are the ratios calculated for a range of known hemispheres.

ρ_b and ρ_c are the measured ratios.

then $\rho_b = \rho_1 + C/B.\rho_2$

$\rho_c = \rho_2 + C/B.\rho_1$ which can be solved to obtain ρ_1 and ρ_2 and hence the shape of the hemi-ellipsoid.

A11.2 Calculation of Central Length

The central length, L is found by obtaining the point of intersection between the ellipse edge and a line at the appropriate collimator angle, Fig. A11.2.

where the equation of the ellipse is $\frac{x^2}{a^2} + \frac{y^2}{b^2} = 1$.

and the intersecting raysum has equation $y = gx$.

A11.3 Calculation of Central Prediction

For a QUAD (26.6°) RSHECT system, the first prediction using IRLST, and the uniform activity is given by

$$AL = \frac{4}{0.75^2 \cdot \frac{4}{\alpha} + 0.125^2 \cdot \frac{8}{\alpha}} \quad \text{where } \alpha = \text{the activity.}$$

In this case the activity is taken as proportional to the area so $\alpha = L.\cos\theta$, see Fig. A11.2

$$\Rightarrow \quad AL = 1.6842.L\cos\theta.$$

A11.4 Calculation of Tangent Area

For the construction illustrated in Fig. A11. the tangent position is given by

$$x_t = a / \left(1 + \frac{b^2}{a^2 g^2}\right)^{\frac{1}{2}}$$

The function of the parallel line to the tangent is found by calculating the constant K for its linear equation.

$$K = g\,[\mathrm{INT}\,(x_t)] + y_t$$

Where INT (x_t) is the integer of x_t. Using this equation along with the equation of the ellipse results in the intercepts x_1 and x_2.

The tangential area is found from the difference of two areas A1 and A2.

A1 is the trapesium beneath the curve of the ellipse, but between x_1 and x_2.

$$A1 = (x_1 - x_2)\,(y_1 + y_2)/2$$

A2 is the area under the ellipse between x and x.

$$A2 = \frac{ab}{2}\left[\frac{\sin 2\theta}{2} + \theta\right]_{\theta_1}^{\theta_2}$$

where $\theta = \sin^{-1}\left\{ x/a \right\}$

Finally the prediction at the extremity of the reconstruction volume is calculated from

$$B = 3.7 \left\{ 2.075^2 \cdot \left[\frac{1}{P_1} + \frac{1}{P_2}\right] + 2.0125^2 \cdot \left[\frac{1}{P_1} + \frac{1}{P_2} + \frac{1}{P_3}\right]\right\}^{-1}$$

where P_1, P_2 and P_3 are the areas coming in from the tangent, see Fig. A11.2.

```
1  REM  PROGRAM TO CALC RATIO A/B FOR
2  REM  A HEMI-ELLIPSOID
3  DIM P(3)
5  HOME
7 PI = 3.1415927
9  INPUT "INPUT THE SYSTEM ANGLE ";GT
10  HOME
11 G =  TAN (PI * (0.5 - GT / 180))
15  PRINT : PRINT "GRADIENT = ",G
20  PRINT : INPUT "MAJOR AND MINOR AXES A & B ";A,B
40  PRINT
50 X = A /  SQR (1 + A ^ 2 * G ^ 2 / B ^ 2)
60 AL = X *  SQR (G ^ 2 + 1)
70  PRINT "INTERCEPT IS AT X = ";X
75 AL = AL * 1.66421 *  COS (GT / 180 * PI)
80  PRINT "ACTIVE LENGTH      = ";AL
90  PRINT : PRINT
100 XT = A /  SQR (1 + B ^ 2 / G ^ 2 / A ^ 2)
110 YD = B *  SQR (1 - XT ^ 2 / A ^ 2)
112 YI = G * XT + YD
114  PRINT "XT,YD,YI ",XT,YD,YI
115  GOTO 305
116 XT =  INT (XT) + 1
117  FOR N = 1 TO 3
120 K = G * (XT - N) + YD
130 A1 = G ^ 2 + B ^ 2 / A ^ 2
140 B1 = 2 * K * G
150 C1 = K ^ 2 - B ^ 2
155  PRINT "A1,B1,C1 ",A1,B1,C1
160 X2 =  SQR (B1 ^ 2 - 4 * A1 * C1)
170 X1 = (B1 + X2) / 2 / A1:T1 =  ATN (X1 / A /  SQR (1 - X1 ^ 2 / A ^ 2)
    )
180 X2 = (B1 - X2) / 2 / A1:T2 =  ATN (X2 / A /  SQR (1 - X2 ^ 2 / A ^ 2)
    )
185  PRINT "T1,T2 ";T1,T2
190 D2 = ( SIN (2 * T2)) / 2 + T2
200 D2 = (D2 - ( SIN (2 * T1)) / 2 - T1) * A * B / 2
210 Y1 = K - G * X1:Y2 = K - G * X2
215 D1 = (X2 - X1) * (Y2 + Y1) / 2
220 P(N) = D1 - D2
230  NEXT N
240 P(3) = P(3) - P(2):P(2) = P(2) - P(1)
245  PRINT "P'S = ",P(1),P(2),P(3)
250 AP = 1.125 * (1 / P(1) + 1 / P(2)) + 31.25E - 3 * (1 / P(1) + 1 / P(2
    ) + 1 / P(3))
260 AP = 3.75 / AP
270  PRINT : PRINT "ACTIVE PERIPH    = ";AP
280  PRINT
290 ADB = AL / AP
300  PRINT "RATIO = ";ADB
305  PRINT
310  INPUT "DO YOU WISH TO RERUN Y/N ";A$
320  IF A$ = "Y" THEN 10
330  STOP
```

Fig A.11.1

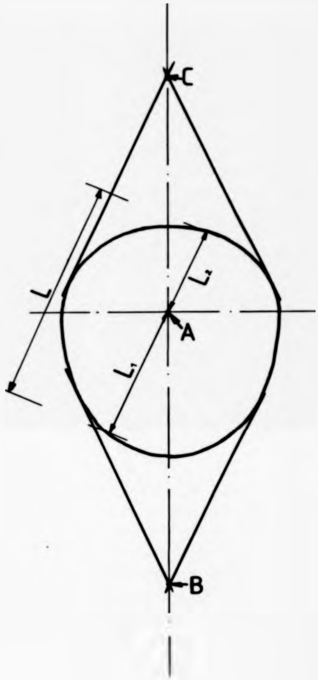

Fig A.11.2

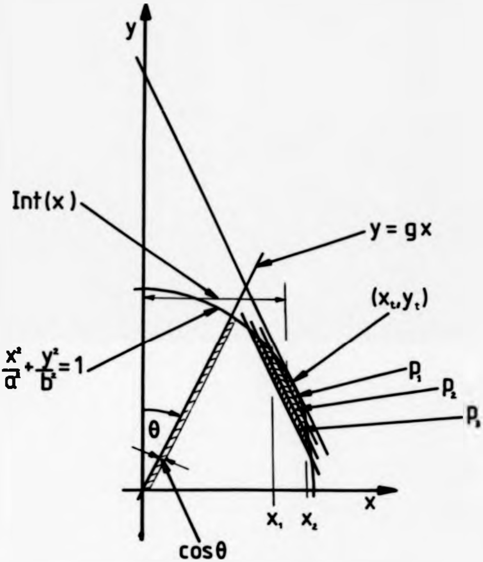

APPENDIX 9

ILSRT PROGRAM FOR A (26.6°) QUAD LECT SYSTEM WITH AN ERROR VOLUME CORRECTION


```
C     THIS PROGRAM IS FOR A QUAD SYSTEM ONLY
C     WITH A CORRECTION BASED ON THE SHAPE OF THE ERROR VOLUME
C     QUADRANT PROJECTION ITERATIVE RECONSTRUCTION TECHNIQUE
      REAL NUM
      DIMENSION P(3136),R(3136),A(3276),DA(3276),ILST(50),IX(4,2),
     CIY(4,2),IRA(28),CL(13),MWD(13)
      DATA (ILST(I),I=1,48)/1,0,1,2,0,1,2,1,28,13,0,0,1,0,781,980,
     C1,0,1,0,0,1,0,1,280,-1,0,1,0,0,-1,0,1/
      IX(1,1)=1
      IX(1,2)=0
      IX(2,1)=0
      IX(2,2)=1
      IX(3,1)=1
      IX(3,2)=2
      IX(4,1)=2
      IX(4,2)=1
      IY(1,1)=1
      IY(1,2)=0
      IY(2,1)=0
      IY(2,2)=1
      IY(3,1)=1
      IY(3,2)=0
      IY(4,1)=0
      IY(4,2)=1
      OPEN(4,ACCESS='SEQUENTIAL',FORM='FORMATTED',STATUS='OLD')
      OPEN(3,ACCESS='SEQUENTIAL',FORM='FORMATTED',STATUS='OLD')
      OPEN(12,ACCESS='SEQUENTIAL',FORM='FORMATTED',STATUS='NEW')
      NPL=1
      NPU=ILST(10)
      WRITE(6,2000)
1     READ(5,8)ILST(17)
      IF(ILST(17).LT.1.OR.ILST(17).GT.2) GOTO 1
      IF(ILST(17).EQ.2) GOTO 30
C     READS IN INITIAL PLANE DISTRIBUTION
      WRITE(6,2010)
      READ(3,8)(A(I),I=1,3276)
      DO 20 I=1,3276
      DA(I)=0.0
20    CONTINUE
      GOTO 40
30    DO 40 I=1,3276
      A(I)=0.0
      DA(I)=0.0
40    CONTINUE
      WRITE(6,2020)
      READ(5,8)ILST(12)
      WRITE(6,2030)
      READ(5,8)ILST(15)
      WRITE(6,2040)
      READ(5,8)ILST(16)
C     READS IN PROJECTION DATA
      WRITE(6,2080)
      READ(4,8)(P(I),I=1,3136)
 10   CONTINUE
C     CALCULATION OF RAYSUMS AND PLANE INCREMENTS
```

```
      WRITE(6,3000)
      DO 100 IT=1,4
      KA=(IT-1)*ILST(9)**2
      DO 110 L=1,ILST(9)
      KB=(L-1)*ILST(9)
      DO 120 K=1,ILST(9)
      IZ=K+KA+KB
      IV=0
      IF (NPL.EQ.1) GOTO 60
      DO 60 N=1,(NPL-1)
      NW=ILST(9)-2*N
      IV=IV+NW**2
 60   CONTINUE
      CT=0
      DO 130 N=NPL,NPU
      NW=ILST(9)-2*N
      KK=K-IX(IT,2)*N
      IF(KK.LT.1.OR.KK.GT.NW) GOTO 130
      LL=L-IX(IT,1)*N
      IF(LL.LT.1.OR.LL.GT.NW) GOTO 130
      IW=IV+(LL-1)*NW+KK
      IWP=IW+IY(IT,2)*NW+IY(IT,1)
      IWM=IW-IY(IT,2)*NW-IY(IT,1)
      CT=CT+A(IW)*0.75
      IF(IT.EQ.2.OR.IT.EQ.4) GOTO 135
      IF(KK.GT.1) CT=CT+A(IWM)*0.125
      IF(KK.LT.NW) CT=CT+A(IWP)*0.125
      GOTO 145
 135  IF(LL.GT.1) CT=CT+A(IWM)*0.125
      IF(LL.LT.NW) CT=CT+A(IWP)*0.125
 145  CONTINUE
      IV=IV+NW**2
 130  CONTINUE
      R(IZ)=CT
 120  CONTINUE
 110  CONTINUE
 100  CONTINUE
C     CALCULATES THE INCREMENTS
      WRITE(6,3100)
      IV=0
      IF (NPL.EQ.1) GOTO 160
      DO 160 N=1,(NPL-1)
      NW=ILST(9)-2*N
      IV=IV+NW**2
160   CONTINUE
      DO 200 N=NPL,NPU
      NLT=ILST(9)-2*N
      DO 210 J=1,NLT
      DO 220 I=1,NLT
      IV=IV+1
      NUM=0
      DEN=0
      DO 240 IT=1,4
      II=I+IX(IT,2)*N
      JJ=J+IX(IT,1)*N
```

```
      IZ=I+(JJ-1)*ILST(9)+(IT-1)*ILST(9)**2
      IF(P(IZ).EQ.0) GOTO 250
      NUM=NUM+0.75*(P(IZ)-R(IZ))/P(IZ)
      DEN=DEN+0.75**2/P(IZ)
      IZP=IZ+IY(IT,2)*ILST(9)+IY(IT,1)
      IZM=IZ-IY(IT,2)*ILST(9)-IY(IT,1)
      IF(IT.EQ.2.OR.IT.EQ.4) GOTO 260
      IF(I.EQ.1) GOTO 270
      IF(P(IZM).EQ.0.0) GOTO 270
      NUM=NUM+(P(IZM)-R(IZM))/P(IZM)*0.125
      DEN=DEN+0.125**2/P(IZM)
270   IF(I.EQ.ILST(9)) GOTO 240
      IF(P(IZP).EQ.0.0) GOTO 240
      NUM=NUM+0.125*(P(IZP)-R(IZP))/P(IZP)
      DEN=DEN+0.125**2/P(IZP)
      GOTO 240
260   IF(JJ.EQ.1) GOTO 290
      IF(P(IZM).EQ.0.0) GOTO 290
      NUM=NUM+(P(IZM)-R(IZM))/P(IZM)*0.125
      DEN=DEN+0.125**2/P(IZM)
290   IF(JJ.EQ.ILST(9)) GOTO 240
      IF(P(IZP).EQ.0.0) GOTO 240
      NUM=NUM+(P(IZP)-R(IZP))/P(IZP)*0.125
      DEN=DEN+0.125**2/P(IZP)
240   CONTINUE
      DA(IV)=NUM/DEN
      GOTO 220
250   A(IV)=0
      DA(IV)=0
220   CONTINUE
210   CONTINUE
200   CONTINUE
C     CALCULATES THE DELTA FACTOR
      WRITE(6,3200)
      NUM=0
      DEN=0
      DO 400 IT=1,4
      KA=(IT-1)*ILST(9)**2
      DO 410 L=1,ILST(9)
      KB=(L-1)*ILST(9)
      DO 420 K=1,ILST(9)
      IZ=K+KA+KB
      IF(P(IZ).EQ.0.0) GOTO 420
      ZCUM=0
      IV=0
      IF(NPL.EQ.1) GOTO 460
      DO 460 N=1,(NPL-1)
      NW=ILST(9)-2*N
      IV=IV+NW**2
460   CONTINUE
      DO 430 N=NPL,NPU
      NW=ILST(9)-2*N
      KK=K-IX(IT,2)*N
      IF(KK.LT.1.OR.KK.GT.NW) GOTO 430
      LL=L-IX(IT,1)*N
```

```
      IF(LL.LT.1.OR.LL.GT.NW) GOTO 430                                  SQU01660
      IW=IV+KK+(LL-1)*NW                                                SQU01670
      IWP=IW+IY(IT,2)*NW+IY(IT,1)                                       SQU01680
      IWM=IW-IY(IT,2)*NW-IY(IT,1)                                       SQU01690
      ZCOM=ZCOM+DA(IW)*0.75                                             SQU01700
      IF(IT.EQ.2.OR.IT.EQ.4) GOTO 440                                   SQU01710
      IF(KK.GT.1) ZCOM=ZCOM+DA(IWM)*0.125                               SQU01720
      IF(KK.LT.NW) ZCOM=ZCOM+DA(IWP)*0.125                              SQU01730
      GOTO 450                                                          SQU01740
  440 IF(LL.GT.1) ZCOM=ZCOM+DA(IWM)*0.125                               SQU01750
      IF(LL.LT.NW) ZCOM=ZCOM+DA(IWP)*0.125                              SQU01760
  450 CONTINUE                                                          SQU01770
      IV=IV+NW**2                                                       SQU01780
  430 CONTINUE                                                          SQU01790
      NUM=NUM+(P(IZ)-R(IZ))/P(IZ)*ZCOM                                  SQU01800
      DEN=DEN+ZCOM**2/P(IZ)                                             SQU01810
  420 CONTINUE                                                          SQU01820
  410 CONTINUE                                                          SQU01830
  400 CONTINUE                                                          SQU01840
      WRITE(6,*) NUM,DEN                                                SQU01850
      D=NUM/DEN                                                         SQU01860
      WRITE(12,1040)                                                    SQU01870
      WRITE(6,*) D                                                      SQU01880
C     CORRECTS THE PLANE DISTRIBUTIONS                                  SQU01890
      WRITE(6,3300)                                                     SQU01900
      IV=0                                                              SQU01910
      IF(NPL.EQ.1) GOTO 560                                             SQU01920
      DO 560 N=1,(NPL-1)                                                SQU01930
      NW=ILST(9)-2*N                                                    SQU01940
      IV=IV+NW**2                                                       SQU01950
  560 CONTINUE                                                          SQU01960
      DO 500 N=NPL,NPU                                                  SQU01970
      NLT=ILST(9)-2*N                                                   SQU01980
      DO 510 J=1,NLT                                                    SQU01990
      DO 520 I=1,NLT                                                    SQU02000
      IV=IV+1                                                           SQU02010
      A(IV)=A(IV)+D*DA(IV)                                              SQU02020
      IF(A(IV).LE.0.0) A(IV)=0.0                                        SQU02030
  520 CONTINUE                                                          SQU02040
  510 CONTINUE                                                          SQU02050
  500 CONTINUE                                                          SQU02060
C     SURVEY OF CENTRAL AXIS PROFILE AFTER FIRST APPROX                 SQU02070
      IF(ILST(13).NE.1) GOTO 970                                        SQU02080
      IV=0                                                              SQU02090
      DO 700 N=1,ILST(10)                                               SQU02100
      NLT=ILST(9)-2*N                                                   SQU02110
      LCT=NLT/2-1                                                       SQU02120
      NLP=LCT*NLT+1+IV                                                  SQU02130
      NUP=NLP+LCT                                                       SQU02140
      CL(N)=A(NUP)                                                      SQU02150
      DO 710 NP=NLP,NUP                                                 SQU02160
      IF(A(NP).NE.0) GOTO 720                                           SQU02170
  710 CONTINUE                                                          SQU02180
      NWB(N)=0                                                          SQU02190
      GOTO 722                                                          SQU02200
```

```
 720  MWD(N)=NUP+1-NP
 722  IV=IV+NLT**2
      WRITE(6,*   ) CL(N),MWD(N)
 700  CONTINUE
C     FINDS MID PLANE,XT,YT AND PLANE CORRECTION,PC
      DO 730 N=1,ILST(10)
      YI=ILST(10)+1-N
      B=CL(YI+1-N)
      IF(B.GT.0) GOTO 735
 730  CONTINUE
 735  MAX=0
      MCX=0
      DO 750 N=1,ILST(10)
      IF(MWD(N).LE.MAX) GOTO 750
      MAX=MWD(N)
      IF(CL(N).LE.MXC) GOTO 750
      MXC=CL(N)
      MID=N
 750  CONTINUE
      XT=MID*0.86625
      DO 755 N=1,ILST(10)
      NN=ILST(10)+1-N
      IF(MWD(NN).LT.MID) GOTO 755
      XT=MWD(NN+1)
      YT=NN
      GOTO 760
 755  CONTINUE
 760  PC=(YI-YT)/3.2
      NPL=2*MID-YT-INT(PC)
      NPU=YT+INT(PC)
      WRITE(6,*)MID,YT,YI,PC
C     ZERO THE EXCLUDED PLANES
 775  IV=0
      DO 780 N=1,(NPL-1)
      NLT=(ILST(9)-2*N)**2
      DO 785 J=1,NLT
      IV=IV+1
      A(IV)=0
 785  CONTINUE
 780  CONTINUE
      DO 790 N=NPL,NPU
      NLT=(ILST(9)-2*N)**2
      IV=IV+NLT
 790  CONTINUE
      DO 795 N=(NPU+1),ILST(10)
      NLT=(ILST(9)-2*N)**2
      DO 800 J=1,NLT
      IV=IV+1
      A(IV)=0
 800  CONTINUE
 795  CONTINUE
C     PRINT ROUTINE FOR PLANES AND KAYSUMS
 970  WRITE(12,1000) ILST(13)
      IF(ILST(15).NE.1) GOTO 900
C     PRINT KAYSUMS
```

```
      WRITE(6,2050)
      DO 910 IT=1,4
      WRITE(12,1010)IT
      KA=(IT-1)*ILST(9)**2
      DO 920 L=1,ILST(9)
      KB=(L-1)*ILST(9)
      DO 930 K=1,ILST(9)
      IZ=K+KA+KB
      IRA(K)=R(IZ)
  930 CONTINUE
      WRITE(12,1020)(IRA(N),N=1,ILST(9))
  920 CONTINUE
  910 CONTINUE
  900 IF(ILST(16).NE.2.AND.ILST(13).NE.ILST(12)) GOTO 990
C     PRINT PLANES
      WRITE(6,2060)
      IV=0
      DO 940 N=1,ILST(10)
      WRITE(12,1030)N
      NW=ILST(9)-2*N
      DO 950 I=1,NW
      DO 960 J=1,NW
      IV=IV+1
      IRA(J)=A(IV)
  960 CONTINUE
      WRITE(12,1020)(IRA(K),K=1,NW)
  950 CONTINUE
  940 CONTINUE
  990 IF(ILST(13).EQ.ILST(12)) GOTO 995
      ILST(13)=ILST(13)+1
      GOTO 10
  995 WRITE(6,2070)
 1000 FORMAT(1H ,6X,10HITERATION ,I3/1H0)
 1010 FORMAT(1H ,6X,7HRAYSUM ,I2/1H0)
 1020 FORMAT(1H ,14(1X,I6)/1H ,14(1X,I6))
 1030 FORMAT(1H ,5X,6HPLANE ,I3/1H0)
 1040 FORMAT(5X,8HDELTA = ,1PE12.4)
 2000 FORMAT(1H ,5X,35HINPUT THE FIRST APPROXIMATION INDEX/
     C1H ,22X,8H1. IDEAL/1H ,22X,21H2. IMPEDANCE OPERATOR/1H /
     C1H ,22X,11HINPUT 1-2  )
 2010 FORMAT(1H0,5X,36HNOW INPUTING THE FIRST APPROXIMATION)
 2020 FORMAT(1H0,5X,41HINPUT THE NUMBER OF ITERATIONS REQUIRED  )
 2030 FORMAT(1H0,5X,44HDO YOU WISH THE RAYSUMS PRINTED 1-YES,2-NO  )
 2040 FORMAT(1H0,5X,26HDO YOU WISH PLANES PRINTED/
     C1H ,22X,24H1. AFTER FINAL ITERATION/
     C1H ,22X,23H2. AFTER EACH ITERATION/1H /
     C1H ,22X,11HINPUT 1-2  )
 2050 FORMAT(1H0,5X,20HNOW PRINTING RAYSUMS)
 2060 FORMAT(1H0,5X,32HNOW PRINTING PLANE DISTRIBUTIONS)
 2070 FORMAT(1H0,15X,11H*** END ***)
 2080 FORMAT(1H0,5X,28HNOW INPUTING THE PROJECTIONS)
 3000 FORMAT(1H0,5X,23HNOW CALCULATING RAYSUMS)
 3100 FORMAT(1H0,5X,26HNOW CALCULATING INCREMENTS)
 3200 FORMAT(1H0,5X,21HNOW CALCULATING DELTA)
 3300 FORMAT(1H0,5X,25HNOW CORRECTING THE PLANES)
```

```
      STOP                                                    SQU03310
      END                                                     SQU03320
```

BIBLIOGRAPHY

ANDREWS, J.R., 1936, "Planigraphy 1; introduction and history", Am. J. Roent, 36, 575-

ANDREWS, J.R. and STAVA, R.J., 1937, "Planigraphy II; mathematical analysis of the methods, description of apparatus and experimental proof", Am. J. Roent, 38, 145-

ANGER, H.O. (1958), "Scintillation Camera". Rev. Scient. Instrum, 29, 27-

BARAT, J.L., BRENDEL, A.J., COLLE, J.P., MAGINEL PELONIER, OHAYON, J., LECCIA, F., BESSE, P. and DUCASSOU, D., 1984, "Gated Single Photon Emission Tomography (GSPECT) as a means of quantitive assessment of LV wall motion", JNM, 25, P44

BENDER, M.A. and BLAU (1962) "The Autoflouroscope" in Progress in Medical Radioisotope Scanning, pg 151. Edited by R.M. Kniseley, G.A. Andrews and C.C. Harris, USAEC Report TID-7673

BERCHE, C., AUBRY, F., LANGLAIS, C., VITAUX, J., PARMENTIER, Cl. and PAOLA, R.D., 1981, "Diagnostic Value of Transverse Axial Tomoscintigraphy for the Detection of Hepatic Metastases: Results on 53 Examinations and Comparison with other Diagnostic Techniques", EJNM, 6, 435-

BERGER, B.C., WATSON, D.D, TAYLOR, G.J., CRADDOCK, G.B., MARTIN, R.P., TEATES, C.D. and BELLER, G.A., 1981 "Quantitative Thallium-201 Exercise Scintigraphy for Detection of Coronary Artery Disease", JNM, 22, 585-

BODENHEIMER, M.M., BANKA, V.S. and HELFANT, R.H., 1980, "Nuclear Cardiology II. The Role of Myocardial Perfusion Imaging Using Thallium-201 in Diagnosis of Coronary Heart Disease", Am. J. Card., 45, 674-

BRACEWELL, R.N., 1956 "Strip Integration in Radio Astronomy", Aust. J. Phys. 9, 198-

BROOKEMAN, V.A. and MAISEY, M.N., 1982, "Performance Characteristics of Seven Pinhole Tomography", BJR, 55, 229-

BUDINGER, T.F., and GULLBERG, G.T., 1974, "Three-dimensional Reconstruction in Nuclear Medicine Emission Imaging", IEEE Trans. Nucl. Sci. NS 21, 2-

BUDINGER, T.F., 1980 "Physical Attributes of Single-Photon Tomography", JNM, 21, 579-

CASSEN, B., CURTIS, L. REED, C. and LIBBY, R., 1951 "Instrumentation for ^{131}I use in Medical Studies", Nucleonics 9, No. 2, 46-

CHANG, L.T., 1978, "A Method for Attenuation Correction in Radionuclide Computed Tomography", IEEE Trans. Nucl. Sci., NS-25, 638-

CHANG, W., HENKIN, R.E. and BUDINGER, E., 1984, "The Sources of Overestimation in Quantification by SPECT of Uptake in a Myocardial Phantom: Concise Communcications", JNM, 25, 788-

CHUI, M.Y., BARRETT, H.H., SIMPSON, R.G., CHOU, C., ARENDT, J.W. and GINDI, G.R., 1979, "Three-dimensional Radiographic Imaging with a Restricted View Angle". J. Opt. Soc. Am., 69, 1323-

CONDON, B., MILLS, J, ARDLEY, R. and TAYLOR, D., 1983 "A Physical Comparison of Two Fixed Angle Tomographic Cardiac Imaging Systems PMB, 28, 131-

DALE, S. EDHOLM, D.E., HELLSTROM, L.GL and LARSSON, S., (1985), "Ectomography - A Tomographic Method for Gamma Camera Imaging". PMB, 30, 1237-

DENDY, P.P, KEYES, W.J., REID, A., UNDRILL, P.E., SMITH, F.W., MALLARD, J.R. and MACDONALD, A.F., 1981, "A Clinical Trial of the Value of a Tomographic Section View to Identify Liver Abnormalities by Radionuclide Imaging with Special Reference to Metastatic Disease", Eur. JNM, 6, 51-

DOHERTY, P.W., KING, M.A. and SCHWIGER, R.B., 1984 "Tomographic Gated Blood Pool Studies: The Parameters for Collection and Reconstruction", JNM, 25, P85

ELL, P.J., DEACON, J.M., DUCASSOU, D. and BRENDEL, A., 1980, "Emission and Transmission Brain Tomography", BMJ, 438-

ELLIOT, A.T., DYMOND, D.S., STONE, D.L., FLATMAN, W., BETT, R., CUNNINGHAME, J.G., SIMMS, H.E. and WILLIS, H.H., 1983, "A Hg-Au Generator for use in First-Pass Nuclear Angiocardiography", PMB, 28, 139-

FABER, T.L., BROWN, W.D., POSKEY, R.W., WILLERSON, J.T., and CORBETT, J.R., 1985, " Comparison of the Results of SPECT Acquisition with Circular Elliptical and Contoured Orbits", JNM, 26, P11

FARIS, J.V., BURT, R.W., GRAHAM, M.C. and KNOEBEL, S.B., 1982 "Thallium-201 Myocardial Scintigraphy: Improved Sensitivity, Specificity and Predictive Accuracy by Application of a Statistical Image Analysis Algorithm, Am. J. Card. 49, 733-

FAZIO, F., FIESCHI, C., COLLICE, M., NARDINI, M., BANFI, F., POSSA, M., and SPINELLI, F., 1980, "Tomographic Assessment of Cerebral Perfusion Using a Single-Photon Emitter (Krypton 81m, and a Rotating Gamma Camera", JNM, 21, 1139-

FAZIO, F., LENZI, G.L., GERUNDINI, P., COLLICE, M., GILARDI, M.C., COLOMBO, R., TADDEI, G., Del MASCHIO, A., et al, 1984, "Tomographic Assessment of Regional Cerebral Perfusion Using i.v. I HIPDM and a Rotating Gamma Camera", J. Comput. Assis. Tom., 8, 911-

FREEDMAN, G.S., 1973 "Tomographic Imaging in Nuclear Medicine", Chapt. 6, Society of Nuc. Med., New York

GARCIA, E., MADDAHI, J., BERMAN, D. and WAXMAN, A, 1981, "Space/Time Quantitation of Thallium-201 Myocardial Scintigraphy" JNM, 22, 309-

GORDON, R., 1974, "A Tutorial on ART", IEEE Trans. Nucl. Sci. N2 21, 78-

GOTTSCHALK, S.C., SMITH, K.A. and WAKE, R.H., undated, "Tomographic Reconstructions With Rotation Slant Hole and Seven Pinhole Collimators on an Anger Camera: Phantom and Clinical Studies", Technicare Corporation

GOTTSCHALK, S.C., SALEM, D., LIM, C.B. and WAKE, R.H., 1983, "SPECT Resolution and Uniformity Improvements by Non-Circular Orbit", JNM, 24, 822-

GREER, K.L, COLEMAN, R.E. and JASZCZAK, R.J., 1983, "SPECT: A Practical Guide for Users", JNM Tech. 11, 61-

HAMILTON, G.W., 1979, "Myocardial Imaging with Thallium-201: The Controversy Over the Clinical Usefulness in Ischaemic Heart Disease", JNM, 20, 1201-

HARKNESS, B.A., ROGERS, W.L., CLINTHORNE, N.H. and KEYES, J.W., 1983 "SPECT: Quality Control Procedures and Artefact Identifiction", JNM. Tech. 11, 55-

HARRIS, C.C., GREER, K.L., FLOYD, C.E., JASZCZAK, R.J., FARROW, E.C. and COLEMAN, R.E., 1984, "Attenuation Coefficients for Tc Photons in Water Filled Phantoms, Determined with a Gamma Camera: Variation with Energy Windows", JNM, 25, P22-

HASEGAWA, B., KIRCH, D., STERN, D., ADAMS, M., SKLAR, J., JOHNSON, T. and STEELE, P., 1982, "Single-Photon Emission Tomography with a 12-Pinhole Collimator", JNM, 23, 606-

JASZCZAK, R., undated, "Data Spectrum Phantom", Scientific and Industrial Equipment (Reading) Ltd.

JASZCZAK, R.J., CHANG, L.T. and STEIN, W.A., 1979, "Whole Body SPECT Using Dual LFOV Scintillation Cameras", PMB, 24, 1123-

JASZCZAK, R.J., GREER, K.L., FLOYD, C.E., HARRIS, C.C. and COLEMAN, R.E., 1984, "Improved SPECT Quantification Using Quantification for Scattered Photons", JNM, 25, 893-

KAWAMURA, J., ITOH, H., YOSHIDA, O., FUJITA, T. and TORIZUKA, K., 1984, "In Vivo Estimation of Renal Column Using a Rotating Gamma Camera for Tc-DMSA Renal Imaging", Eur. JNM, 9, 168-

KIRCH, D.L., VOGEL, R.A., LeFREE, M.T., STERN, D.M., SKLAR, J., HASEGAWA, B.H. and STEELE, P.P., 1980, "An Anger Camera/Computer System for Myocardial Perfusion Tomography Using a Seven Pinhole Collimator", IEEE Trans. Nucl. Med. NS27, 412-

KORAL, K.F., CLINTHORNE, N.H., ROGERS, W.L. and KEYES, J.W., 1982, "Feasibility of Sharpening Limited Angle Tomography by Including an Orthogonal Set of Projections", Nuc. Instr. and Meth., 193, 223-

KORAL, K.F., NOLDER, C., CILIAX, G., ROGERS, W.L. and KEYES, J.W., 1984, "Simulated ECT of the Left Ventricle Using Rotating Slant-Hole Collimator and Two Camera Positions", JNM, 25, 343-

KUHL, D.E. and EDWARDS, R.Q., 1963, "Image Separation Radio-isotope Scanning", Radiology, 80, 653-

LaFONTAINE, R., GRAHAM, L.S., and STEIN, M.A., 1984, "Effects of Asymmetric Photopeak Windows on Flood Field Uniformity and Spatial Resolution for Scintillation Cameras", JNM, 25, P22

LeFREE, M.T., VOGEL, R.A., KIRCH, D.L. and STEELE, P.P., 1981, "Seven Pinhole Tomography - A Technical Description", JNM, 22, 48-

LeJEUNE, J.J., MAUBLANT, J., LAHELLEL, M. and VEYRE, A., 1982, "Emission Computed Tomography vs Perfusion Scanning in Lung Disease", Eur, JNN, 7, 171-

MACEY, D.J., DeNARDO, G.L., DeNARDO, S.J., and SEIBERT, J.A., 1985, "A Modified Post Processing Attenuation Correction Method for SPECT", JNM, 26, P35.

MAEDA, H., ITOH, H. and ISHIU, Y., 1981, "Determination of the Pleural Edge by Gamma Ray Transmission Computed Tomography", JNM, 22, 815-

MAGISTRETTI, P.L., UREN, R.F., PARKER, J.A., ROYAL, H.D., FRONT, D., and KOLODNY, G.M., 1983, "Monitoring of Regional Cerebral Blood Flow by Single Photon Emission Tomography of I-123-N-Isopropyl-Iodoamphetamine in Epilelatics", Ann. Radiol (Paris), 26, 68-

MASSIE, B., BOTVINICK, E., ARNOLD, S., SHAMES, D., BRUNDAGE, B., HANLON, J.T. and SHELDON, K., 1981, "Contrast Enhancement of Thallium-201 Myocardial Scintigrams: Improved Sensitivity with Diminished Specificity in Coronary Disease Detection", Am. Heart, J., 102, 37-

MAUBLANT, J., CASSAGNES, J., LeJUENE, J.J., MESTAS, D., VEYRE, A., JALLUT, H. and MEYNIEL, G., 1983, "A Comparison Between Conventional Scinitigraphy and Emission Tomography with Thallium-201 in Detection of Myocardial Infarction: Concise Communication", JNM, 23, 204-

MAYNEORD, W.V., TURNER, R.C., NEWBERY, S.P. and HOOT, H.D., 1951, "A Method of Making Visible the Distribution of Activity in a Source of Ionizing Radiation", Nature, Lond. 168, 762-

McKILLOP, J.H., MURRAY, R.G., TURNER, J.G., BESSENT, R.G., LORIMER, A.R. and GREIG, W.R., 1979, "Can the Extent of Coronary Artery Disease by Predicted From Thallium-201 Myocardial Images", JNM, 20, 715-

McKILLOP, J.H., MURRAY, R.G., TURNER, J.G., BESSENT, R.G., 1980, "A Comparison of Visual and Semi-Quantitative Analysis of Stress Thallium-201 Myocardial Images in Patients with Suspected Ischaemic Heart Disease", Radiology, 136, 187-

McKILLOP, J.H., FAWCETT, H.D., BAUMERT, J.E., McDOUGALL, J.R., DeBUSK, R.F., HANSON, D.C. and GORIS, M.L., 1981 "ECG Gating of Thallium-201 Myocardial Images: Effect on Detection of Ischaemic Heart Disease", JNM, 22, 219-

MORTELMANS, L.A., DeROO, M.J., 1983, "Diagnostic Value of SPECT in a Case of Lower Neck Uptake on Bone Scan", Clin. Nuc. Med.8, 616

MUEHLLEHNER, G., 1970, "Rotating Collimator Tomography", JNM, 11, 347-

MUELLER, T.M., MELVIN, M.D., MARCUS, L., ERHARDT, J.C., CHAUDHURI, T. and ABBOUD, F.M., 1976, "Limitations of Thallium-201 Myocardial Perfusion Scintigrams", Circ., 54, 640-

MURRAY, R.G., McKILLOP, J.H., BESSENT, R.G., TURNER, J.G., LORIMER, A.R., HUTTON, I., GREIG, W.R., and LAWRIE, T.D.V., 1981, "Baysian Analysis of Stress Thallium-201 Scintigraphy", Eur. JNM, 6, 201

MYERS, M.J., BUSEMAN, SOKOLE, E. and DeBAKKER, J., 1983, "A Comparison of Rotating Slant Hole Collimator and Rotating Camera for Single Photon Emission Tomography of the Heart", PMB, 28, 581-

OLDENDORF, W.H., 1961, "Isolated Flying Spot Detection of Radio-density Discontinuties - Displaying the Internal Structural Pattern of a Complex Object", IRE. Trans. on Bio-Medical Electronics 8, 68-

OSBORNE, D.R.S., JASZCZAK, R. and COLEMAN, R.E., 1983, "Single Photon Emission Computed Tomography and its Application in the Lung", Rad. Clin. of North America, 21, 789-

OYAMADU, H., TERUI, S., MAKUUCHI, M., YAMAZAKI, S., HASEGAWA, H. and OZAKAKI, N., 1984, "Segmental Assessment on Ordinary Scintigrams and SPECT Images of the Liver", EJMN, 9, 161-

PRIGENT, F., FRIEDMAN, J., MADDAHI, J., BEITENDORF, L., GARCIA, E., AREEDA, J., VAN TRAIN, K., WAXMAN, A. and BERMAN, D., 1983 "Comparison of Rotational Tomography with Planar Imaging for Thallium-201 Stress Myocardial Scintigraphy", JNM, 24, P18

RATIB, O., HENZE, E., HOFFMAN, E., PHELPS, M.E. and SCHELBERT, H.R., 1982, "Performance of the Rotating Slant Hole Collimator for the Detection of Myocardial Perfusion Abnormalties", JNM, 23, 34-

REID, A., DENDY, P.P., GEMMELL, H.G. and SMITH, F.W., 1983, "Value of Tomographic Section Views in Identifying Liver Abnormalities by Scintigraphy", Acta. Rad. Diag. 24, 107-

RIGO, P., BAILEY, I.K., GRIFFITH, L.S.C., PITT, B., BURROW, R.D., WAGNER, H.N. and BECKER, L.C., 1980, "Value and Limitation of Segmental Analysis of Stress Thallium Myocardial Imaging for Localisation of Coronary Artery Disease", Circ. 61. 973-

RITCHIE, J.L., WILLIAMS, D.L., CALDWELL, J.H., STRATTON, J.R., HARP, G.D., VOGEL, R.A. and HAMILTON, G.W., 1981, "7-Pinhole Emission Tomography with Thallium-201 in Patients with Prior Myocardial Infarction", JNM, 22, 107-

RIZI, H.R., KLINE, R.C., THRALI, J.H., BESOZIA, M.C., KEYES, J.W., ROGERS, W.L., CLARE, J. and PITT, B., 1981, "Thallium-201 Myocardial Scintigraphy: A Critical Comparison of 7-Pinhole Tomography and Conventional Planar Imaging", JNM, 22, 493-

ROFF, U., NELSON, T.R. and RITENOW, E.R., 1984, "Improvement of SPECT Imaging for Myocardial Perfusion Studies Using a Media Filter Pre-Processing Technique", JNM, 25, P14

ROGERS, W.L., CLINTHORNE, N.H., and HARKNESS, B.A., 1982, "Field Flood Requirements for Emission Computed Tomography with an Anger Camera", JNM, 23, 162-

RONALDSON, R.M., KAHN, O., RAPHAEL, M.J., JARRITT, P.H., and ELL, P.J., 1982, "Emission Tomography in Embolic Lung Disease: Angiographic Correlations", Clinical Radiology, 33, 389-

SAKATA, T., ISHIMARU, T., MAEDA, H., OKAHASHI, S., KAWAI, T., SUEZAWA, Y., YAMASAKI, K., TAKEUCHI, M. and AGACHI, H., 1983, "Single Photon Emission Computed Tomography (SPECT) in Bone Lesion", Kaku, Igaku, 20, 667-

TAMAKI, N., MUKAI, T., ISHII, Y., YONEKURA, Y., KAMBARA, H., KAWAI, C. and TONZUKA, K., 1981, "Clinical Evaluation of Thallium-201 Emission Myocardial Tomography Using a Rotating Gamma Camera: Comparison with 7-Pinhole Tomography", JNM, 22, 849-

TODD-POKROPEK, A., 1983, "Non-Circular Orbits for the Reduction of Uniformity Artefacts in SPECT", PMB, 28, 309-

TODD-POKROPEK, A., MARSH, R., GILARDI, M.C., GEVDI, P. and FAZIO, F., "An Object Independent Attenuation Correction in SPECT: Estimating the Effects of Scatter and Collimator RSF", JNM, 25, P14-

UNDERWOOD, S.R., WALTON, S., LAMING, P.J., JARRITT, P.H., ELL, P.J., EMANUEL, R.W., and SWANTON, R.H., 1985, "Left Ventricular Volume and Ejection Fraction Determined by Gated Blood Pool Emission Tomography", Br. Heart. J., 53, 216-

UNDERWOOD, S.R., ELL, P.J., JARRITT, P.H., ENOWEL, R.W. and SWARTON, R.H., 1984, "ECG Gated Blood Pool Tomography in the Determination of LV Volume, Ejection Fractions and Wall Motion", JNM, 25, P87.

UREN, R.F., MAGISTRETTI, P.L, and ROYAL, H.D., 1982, "Single Photon Emission Computed Tomography with Tc-99m Gluocoheptonates and I-123 Iodamphetamine in Cerebral Infarction", Clin. Nuc. Med. 7, 385-

VOGEL, R.A., KIRCH, D., LeFREE, M. and STEELE, P., 1978, " A New Method of Multiplanar Emission Tomography Using a 7-Pinhole Collimator and an Anger Scintillation Camera", JNM, 19, 648-

WATSON, N.E., COWAN, R.J., BALL, M.R., MOODY, D.M., LASTER, D.W., and MAYNARD, C.D., 1980, "A Comparison of Brain Imaging with Gamma Camera, Single Photon Emission Computed Tomography and Transmission Computed Tomography: Concise Communication", JNM, 21, 507-

WEBB, S., FLOWER, M.A., OTT, R.J. and LEACH, M.O., 1983, "A Comparison of Attenuation Correction Methods for Quantitative SPECT", PMB, 28, 1045-

WHITE, D.R., SPELLER, R.D. and TAYLOR, P.M., 1981, "Evaluating Performance Characteristics in Computerised Tomography", BJR, 54, 221-

WILLIAMS, D.L., RITCHIE, J.L., HARP, G.D., CALDWELL, J.H., and HAMILTON, G.W., 1980 "In Vivo Simulations of Thallium-201 Myocardial Scintigraphy by 7-Pinhole Emission Tomography", JNM, 21, 821-